

Editor-in-Chief B.E.Paton

Editorial board:

- Yu. S. Borisov V. F. Grabin
A. Ya. Ishchenko V. F. Khorunov
B. V. Khitrovskaya I. V. Krivtsun
S. I. Kuchuk-Yatsenko
Yu. N. Lankin V. K. Lebedev
V. N. Lipodaev L. M. Lobanov
V. I. Makhnenko A. A. Mazur
O. K. Nazarenko I. K. Pokhodnya
I. A. Ryabtsev Yu. A. Sterenbogen
N. M. Voropai K. A. Yushchenko
A. T. Zelnichenko

International editorial council:

- N. P. Alyoshin (Russia)
U. Diltey (Germany)
Guan Qiao (China)
D. von Hofe (Germany)
V. I. Lysak (Russia)
N. I. Nikiforov (Russia)
B. E. Paton (Ukraine)
Ya. Pilarczyk (Poland)
P. Seyffarth (Germany)
G. A. Turichin (Russia)
Zhang Yanmin (China)
A. S. Zubchenko (Russia)

Promotion group:

- V. N. Lipodaev, V. I. Lokteva
A. T. Zelnichenko (exec. director)
Translators:
I. N. Kutianova, V. F. Orets,
T. K. Vasilenko, N. V. Yalanskaya
Editor
N. A. Dmitrieva
Electron galley:
I. S. Dmitruk, T. Yu. Snegiryova

Address:

E.O. Paton Electric Welding Institute, International Association «Welding», 11, Bozhenko str., 03680, Kyiv, Ukraine
Tel.: (38044) 287 67 57
Fax: (38044) 528 04 86
E-mail: journal@paton.kiev.ua
http://www.nas.gov.ua/pwj

State Registration Certificate KV 4790 of 09.01.2001

Subscriptions:

\$324, 12 issues per year, postage and packaging included. Back issues available.

All rights reserved.

This publication and each of the articles contained herein are protected by copyright. Permission to reproduce material contained in this journal must be obtained in writing from the Publisher. Copies of individual articles may be obtained from the Publisher.

CONTENTS

SCIENTIFIC AND TECHNICAL

Makhnenko V.I., Velikoivanenko E.A. and Olejnik O.I. Risk analysis as a method for formalising decision making on unscheduled repair of welded structures ..... 2
Poznyakov V.D. Improvement of delayed cracking resistance of welded joints of cast hardenable steels ..... 7
Ryabtsev I.I. Calculation-experimental evaluation of the efficiency of alloying the high-alloy deposited metal with phosphorus ..... 13
Kuzmin S.V., Chuvichilov V.A. and Lysak V.I. Peculiarities of plastic deformation of near-weld zone metal in explosion welding according to scheme of double-sided symmetrical cladding ..... 18
Tsybulkin G.A. Correction of a manipulation robot motion path taking into account additional measurements ..... 22

INDUSTRIAL

Garf E.F. and Snisarenko V.V. Development and application of tubular welded structures ..... 25
Kozulin S.M., Lychko I.I. and Podyma G.S. Electroslag surfacing of rotating kiln gear shaft teeth ..... 31
Zagornikov V.I. Procedure for repair of blades of titanium alloy VT3-1 by electron beam welding ..... 35
Levchenko O.G. and Levchuk V.K. Safe level of electromagnetic field intensity in resistance welding ..... 38

BRIEF INFORMATION

Dobrushin L.D., Petushkov V.G. and Bryzgalin A.G. Application of explosion energy for treatment of welded joints on decomposers and mixers at the Nikolaev Alumina Plant ..... 47
News ..... 48

NEWS

To 80th anniversary of Prof. Boris A. Movchan ..... 48
Developed at PWI ..... 12, 34



# RISK ANALYSIS AS A METHOD FOR FORMALISING DECISION MAKING ON UNSCHEDULED REPAIR OF WELDED STRUCTURES

V.I. MAKHNENKO, E.A. VELIKOIVANENKO and O.I. OLEJNIK

E.O. Paton Electric Welding Institute, NASU, Kiev, Ukraine

The ideology of formalising decision making on the scope and terms of repair of welded structures by using their technical diagnostics data is considered. It is based on prediction of the probability of failure due to detected defects for a forthcoming period of operation, and is combined with the advanced risk analysis tools developed in allied activity fields.

*Keywords:* risk analysis, technical diagnostics, detected defects, failure probability

The concept based on «prediction and prevention» receives an increasingly wide acceptance now, and is replaced by the old «detection and removal» concept to ensure safe operation of critical structures.

According to the new concept, prediction of the remaining safe service life is based on the corresponding information generated by stress loading monitoring, results of technical diagnostics of the state of a structure containing geometrical defects (especially discontinuities), as well as data on degradation of the mechanical properties responsible for resistance to different types of fracture and related to service conditions. Appropriate calculation codes (algorithms) based on up-to-date achievements in deformation and fracture mechanics, calculus mathematics and computer facilities are used for this purpose.

The system of safety factors for stress loading of a structure, as well as characteristics of a material determining its fracture resistance, is employed to provide a reliable prediction by calculations. The system is intended to compensate for measurement errors in technical diagnostics and probable fluctuations of loading and fracture resistance properties of the material. The probability theory approaches have been widely used in the last decades for these purposes. They apply to the cases where the probability of failure, i.e. violation of integrity, is determined by using the set laws of randomly varying characteristics (load, measured geometrical sizes of defects, degree of degradation of resistance of the material to this or that type of fracture), and the decision on further safe operation of the structure is made on this basis. Most often the appropriate decision making is based on the prescribed failure probabilities permitted by standards for the corresponding structures operating under specific service conditions [1]. Development of the regulatory base is a labour-consuming and very important job. Nevertheless, such developments are available not only in the industries where requirements for the reliability are very high (e.g. aircraft engineering), but also in civil engineering [2–4], pipeline transport [5,

6], etc. Naturally, estimation of the failure probability is associated with a larger amount of calculations, compared with deterministic calculation of the maintenance of integrity. However, with the state-of-the-art in computer facilities, this drawback is no longer important. At the same time, owing to the probability approach, for formalisation of decisions it is possible to use the established risk analysis methods developed in allied activity fields (e.g. in banking), as well as other methods, and thus avoid as much as possible any subjectivism in decision making on prevention of emergency situations for the predicted service life of structures.

Consider this issue in more detail. Let an examination object have  $n = 1, 2, \dots, n, \dots, N$  independent defects with failure probability  $P_1, P_2, \dots, P_n, P_N$  determined for each of them for predicted period  $\tau$ . Note that all  $P_n < 1$ . However, we can distinguish several values of  $P_1, P_2, \dots, P_k$ , for which condition  $P_n \ll 1$  is not met.

In this case, probability  $P_N(\tau)$  that failure due to one of the defects takes place at least for predicted period  $\tau$  can be determined from the known relationship:

$$P_N(\tau) = 1 - \left[ \prod_{n=1}^k (1 - P_n) \right] \exp \left( - \sum_k^N P_n \right) \quad (1)$$

where  $\prod_{n=1}^k (1 - P_n)$  is the operator of the product of values  $(1 - P_n)$  and  $n = 1, 2, \dots, k$ .

With specific values of  $P_N(\tau)$ , it is possible to estimate contribution of each of  $N$  defects to probability  $P_N(\tau)$  from (1).

Consider the case of financial losses alone, where the losses are associated with failure of a given object. Designate the costs of removal of failure consequences for the object as  $Q$ , and costs of removal (repair) of  $n$ -th defect  $q_n$  as  $(q_n + q_0)$ , where  $q_0$  are the repair costs that are independent of peculiarities of a defect, quantity of defects and other factors, i.e. the costs of scope  $M$  of repair of the defects can be expressed in terms of the following sum:



$$\Phi(M) = q_0 + \sum_{n=1}^M q_n \quad (2)$$

As the risk of financial losses related to removing consequences of formation of defects can be represented as product  $QP_{N-M}(\tau)$ , comparison of  $\Phi(M)$  with  $QP_{N-M}(\tau)$  determines the necessity of repair and its scope  $M$  for time  $\tau$  of the predicted operation

$$\Phi(M) = QP_{N-M}(\tau) \quad (3)$$

Figure 1 shows the risk analysis diagram for financial losses, which relates the time of operation of a given object to the next examination,  $\tau$ , to quantity  $N$  of the detected defects, their quality through  $P_n(\tau)$ , costs  $Q$  for removal of the consequences of failure and repair,  $q_0$  and  $q_n$ , and scope  $M$  of the defects removed by repair.

The key point in implementation of the above risk analysis scheme is determination of  $P_n(\tau)$  for the detected defects.

As there is no way to solve this problem experimentally, numerical methods are used at present for these purposes. They are based on the corresponding deterministic fracture criteria, as well as on the experimentally observed spread (variation) of load values, geometrical sizes of defects, and parameters of resistance of a material to characteristic types of fracture.

The fracture criterion for a given specific defect can be written down as follows:

$$Y(X_1, X_2, \dots, X_n, Z_1, Z_2, \dots, Z_m) = 0, \quad (4)$$

where  $X_1, X_2, \dots, X_n$  are the parameters that have appreciable stochasticity; and  $Z_1, Z_2, \dots, Z_m$  are the parameters with insignificant variations, i.e. they are considered to be deterministic.

For parameters  $X_1, X_2, \dots, X_n$ , their mean values  $\bar{X}_1, \bar{X}_2, \dots, \bar{X}_n$  and normalised distribution density  $\varphi_{X_1}, \varphi_{X_2}, \dots, \varphi_{X_n}$  are known. Most often for these purposes the use is made of the truncated normal distribution law, allowing for normalising (Figure 2), having the following form:

$$\varphi_X = 0, \quad \bar{\varphi}_X = \frac{1}{S} \left[ \frac{1}{\sqrt{2\pi}\xi_X} \exp \left[ -\frac{1}{2} \left( \frac{X - \bar{X}}{\xi_X} \right)^2 \right] \right], \quad (5)$$

where  $S = \int_A^B \varphi_X dX$ ; and  $\xi_X$  is the standard deviation of the  $X$  values.

Probability  $P(Y < 0)$ , where  $Y < 0$  is taken from (4), is determined by the Monte-Carlo method [7], i.e. the sample of the  $Y(X, Z)$  values is formed according to (4) for different combinations of values of parameter  $X$  determined by the law of random numbers. The table of correspondence between random numbers  $Z$  within  $0 \leq Z \leq 1$  and  $X$  values within  $A \leq X \leq B$  is compiled for each value of  $X$ . This is done by using the rule that random number  $Z$  corresponds

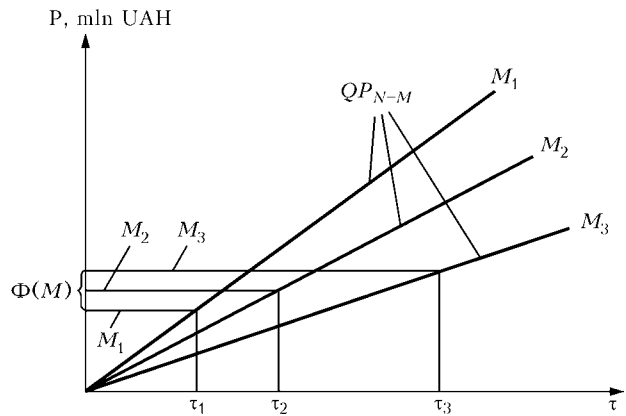


Figure 1. Diagram of risk analysis relating probability repair costs  $QP_{N-M}(\tau)$  to volume  $M$ , and costs of repaired defects  $\Phi(M)$  depending upon time  $\tau$  till next examination of object:  $M_1 < M_2 < M_3$ ;  $P$  — financial expenses

to a value of  $X$ , the probability of which is not less than the value of  $Z$ , i.e.

$$Z = \int_A^X \bar{\varphi} dX. \quad (6)$$

Therefore, if the law of the normalised density of distribution of the  $X$  values within the  $A \leq X \leq B$  range is known, equation (6) allows each value of  $X$  to be unambiguously related to random number  $X$  within the  $0 \leq Z \leq 1$  range.

It should be noted at this point that for such characteristics of a material as the critical values of stress intensity factor  $K_{IC}$ , which determine brittle fracture resistance, stochasticity is often described by the Weibull law, i.e. we will obtain the following instead of (6):

$$Z = 1 - \exp \left[ - \left( \frac{K_{IC} - K_0}{K_d - K_0} \right)^\eta \right], \quad (7)$$

where  $K_0, K_d$  and  $\eta$  are the distribution parameters of the Weibull law, which are usually determined by the results of 12–15 experiments [8], when the mean value of  $K_{IC}^m$ , for which  $Z = 0.5$ , as well as the lower,  $K_{IC}^l$ , and upper,  $K_{IC}^u$ , limits of this value, for which  $Z = 0.05$  and  $0.95$ , respectively, are known.

As follows from the above-said, most important here are the deterministic fracture criteria (4). As

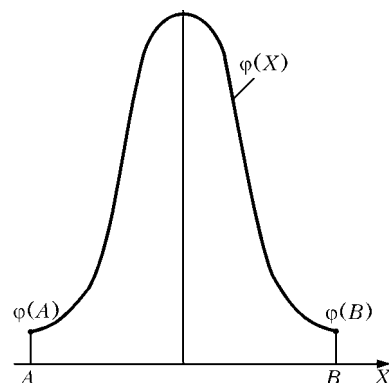


Figure 2.  $X$  value distribution density

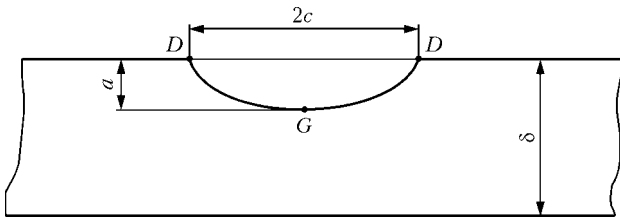


Figure 3. Semi-elliptical crack  $2c \times a$  in size, located in pipe wall

applied to welded joints (connections), this issue is adequately considered in modern literature, in study [9] in particular.

As an example, consider a region of pipeline with diameter  $d = 1420$  mm and wall thickness  $\delta = 19$  mm, where defects of the following two types were detected:

- surface cracks,  $2c_j \times a_j$  in size (Figure 3), along the axial weld in pipe, variants  $j = 1, 2, 3$ , and along the circumferential weld  $j = 4, 5$  (Table 1);
- local thinnings (Figure 4),  $s_j$  (along the pipe axis) and  $c_j$  (along the circumference) in size, with minimal measured thickness  $\delta_{meas}^{(j)}$ ; corresponding geometrical sizes of the defects are given in Table 2 for  $j = 6-10$ .

The defects are the stress corrosion ones. The rate of corrosion growth of the cracks under static loading is set by parameters of the corresponding diagram of static corrosion cracking, i.e. the threshold value of stress intensity factor  $K_{ISCC}$  and crack propagation rate  $W_{max}$  (Figure 5). Stochasticity of these parameters causes no doubts. The Weibull distribution is used for  $K_{ISCC}$  at  $K_0 = 2 \text{ MPa}\cdot\text{m}^{1/2}$ ,  $K_d = 21.7 \text{ MPa}\cdot\text{m}^{1/2}$  and  $\eta = 4$ . Accordingly,  $K_{ISCC} = 20 \text{ MPa}\cdot\text{m}^{1/2}$ . For  $W_{max}$ , the truncated normal law (5) is used at  $\bar{W}_{max} = 4.4$  mm/year,  $\xi_W = 0.4$  mm/year,  $A_W = 4.0$  mm/year, and  $\bar{B}_W = 4.8$  mm/year.

The values of stress intensity factor  $K_I$  within the crack zone are determined through crack sizes  $a$  and  $c$ , and through membrane and bend stresses,  $\sigma_m$  and  $\sigma_b$ , respectively, which are normal to the crack plane [10]. According to [10], the stress intensity factors are calculated as follows:

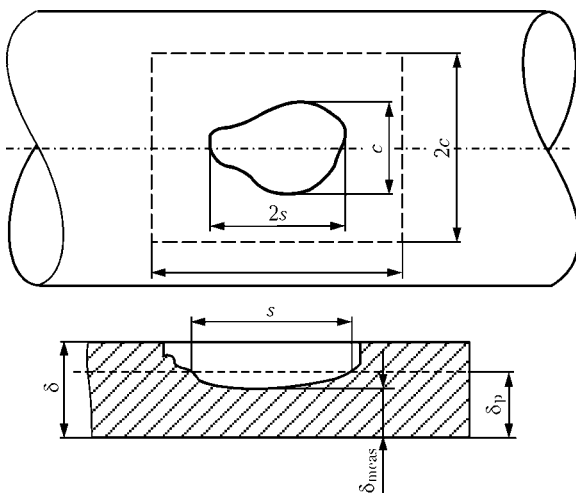


Figure 4. Local thinning  $c \times s$  in pipe wall ( $2c \times 2s$  — control zone)

Table 1. Geometrical sizes of crack, mm

j	$\bar{a}$	$\bar{c}$	$\xi_a$	$\bar{A}_a$	$\xi_c$	$\bar{A}_c$	Load, MPa		
							$\bar{\sigma}_m$	$\xi_{\sigma}$	$A_{\sigma}$
1	1.6	20	1	0.6	2	16	235.0	10	225.0
2	1.6	50	1	0.6	4	46	235.0	10	225.0
3	1.6	200	1	0.6	4	196	235.0	10	225.0
4	1.6	200	1	0.6	4	196	117.5	10	107.5
5	1.6	600	1	0.6	4	596	117.5	10	107.5

Table 2. Geometrical sizes of thinning, mm

j	$\bar{s}$	$\bar{c}$	$\delta_{meas}$	$\xi_s$	$A_s$	$\xi_{\delta_{meas}}$	$A_{\delta_{meas}}$	$\xi_c$	$A_c$
6	40	500	11.5	2	20	0.5	10.5	5	250
7	40	500	12.0	2	20	0.5	11.0	5	250
8	100	500	12.0	2	50	0.5	11.0	5	250
9	150	500	15.5	2	75	0.5	14.5	5	250
10	150	500	16.0	2	75	0.5	15.0	5	250

$$K_{Ij}(j) = \frac{\sqrt{\pi a}}{Q} F_j(\sigma_m + H_j \sigma_b), \quad (j = D, G), \quad (8)$$

where

$$Q = 1 + 1.464(a/c)^{1.65};$$

$$F_j = [M_1 + M_2(a/\delta)^2 + M_3(a/\delta)^4] g_j;$$

$$M_1 = 1.11 + 0.09(a/c);$$

$$M_2 = -0.54 - \frac{0.89}{0.2 + a/c};$$

$$M_3 = 0.5 - \frac{1}{0.65 + a/c + 14(1 - a/c)^{24}};$$

$$g_D = 1, \quad g_G = [1 + (0.1 + 0.35)(a/\delta)^2] \sqrt{a/c};$$

$$H_G = 1 - (1.22 + 0.12a/c)a/\delta + [0.55 - 1.05(a/c)^{0.75} + 0.47(a/c)^{1.5}] (a/\delta)^2;$$

$$H_D = 1 - 0.34(a/\delta) - 0.11(a/c)(a/\delta).$$

The values of  $K_I$  at the crack apex (points  $D$  and  $G$  in Figure 3) are calculated from the above relationships, and the rate of growth of a crack with sizes  $da/d\tau$  and  $dc/d\tau$  is determined from the diagram shown in Figure 5.

Crack sizes  $a/\tau$  and  $c/\tau$  are found by successive tracing against time. It is considered that the critical state is the state which generates conditions for spontaneous growth of a crack  $a(\tau) \times 2c(\tau)$  in size.

Condition of the spontaneous growth of a crack can be determined from the well known brittle-tough fracture criterion [9]:

$$K_r(L_r) = (1 - 0.14L_r^2) [0.3 + 0.7 \exp(-0.65L_r^6)], \quad (9)$$

where  $K_r = K_I(\tau) / K_{IC}$  characterises the risk of brittle fracture;  $L_r = \sigma_{ref} / \sigma_y$  is the risk of purely tough fracture within the crack zone by the mechanism of plastic instability;  $\sigma_y$  is the yield strength of the material;



and  $\sigma_{ref}$  are the stresses that depend upon the rated membrane  $\sigma_m$  and bend stresses  $\sigma_b$ , respectively [11].

According to [11], the calculation of  $\sigma_{ref}$  for cracks along the generating line is made as follows:

$$\sigma_{ref} = \frac{1}{3} \{ \sigma_b + [(f\sigma_b)^2 + 9(M_s\sigma_m)^2]^{0.5} \}, \quad (10)$$

where

$$f = 1 - 20 \left( \frac{a}{2c} \right)^{0.75} \alpha^3, \quad \alpha = \frac{a/\delta}{1 + \delta/c};$$

$$M_s = \frac{1 - 0.85a/\delta/M_t}{1 - 0.85a/\delta};$$

$$M_t = \frac{1.0005 + 0.49001\lambda + 0.32409\lambda^2}{1.0 + 0.50144\lambda - 0.01106\lambda^2}; \quad \lambda = \frac{1.818a}{\sqrt{\delta d/2}}.$$

The calculation of  $\sigma_{ref}$ , according to [11], for cracks along the circumference at  $\sigma_b = 0$  is made as follows:

$$\sigma_{ref} = \sigma_m Z, \quad (11)$$

where

$$Z = \left\{ \frac{2}{\pi} - \frac{(\bar{\alpha}/\delta) \theta}{\pi} \left[ \frac{2 - 2(2\delta/d) + 2a/d}{2 - 2\delta/d} \right] \right\}^{-1};$$

$$\bar{\alpha} = \arccos A \sin \theta; \quad \theta = \frac{2\pi c}{4d};$$

$$A = X \frac{(1 - \tau)(2 - 2\tau + X\tau) + (1 - \tau + X\tau)^2}{2[1 + (2 - \tau)(1 - \tau)]};$$

$$X = \frac{a}{\delta}; \quad \tau = \frac{2\delta}{d}.$$

Stochasticity shows up here both in stresses  $\bar{\sigma}_m$  (see Table 1) and  $\sigma_b$ , and in such characteristics of the material as  $K_{IC}$  and  $\sigma_y$ . The truncated normal law of the probability density distribution (5) at  $\bar{\sigma}_y = 350$  MPa,  $\xi_\sigma = 20$  MPa,  $A_{\sigma_y} = 320$  MPa and  $B_{\sigma_y} = 380$  MPa is used to determine  $\sigma_y$ .  $K_{IC}$  is estimated by using the Weibull law (7) at  $K_0 = 20$  MPa·m<sup>1/2</sup>,  $\eta = 4$  and  $K_d = 107.7$  MPa·m<sup>1/2</sup>. Accordingly, mean value  $\bar{K}_{IC} = 100$  MPa·m<sup>1/2</sup>. Table 3 gives correspondence between the random values of  $Z$ ,  $K_{ISCC}$  and  $K_{IC}$ . Results of the calculation of failure probability for cracks with  $j = 1-5$ , according to Table 1, depending upon service time  $\tau$ , are shown in Figure 6. It can be seen that the certain incubation period, when the crack growth is determined by a random violation of condition  $K_{IC} > K_{ISCC}$  at the tracing steps, is followed by the period of a quite intensive growth of cracks up to the moment when a crack is transformed into a through one (where  $a \approx \delta$ ), after which the failure probability grows slowly, as it is determined now by increase in size  $2c$ .

For the second type of defects, i.e. local thinnings ( $j = 6-10$ ) (see Table 2), the failure criterion, according to [12], can be written down in the following form:

$$\delta_{meas}^{min} - v_c \tau - [\delta_p] R_{s,c} = 0, \quad (12)$$

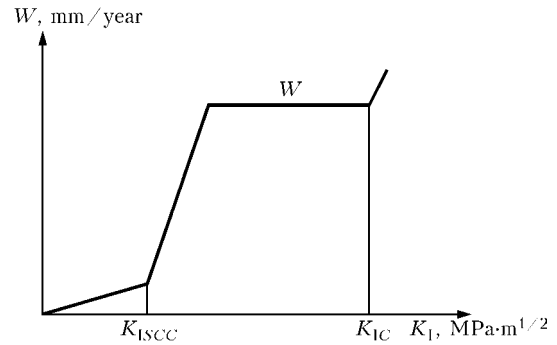
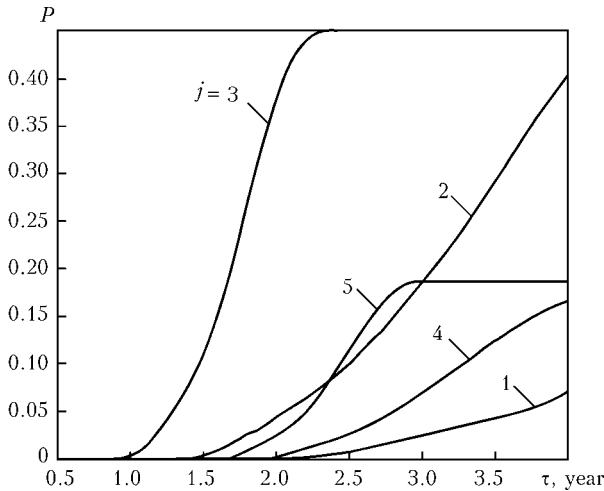


Figure 5. Diagram of static corrosion cracking

where  $\delta_{meas}^{min}$  is the minimal measured thickness of a pipe;  $v_c$  is the surface corrosion rate;  $\delta_p$  is the admissible (calculated) thickness of a defect-free pipe, based on the strength conditions;  $\tau$  is the predicted service time; and  $R_{s,c}$  according to [12] (see also [9]), is shown in Figure 7;

Table 3. Correspondence between random values of  $Z$ ,  $K_{ISCC}$  and  $K_{IC}$  for a considered pipe material

Z	$K_{ISCC}$ , MPa·m <sup>1/2</sup>	$K_{IC}$ , MPa·m <sup>1/2</sup>
0.8095667	24.35589	119.5234
0.8579873	25.28505	123.6599
0.4322595	19.08786	96.07135
0.3141314	17.43731	88.72343
0.050000	11.37522	61.73637
0.8706391	25.55849	124.8771
0.09593023	13.10156	69.42165
0.2225395	15.95394	82.11980
0.8249169	24.63388	120.7610
0.7943811	24.09273	118.3519
0.950000	27.91743	135.3786
0.05106258	11.42594	61.96219
0.950000	27.91743	135.3786
0.950000	27.91743	135.3786
0.8305760	24.73983	121.2327
0.1832684	15.21426	78.82693
0.1558958	14.63995	76.27024
0.1917861	15.38211	79.57417
0.6983891	22.61277	111.7635
0.3617200	18.12585	91.78867
0.9038577	26.37022	128.4908
0.7445055	23.29188	114.7867
0.4923106	19.87538	99.57719
0.2371828	16.21029	83.26105
0.3804549	18.38694	92.95100
0.2091601	15.71121	81.03925
0.2628518	16.63960	85.17223
0.6154635	21.47819	106.7125
0.4542154	19.37802	97.36305



**Figure 6.** Failure probability against service time for crack-like defects with  $j = 1-5$  (accordingly,  $c = 20-600$  mm) at  $a = 1.6$  mm

$$R_s, c = 0.2 \text{ at } \lambda = \frac{1.285s}{\sqrt{d\delta_p}} \leq 0.3475 \text{ and } c/d \leq 0.348;$$

$R_s = f(\lambda)$  according to Figure 7, at  $\lambda > 0.3475$ ;

$$R_c = \frac{10.51(c/d)^2 - 0.73589}{13.838(c/d)^2 + 1} \text{ at } c/d > 0.3475.$$

Stochasticity in this criterion is related to geometrical sizes of the thinning zone,  $s$ ,  $c$  and  $\delta_{meas}^{min}$ , as well as to corrosion rate  $v_c$ . To determine these values, it is possible to use the truncated normal distribution law (5). Tables 1 and 2 give the corresponding characteristics of this distribution for the said parameters, and Figure 8 shows the kinetics of variation of failure probability  $P_j$  ( $j = 6-10$ ), which is calculated by using the deterministic data with respect to  $d = 1420$  mm and  $\delta_p = 16$  mm. As follows from these data, for thinnings with  $j = 6, 7$ , the failure is determined by fracture along the circumference, and for the rest of the thinnings ( $j = 8-10$ ) it is determined by fracture along the generating line, the key factor being decrease in the  $\delta_{meas}$  values with time due to corrosion.

The data of Figures 6 and 8 from equation (1) can be used to calculate the failure probability at least by one of the defects considered with  $j = 1-10$  (curve  $P$  ( $M = 0$ ) in Figure 9), which corresponds to  $M = 0$  of the removed (repaired) defects. It can be seen from the Figure that the failure probability after a year and

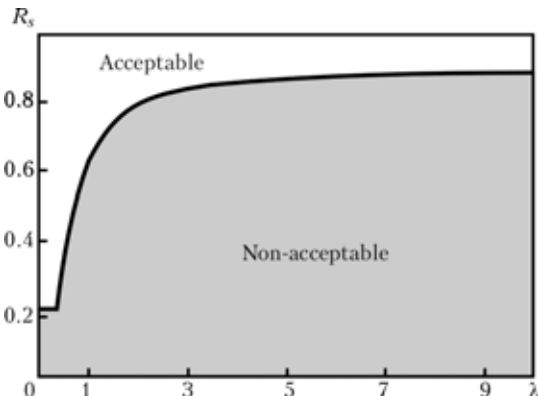


**Figure 7.** Condition of acceptability of defects of the type of local thinning by size  $s$

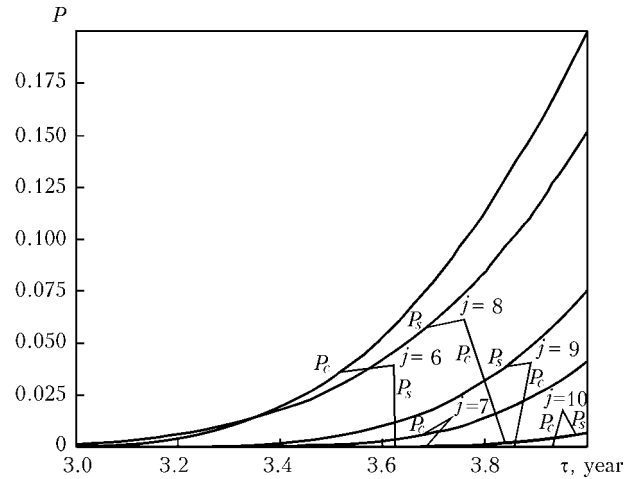


**Figure 8.** Failure probability against service time for defects of the type of thinning with  $j = 6-10$  by direction  $c$  — ( $P_c$ ) and  $s$  — ( $P_s$ )

a half service is more than 0.12, and after 2 years it is over 0.42. In this Figure, the curves of a relative cost of repair,  $\Phi(M)/Q$ , show that the necessity of repair becomes unquestionable as early as after two years of operation for economical reasons as well, i.e. the risk analysis shows that the given region can remain in operation without repair for no longer than a year and a half.

Curves  $P(M)$  in Figure 9 (at  $M = 1, 2, \dots, 9$ ) give an idea of the risk of failure on a condition of removal of scope  $M$  of the most dangerous defects, i.e.  $M = 1$  corresponds to removal of defect with  $j = 3$  (see Tables 1 and 2),  $M = 2$  — additional removal of defect with  $j = 2$ ;  $M = 3$  —  $j = 5$ ;  $M = 4$  —  $j = 6$ ;  $M = 5$  —  $j = 4$ ;  $M = 6$  —  $j = 8$ ;  $M = 7$  —  $j = 1$ ;  $M = 8$  —  $j = 9$ , and  $M = 9$  —  $j = 7$ .

It can be seen from the Figure that in the case of a forthcoming four years' operation to the next diagnostics, it is economically beneficial to remove seven most dangerous defects (curve  $M = 7$ ).

Therefore, it can be concluded from the example considered that plotting the risk analysis diagrams for the detected defects in welded structures formalises to a substantial degree the process of decision making on the necessity of a forthcoming repair, as well as its scope.

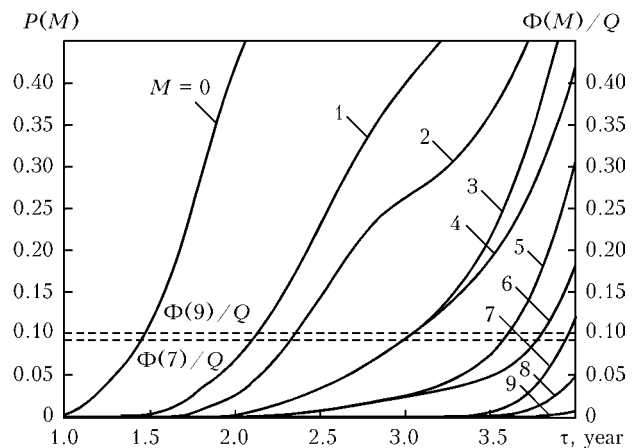


**Figure 9.** Diagram of risk analysis for substantiation of the required scope of repair ( $M = 1-9$  — see explanations in the text)



1. Bolotin, V.V. (1982) *Methods of probability and reliability theory in analysis of structures*. Moscow: Strojizdat.
2. Rajzer, V.D. (1986) *Methods of reliability theory in problems of regulation of design parameters for building structures*. Moscow: Strojizdat.
3. Rzhantsyn, A.R. (1978) *Theory of reliability design of building structures*. Moscow: Strojizdat.
4. Perelmuter, A.V. (2000) *Selected problems of reliability and safety of building structures*. Kiev: UkrNIIproektstalkonstruktziya.
5. ISO SD 16708: Petroleum and natural gas industries. Pipeline transportation systems. Based limit state methods. Filed Oct. 2000.
6. Caley, T., Gonzalez, I.L., Hallen, I.M. (2002) A study on the reliability assessment methodology for pipelines with active corrosion defects. *Int. J. Pressure Vessels and Piping*, **1**, 3–6.
7. Metropolis, N., Ulam, S. (1949) The Monte Carlo method. *Amer. Statist. Assoc.*, **44**(248), 335–341.
8. Margolin, B.E., Shvetsova, V.A., Gulenko, A.G. et al. (2003) Prediction of crack resistance of hull reactor steel based on the «Master curve» concept and probabilistic model. *Problemy Prochnosti*, **1**, 5–21.
9. Makhnenko, V.I. (2006) *Resource of safe service of welded joints and assembly units in modern structures*. Kiev: Naukova Dumka.
10. MR 125-01-90: Calculation of stress intensity factors and section weakening coefficients for defects in welded joints. Kiev.
11. Zahoor, A. (1989) *Ductile fracture handbook*. Palo Alto, CA: Electric Power Institute.
12. (2000) *Fitness-for-service: Recommended practice 579*. Washington: American Petroleum Institute.

## IMPROVEMENT OF DELAYED CRACKING RESISTANCE OF WELDED JOINTS OF CAST HARDENABLE STEELS

V.D. POZNYAKOV

E.O. Paton Electric Welding Institute, NASU, Kiev, Ukraine

Results of evaluation of delayed fracture resistance of the HAZ metal in welded joints on cast steel of 35L type depending on weld saturation with diffusible hydrogen, welding heat input and preheating temperature, are given. Data on the influence of welding technique on formation of the stressed state of rigidly fixed joints of heavy metal sections are presented.

*Keywords:* cast carbon steel, cold cracks, preheating, diffusible hydrogen, welding stresses, welding technology, restoration of metal structures

Engineering structures and mechanisms, which are past their design life or are close to this condition, are currently operating in Ukraine and other CIS countries. In most of the cases they are unique. The weight of some of them is greater than 100 t, and metal thickness is 80 mm. They include the basic components of crushers, hydraulic and mechanical presses — processing equipment operated in open mining and processing enterprises and metallurgical works, as well as engineering plants. They are made of cast steels of 25L and 35L type with carbon content of 0.25–0.40 %.

As shown by experience, during long-term service the metal, of which the above structures are made, accumulates micro- and macrodamage. When cracks reach critical dimensions, it becomes necessary to repair the item. Welding is one of the simplest methods of restoration of the integrity and geometrical dimensions of metal structures. This process can be performed directly in the site of equipment operation (the equipment is usually not dismantled) in a short time and at relatively low material costs.

Metal structures are usually reconditioned using standard technologies, developed for manufacturing new products. They, however, do not take into account a number of features characteristic for repair — high restraint of the welded joints, limited capabilities for selection of the methods of defect removal, edge preparation and welding performance, i.e. factors, essen-

tially influencing the properties of the components being welded [1–4]. The above specific features of welding in repair led the authors of [5] to the following conclusions: selection of welding technology for metal structure reconditioning requires a fundamentally different approach than that used for initial welding. One of the main problems to be solved in this case is the need to find the processes, which would provide a low level of residual stresses in the welds. This is necessary not only to eliminate the possibility of crack formation in the joint at the stage of welding operations performance, but also for improvement of the item performance in further service.

Increased carbon content in cast 25L and 35L steels itself predetermines considerable difficulties in their welding. They are due to the possibility of formation of a hardening martensite structure in the metal of welded joint HAZ, which is known [6] to drastically lower the cold cracking resistance of the metal. To avoid its formation, it is recommended to perform welding of the joints with preheating up to the temperatures of 200–300 °C. However, considering the complex configuration and great thickness of the metal, of which the structures are made, and the fact that during repair welding operations are performed, as a rule, in cramped conditions, it is difficult to fully implement such a technological operation in practice.

In this connection it became necessary to perform research aimed at finding new more effective technological solutions, providing an improvement of delayed cracking resistance of welded joints of steels with more than 0.25 % C, which is manifested in the



possibility of lowering the preheating temperature to 80–100 °C. To solve the posed task, it was necessary to assess the influence of the welding heat input, preheating temperature, level of weld saturation by hydrogen on delayed cracking resistance of the HAZ metal of steel joints with an increased carbon content, and determine the influence of welding techniques on development of residual stresses in welded joints of thick metal.

Resistance of the HAZ metal to delayed fracture was studied using the well-known implant method [6]. To conduct testing, samples were taken from the bed of a crusher, which had been operating for more than 12 years in one ore mining and processing works. The samples had the following composition, wt.%: 0.42C; 0.41Si; 0.67Mn; 0.34Cr; 0.36Ni; 0.025S; 0.035P.

Deposition of the connecting welds was performed with ANP-10 electrodes of 4.0 mm diameter, which ensured the welding heat input in the range of 10–21 kJ/cm. Sample cooling rate was adjusted by smoothly changing the preheating temperature from 20 to 100 °C. Concentration of diffusible hydrogen in the deposited metal was assessed by the chromatographic method and changed from 7 to 15 ml/100 g by lowering the temperature and duration of electrode baking. Generalized data obtained from the investigation results are given in Figure 1.

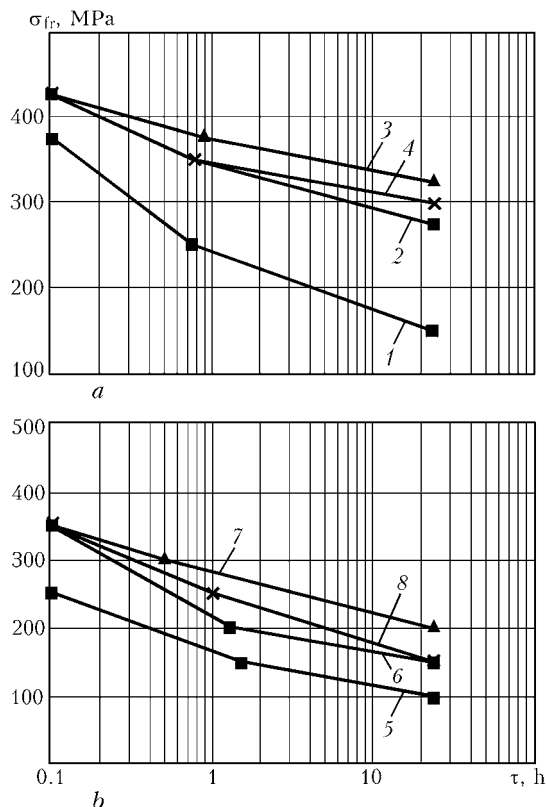


**Figure 1.** Delayed fracture resistance of HAZ metal of 35L steel at the diffusible hydrogen content in the deposited metal of 8 (a) and 15 (b) ml/100 g depending on the preheating temperature and welding heat input: 1, 4, 5, 8 —  $T_{pr} = 20$ ; 2, 6 — 60; 3, 7 — 100 °C; 1–3, 5–7 —  $Q_w = 10$ ; 4, 8 — 20 kJ/cm

The highest delayed fracture resistance is found in samples welded with preheating up to temperatures of 80 to 100 °C in the modes ensuring  $Q_w \approx 10$  kJ/cm, at the diffusible hydrogen content in the deposited metal of up to 8 ml/100 g. Critical stresses, at which the above samples did not fail for 24 h, were equal to  $\sigma_{cr} \approx 325$  MPa. Analysis of the thermokinetic diagram of austenite decomposition in steel 35 [7] close by composition and mechanical properties to steel 35L, shows that under these conditions of welded joint cooling ( $w_{6/5} \leq 10$  °C/s) the HAZ metal develops a structure consisting of bainite and pearlite. At their more intensive cooling characteristic for welding without preheating ( $w_{6/5} \approx 20$  °C/s) and with preheating to 60 °C ( $w_{6/5} \approx 12$  °C/s), the HAZ metal develops a predominantly martensitic structure with a low cold cracking resistance. At the cooling rate of 12 °C/s, it consists of martensite by almost 50 %. Further increase of the intensity of sample cooling up to  $w_{6/5} \geq 12$  °C/s promotes the martensite quantity in the HAZ metal increasing to 80 %. In our opinion, this accounts for the fact that under such welding conditions even in the case, when the diffusible hydrogen concentration in the deposited metal is low ( $\approx 7$  ml/100 g), cracks in the HAZ metal of 35L steel form at stresses not exceeding 150 MPa. At a limited content of diffusible hydrogen in the deposited metal (up to 8 ml/100 g) a high delayed cracking resistance ( $\sigma_{cr} \approx 300$  MPa) is also found in samples, welded at higher modes ( $Q_w \approx 20$  kJ/cm). However, as is known [8], increase of welding heat input promotes an increase of the level of residual stresses in welded joints, so that this technology variant, will, probably, not allow avoiding formation of cold cracks in them.

Diffusible hydrogen has a significant influence on delayed cracking of HAZ metal of 35L steel welded joints. Increase of its concentration in the deposited metal from 8 to 15 ml/100 g leads to a significant lowering of the metal capability to resist cold cracking. Even in welding at increased modes ( $Q_w \approx 20$  kJ/cm) they can form at stresses, the value of which does not exceed 150 MPa. Preheating in these cases is also low-efficient. Sample heating up to the temperature of 100 °C allowed increasing  $\sigma_{cr}$  only up to 200 MPa.

On the whole, the performed research indicates that in order to ensure a high resistance of welded joints of steels of 35L type to cold cracking, it is necessary to lower not only the concentration of diffusible hydrogen in the deposited metal, but also the level of stresses in welded joints.

It is known that in rigidly restrained welded joints with multilayer welds the residual stresses can reach the deposited metal yield point. This is significantly higher than the loads which the HAZ metal of 35L steel can take without fracture. Under such conditions formation of cold cracks in welded joints cannot be avoided. In this connection, quite a lot of research is devoted to the problem of formation of residual stresses in welded joints, influence of various techno-



logical factors on this process and finding the methods for their adjustment. It is also known that the main cause for formation of stresses and strains in welding is a non-uniform widening and narrowing of different sections of the joint, resulting from the action of a concentrated heat source on the metal [9, 10]. Therefore, the problems of a relative lowering of the overall level of residual stresses in welded joints can be solved by adjustment of the heat input or heat removal from the weld zone, conditions of metal heating and cooling, change of the technological processes of welding, etc. [11, 12]. In this case, it appeared rational to study the influence of welding technique on formation of residual welding stresses in thick metal joints.

Investigations were performed using a special technological sample, simulating one of the components of thick-walled structures, where cracks are the most frequent. Such a technological sample (Figure 2) is a massive butt joint reinforced by stiffeners with a V-shaped edge preparation of 500 mm length and 400 mm width. Joint rigidity results from fastening one of its ends by a massive run-off tab and mounting two stiffeners. Such dimensions and design of the technological sample, first, eliminate angular deformation of the sample and influence of other unforeseen factors on the research progress, and, secondly, promote formation in the joints of residual stresses close to those, which form in welding of rigidly fastened item components.

Manual arc welding as one of the metal joining methods the most widely used in repair was accepted as the basic technology for investigations, and high-strength steel of 14KhG2SAFD grade having a high cold cracking susceptibility similar to 35L steel, was accepted as the basic steel. Rolled sheets of 40 mm thickness and the following composition were used, wt. %: 0.13C; 0.57Si; 1.42Mn; 0.44Cr; 0.16Ni; 0.39Cu; 0.08Al; 0.04Ti; 0.01Nb; 0.08V, which have the following mechanical properties:  $\sigma_{0.2} = 635$  MPa;  $\sigma_t = 784$  MPa;  $\delta_5 = 17.8$  %;  $\psi = 59.0$  %.

The root weld was welded by FOX EV 50 electrodes of 3.2 mm diameter in the following mode:  $I_w = 140-150$  A,  $U_a = 24-25$  V,  $v_w = 7-8$  m/h. The groove was filled using ANP-10 electrodes of 4.0 mm diameter in the following welding modes:  $I_w = 160-170$  A,  $U_a = 25-26$  V,  $v_w = 9-10$  m/h. Composition and mechanical properties of the metal deposited with ANP-10 and FOX EV 50 electrodes, are given in the Table. Before welding the electrodes were baked in a furnace at the temperature of 430–450 °C for 2 h, this providing a low concentration of diffusible hydrogen (4.0–4.5 ml/100 g) in the deposited metal, the con-

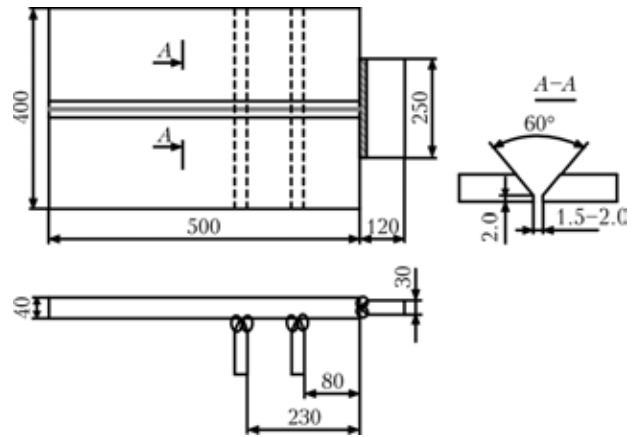


Figure 2. Schematic of a technological sample

tent of which was determined by the chromatographic method [13]. After the individual weld layers were made (all together 14 such layers were made in each joint), the samples were cooled to the ambient temperature, and welding was resumed only after that.

Four technological variants of welding were studied. Sample #1 (basic variant) was welded by the traditional process in the gravity position (Figure 3, a). The second and third samples were conditionally divided into three blocks, each of which had the length of 165 mm. These blocks were welded one by one in succession in the direction from the rigidly restrained base of the joint towards its relatively free top (Figure 3, b). The main difference between these joints consisted in that sample #3 was made with weld peening, and sample #2 without it. Sample #4 was conditionally divided into two blocks of 335 and 165 mm length, its welding was performed in keeping with the schematic given in Figure 3, c.

Two batches of technological samples were made for each of the above technological variants of welding. One batch of samples was used for evaluation of the stressed state of welded joints, the second --- for evaluation of their delayed cracking resistance. Residual stresses in welded joints were determined at the start, in the mid-section and at the end of welds by the method of mechanical strain gauging. For this purpose, special rosettes with 17 mm distance between the holes were prepared on the sample surface.

Investigations, the results of which are given in Figure 4, indicated that the stressed state of welded joints depends on the welding technique and sequence of block welding up. The highest transverse and longitudinal stresses ( $\sigma_y = 500-590$  MPa,  $\sigma_x = 750-760$  MPa) form in samples welded in the gravity position (sample #1). They are much lower ( $\sigma_y \leq$

Composition and mechanical properties of metal deposited with electrodes of ANP-10 and FOX EV 50 grades

Electrode grade	Composition, wt. %					Mechanical properties (not less than)		
	C	Mn	Si	S	P	$\sigma_t$ , MPa	$\delta_5$ , %	$KCV_{+20}$ , J/cm <sup>2</sup>
ANP-10	0.11	1.8	0.5	0.020	≤ 0.023	760	18	120
FOX EV 50	0.07	1.1	0.5	0.009	0.012	590	30	220

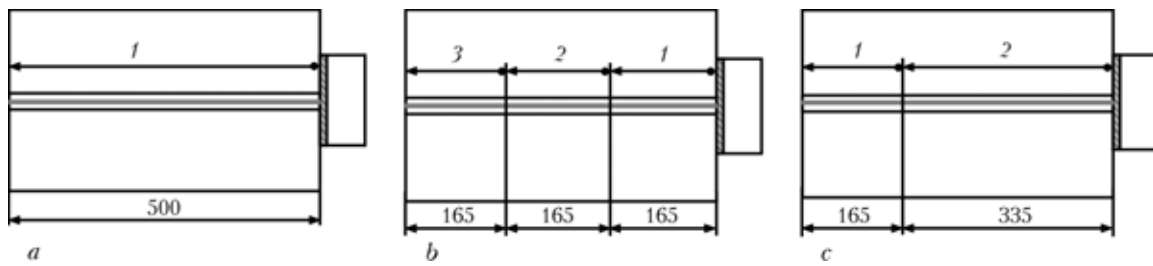


Figure 3. Schematic of the sequence of welding the technological samples #1 (a), 2 and 3 (b), 4 (c)

$\leq 250$  MPa,  $\sigma_x = 500$ –560 MPa) in joint #3 welded by the block method with layer-by-layer weld peening.

Rather close in value transverse stresses ( $\sigma_y = 350$ –400 MPa) were recorded at the start and in the middle of joints #2 and 4, but they are distributed in a different way along the sample length. In technological sample #4 welded in the direction from the sample unrestrained end to the rigidly restrained part of the joint, transverse stresses are rather uniformly distributed along the weld. In the case when the sequence of block welding up was changed, and welding was started from the rigidly restrained end of the sample (sample #2), not more than 300 MPa stresses form from the opposite, less restrained side of the joint. Longitudinal stresses in such joints are lower than in sample #1, but they are still quite high and non-uniformly distributed along the sample length. The highest stresses ( $\sigma_x = 630$ –680 MPa) in technological sample #4 were formed at the start and end of the weld and were somewhat lower ( $\sigma_x \approx 550$  MPa) in its middle part. In sample #2 the longitudinal stresses rise monotonically from 530 (weld start) up to 670 MPa at its end. Such a nature of residual stress distribution in the above technological samples is, obviously, related both to the features of sample fastening and to the change of welding direction and sequence of block welding up. It should be noted that from the view point of cold crack formation in welded joints with multilayer welds the most unfavourable stressed state developed in sample #1.

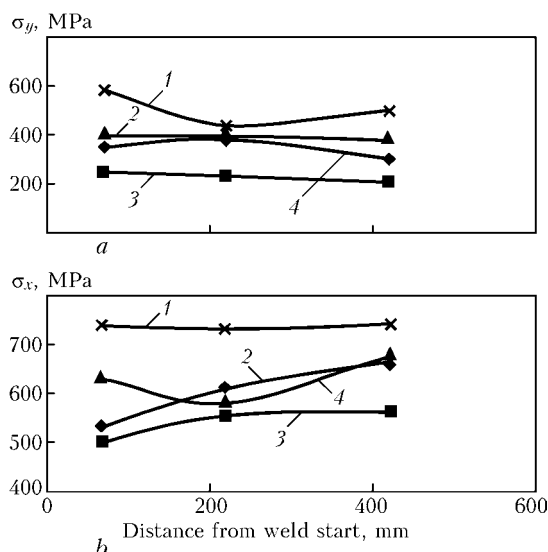
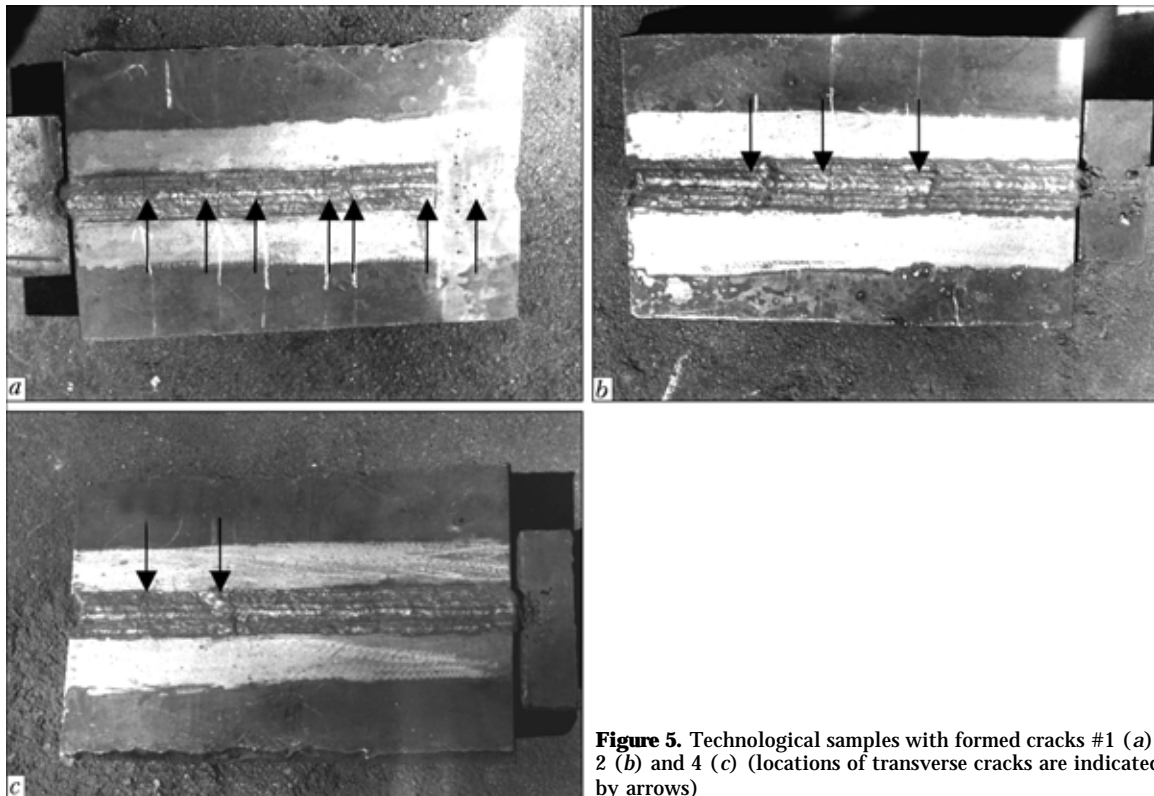


Figure 4. Distribution of transverse (a) and longitudinal (b) stresses in weld metal of technological sample #1 (1), 2 (2), 3 (3) and 4 (4)

Layer-by-layer peening of welds had a significant influence on stress formation in the welded joints (sample #3). As shown by investigations, application of this technique may allow reducing the level of residual welding stresses in such joints relative to the reference welding sample (#1) almost 2.5 times, and relative to sample #2, which was welded in the same sequence, but not peened, 1.4–1.6 times. Weld peening had a less pronounced, but still positive effect also on formation of longitudinal stresses. They decreased by 40–50 % relative to the basic sample. Different influence of peening on the change of the conditions of formation of the longitudinal and transverse stresses is, obviously, related to the features of metal deformation in the longitudinal (section length of 165 mm) and transverse (width of 10–40 mm) directions relative to weld axis. It may be assumed that the combination of the two techniques (block welding and weld peening) may have a positive influence on cold cracking resistance of thick-walled welded joints. This was also confirmed by subsequent studies.

Cold cracking resistance of welded joints was assessed using the same samples, as for investigation of their stressed state. The difference between them consisted only in formation of the weld root layer. In this case, it was made so that a stress raiser in the form of a lack-of-penetration formed in the joint. During welding of the joints, the results of testing which were used to assess the cold cracking resistance of the technological samples, and for some time after welding was over, the samples were controlled by several methods. In welding and during the first two days after it, the welded joint behaviour was controlled by the method of acoustic emission [14], and then for the next 40 days visually and every five days by the dye-penetrant method. Portable permanent-magnet magnetizing device of MAGEKS-1 grade and concentrate of magnetic suspension DIAGMA-1100 were used for these purposes. If cracks in the welded joints were not visually observed, the final conclusion about the cracking resistance of the technological samples was made by the results of metallographic investigations of the macrosections. Sections in the quantity of 12 pcs were cut out in the transverse and longitudinal directions relative to the weld axis, four samples each from the start, middle and end of the sample.

Observation of development of acoustic signals showed that during the first two days no cracking was found in any of the above welded joints. The first cracks which formed in technological samples #1, 2 and 4 were detected much later. First the transverse



**Figure 5.** Technological samples with formed cracks #1 (a), 2 (b) and 4 (c) (locations of transverse cracks are indicated by arrows)

cracks were found in sample #1 welded in the gravity position. The first four cracks on the surface of welds of this joint were detected only 7 days after completion of welding. After five more days their total amount reached seven. In this technological sample the cracks formed uniformly along the entire sample length, and affected solely the weld (Figure 5, a).

Ten days after welding cracks were detected in samples #2 and 4. Unlike joint #1 their quantity was much smaller — three and two, respectively (Figure 5, b, c). Less intensive nature of development of cracks in these welded joints is related, probably, to a more favourable (smaller) than in technological sample #1 formation of stresses. Note the fact that in sample #2 two out of three cracks, and in sample #4 one out of two crack formed in the section of joining blocks, in which weld craters are located. These are known to be exactly the weld sections the most prone to cold and hot microcrack formation. Further on such microcracks may initiate development of transverse cracks. This circumstance should be taken into account in development of the technological process of welding and care should be taken to ensure thorough grinding out of these weld sections.

Further research showed that the highest delayed cracking resistance is found in joints made by the block method with layer-by-layer weld peening (sample #3). Cracks in samples welded by this technology were not found even 40 days after welding. Results of metallographic studies confirmed the fact of the absence of cracks in this sample. In our opinion, absence of cold cracks in joint #3 can be attributed to at least two factors — lowering of the overall level of residual stresses in this sample and refinement of

the weld metal structure, which occurred at peening. As is known, the metal, which at all other conditions being equal, has a lower grain point offers better resistance to brittle fracture [15]. It is also possible that peening resulted in elimination of local peak stresses in the weld metal, occurring in the welded joints [16].

On the whole the results of the conducted investigations are indicative of the fact that cold crack formation in the joints of hardenable steels with multilayer welds greatly depends on the level of residual stresses, which form during welding. This is confirmed by the universally accepted opinion about the need to find ways for lowering them. Among the considered techniques, the stresses are lowered in the most effective manner as a result of weld peening and conducting the process by the block technique with breaking up of the joints into short sections (up to 200 mm). Use of a technology based on these principles allowed us eliminating the possibility of crack formation in rigidly-restrained welded joints of 14KhG2SAFD steel even in welding without preheating.

Undoubtedly, conditions of welding thick metal in practice can differ essentially from those reproduced by us when studying the technological samples under the laboratory conditions, and, therefore, preheating as a technological operation, should not be eliminated. On the other hand, the data of the performed research show that it can be significantly reduced. This is also indicated by our experience, gained in repair of basic components of crushers made of cast steel 25L and 35L 80–100 mm thick.

Welding technology developed with the direct participation of specialists of the E.O. Paton Electric Welding Institute at OJSC «Karelsky Okatysh» from



2003 till 2004 was used to perform restoration repair of eight beds of KKD, KSD and KMD crushers. In terms of technology the repair process included the following operations:

- determination by the nondestructive testing methods of the extent and depth of crack location;
- cutting out the cracks and edge preparation for welding;
- quality control of surfaces of the metal to be joined prepared for welding;
- preheating (80–100 °C);
- welding of the joints;
- work on lowering of the level of residual stresses in welded joints (layer-by-layer peening of welds);
- removal of weld metal reinforcement with ensuring its smooth transition to the base metal;
- quality control of welded joints.

At present the above equipment is operating in the design mode. Costs of crusher restoration were not higher than 25 % of the bed initial cost.

In conclusion it should be noted that the conducted research and gained experience of reconditioning operation allow an optimistic estimate of the role of technological methods of improvement of the delayed cracking resistance of cast hardenable steels.

1. Maccocaire, C. (1991) Repair welding: how to set up a shop. *Welding J.*, **8**, 54–56.
2. Ye Dong-lin, Yongfu He, Rangez Zhang et al. (1982) A study on cracks on the oxygas cut surfaces of weld grooves of 14MnMoVN steel plates during cold forming. *Transact. of China Welding Inst.*, **4**, 159–164.
3. Larionov, V.P. (1986) *Electric arc welding of structures in northern version*. Novosibirsk: Nauka.
4. Volkov, A.S. (1974) Causes of appearance of defects near the repaired zones of welds. *Svaroch. Proizvodstvo*, **8**, 33–34.
5. Irving, R.R. (1980) Can industry afford the high cost of weld repair? *Iron Age*, **3**, 49–55.
6. Makarov, E.L. (1981) *Cold cracks in welding of alloy steels*. Moscow: Mashinostroenie.
7. Shorshorov, M.Kh., Belov, V.V. (1972) *Phase transformations and change of properties of steel in welding*: Atlas. Moscow: Nauka.
8. Korolkov, P.M., Dikun, V.N. (1993) Influence of technological welding processes and volume heat treatment on welding stress level in spherical vessels for liquid ammonia. *Montazh i Spets. Raboty v Stroitelstve*, **8**, 24–26.
9. Vinokurov, V.A., Grigoriants, A.G. (1984) *Theory of welding strains and stresses*. Moscow: Mashinostroenie.
10. Trochun, I.P. (1964) *Internal forces and deformations in welding*. Moscow: Mashgiz.
11. Berezhnitska, M.P. (2001) Methods of determination of residual stresses and their relaxation. *Fiziko-Khim. Mekhanika Materialiv*, **6**, 69–74.
12. Makhnenko, V.I. (1976) *Computational methods for investigation of kinetics of welding stresses and strains*. Kiev: Naukova Dumka.
13. Pokhodnya, I.K., Paltsevich, A.P. (1980) Chromatographic method for determination of diffusion hydrogen in welds. *Avtomatch. Svarka*, **1**, 37–39.
14. Musiyachenko, V.F., Zhdanov, S.L. (1987) Application of acoustic emission method for investigation of cold cracking process in high-strength steel welded joint. *Diagnostika i Prognoz. Razrusheniya Sv. Konstruktsij*, Issue 5, 73–77.
15. Lazko, V.E., Borisov, M.T., Kovalchuk, V.D. et al. (1977) Effect of cerium on delayed fracture of high-strength weld metal. *Avtomatch. Svarka*, **2**, 27–29.
16. Sarak, V.I., Suvorova, S.O., Filippov, G.A. (1974) About internal microstresses resulting from martensite transformation in steel. *Metallofizika*, **54**, 94–97.

## COMPUTERISED SYSTEM FOR HIGH-FREQUENCY PEENING OF WELDED JOINTS

High-frequency peening (HFP) was developed from the technologies of plastic surface deformation (surface cold working) of metals. Plastic surface deformation of metal in HFP is achieved through affecting the surface to be treated by the shock pulses exerted by deforming elements of the tool and formed by the ultrasonic generator. In HFP only the weld to base metal fusion zone 4–7 mm wide is subjected to plastic deformation. HFP leads to a 8–10 times extension in cyclic life and a 30–200 % increase in fatigue limit on a base of  $2 \cdot 10^6$  stress alteration cycles, depending upon the cyclic loading conditions (cycle asymmetry), main mechanical properties of the material treated, stress concentration, shape of the joint, residual stresses and other factors. To ensure maximal increase in fatigue resistance of different types of welded joints, the optimal parameters of strengthening are determined and set using special software. The HFP process flow diagram was developed to increase fatigue resistance of welded joints in members of load-carrying structures.



**Purpose.** Increase in fatigue resistance of weldments in metal structures during their fabrication and operation.

**Application.** Ship building, bridge construction, aircraft engineering, heavy engineering.

General view of computerised HFP system

Contacts: Kirian V.I.

E-mail: office@paton.kiev.ua; kiryan@svitonline.com



# CALCULATION-EXPERIMENTAL EVALUATION OF THE EFFICIENCY OF ALLOYING THE HIGH-ALLOY DEPOSITED METAL WITH PHOSPHORUS

I.I. RYABTSEV

E.O. Paton Electric Welding Institute, NASU, Kiev, Ukraine

The probability of formation of phosphides of some alloying elements (V, Mo, Cr, Mn, Co, W, Al, Fe, Ni, Si) was determined by using thermodynamic calculations. As shown by examinations of microstructure of metal deposited with flux-cored wires, which contain phosphorus, vanadium and phosphorus, molybdenum and phosphorus, and titanium and phosphorus, all of the above alloying elements lead to spheroidisation of phosphide inclusions, which makes promising the use of phosphorus as an alloying element for high-alloy surfacing consumables.

*Keywords:* arc surfacing, deposited metal, tool steel, phosphorus, phosphides, phosphide eutectics, thermodynamic calculations, prospects

As shown in studies [1–4], phosphorus can be used to advantage as an alloying element to improve tribological properties of deposited metal of the type of low-alloy steels. Investigations were carried out on the basis of the available experience to study the possibility of alloying the deposited metal of the type of tool steels, having the Fe–Si–Mn–W–Cr–V, Fe–Si–Mn–Cr–Mo–V–Ni and Fe–Si–Mn–Cr–Mo–V–W alloying systems, with phosphorus. It was established [4] that the key problem in this case consists in a decreased crack resistance of the deposited metal at its phosphorus content of over 1.2 wt.%. The cause of cracking is a continuous network of the phosphide eutectic formed along the grain boundaries, which is characterised by increased hardness and brittleness.

It is a known fact that phosphorus can dissolve in iron and, at the same time, form inclusions of the phosphide phase in the form of compact phosphides or phosphide eutectics [5]. In unalloyed steels, phosphorus forms low-melting point brittle phosphide eutectics of the type of FeP–Fe<sub>3</sub>P. In high-alloy steels, some alloying elements may form refractory phosphides, such as TiP (melting point --- 1962 °C), Ti<sub>2</sub>P (1895 °C), CrP (1575 °C), Cr<sub>3</sub>P (1482 °C) and Co<sub>2</sub>P (1361 °C) [6]. To improve crack resistance and some other service properties of the deposited metal, it is necessary to alloy it and fix phosphorus to form more refractory phosphides, which are the first to precipitate and have a compact shape in solidification of the deposited metal.

The probability of formation of these or those phosphides in simultaneous alloying the deposited metal with several elements can be evaluated by using thermodynamic calculations of equilibrium of chemical reactions leading to their formation. Such calculations make it possible to conduct theoretical analysis of different technological processes by avoiding complex and expensive experiments [7].

The entropy method was chosen to calculate isobaric potentials of the reactions of formation of alloying element phosphides. With this method the calculations are relatively simple and sufficiently reliable, providing the data on thermodynamic characteristics of initial components and reaction products are available. Isobaric potentials of the reactions of formation of phosphides were calculated using the following equation taken from study [7]:

$$\Delta Z_T^0 = \Delta H_{298}^0 - T\Delta S_{298}^0.$$

To make calculations by using the above formula, it is necessary to know enthalpy  $\Delta H_{298}^0$  of the formation of phosphides of alloying elements and difference  $\Delta S_{298}^0$  between the values of absolute entropies of initial elements and formed phosphides.

Isobaric potentials of the reactions of formation of phosphides were calculated at room temperature and at a temperature of the weld pool (Table 1). According to the data by Frumin I.I. [8], in submerged-arc welding of low-carbon steel using flux AN-348A, mean temperature  $T$  of the weld pool is (1770±100) °C, or 2043 K (rounded to 2050 K).

The calculated values of isobaric potentials of the formation of phosphides, obtained at two different temperatures, were plotted in the diagram (Figure 1). Plotting of several straight lines for reactions in the diagram makes it possible to estimate the direction of a reaction of formation of different phosphides, as well as the value of an isobaric potential of each of them, and, by comparison, find the favourable thermodynamic conditions for them to occur, as well as a higher or lower stability of the formed products of a corresponding reaction.

Among the alloying elements used for tool steels, it is the formation of phosphides of vanadium, molybdenum and chromium that is most probable in terms of thermodynamics. Isobaric potentials of the reactions of formation phosphides of tungsten and cobalt, which are also used to alloy tool steels, are at a level of isobaric potentials of the reactions of formation of iron phosphides, and their formation in the deposited

**Table 1.** Entropies  $S_{298}^0$  of alloying elements [9], entropies  $S_{298}^0$  and enthalpies  $\Delta H_{298}^0$  of their phosphides [6, 10–13], and isobaric potentials  $\Delta Z_T^0$  of reactions of formation of phosphides at 298 and 2050 K

Chemical element	$S_{298}^0$ of alloying elements, J/(mol·K)	Phosphide	$S_{298}^0$ of phosphides, J/(mol·K)	$\Delta S_{298}^0$ , J/(mol·K)	$\Delta H_{298}^0$ , kJ/mol	$\Delta Z_T^0$ , kJ/(g·mol), at temperature, K	
						298	2050
Al	28.33	AlP	47.28	-22.14	-164	-157.40	-118.60
Mn	32.01	<b>MnP</b>	<b>49.16</b>	<b>-23.94</b>	<b>-186</b>	<b>-178.86</b>	<b>-136.92</b>
		Mn <sub>2</sub> P	76.98	-28.13	-172	-163.62	-114.33
		Mn <sub>3</sub> P	104.52	-32.60	-181	-170.27	-114.20
Si	18.83	SiP	32.64	-27.28	-69	-60.87	-13.076
Fe	27.28	Fe <sub>2</sub> P	72.38	-23.27	-147	-140.07	-99.30
		<b>Fe<sub>3</sub>P</b>	<b>101.67</b>	<b>-21.26</b>	<b>-162</b>	<b>-155.66</b>	<b>-118.42</b>
Cr	23.47	CrP	39.74	-24.82	-168	-160.60	-117.12
		<b>Cr<sub>3</sub>P</b>	<b>87.88</b>	<b>-23.62</b>	<b>-252</b>	<b>-244.96</b>	<b>-203.58</b>
V	28.91	V <sub>2</sub> P	33.25	-65.66	-327	-307.44	-192.40
Ni	29.87	NiP	93.12	+22.16	-108	-114.60	-153.43
Co	30.04	<b>Co<sub>2</sub>P</b>	<b>77.40</b>	<b>-23.77</b>	<b>-174</b>	<b>-166.92</b>	<b>-125.27</b>
		CoP	50.21	-20.92	-158	-151.77	-115.11
Mo	28.66	Mo <sub>2</sub> P	90.45	-7.96	-255	-252.63	-238.68
W	32.64	WP	52.41	-21.32	-172	-165.65	-128.29
P	41.09	----	--	--	--	--	--

Note. In the case of formation of two or three phosphides of the same alloying element, shown in bold type are the most probable products of their formation.

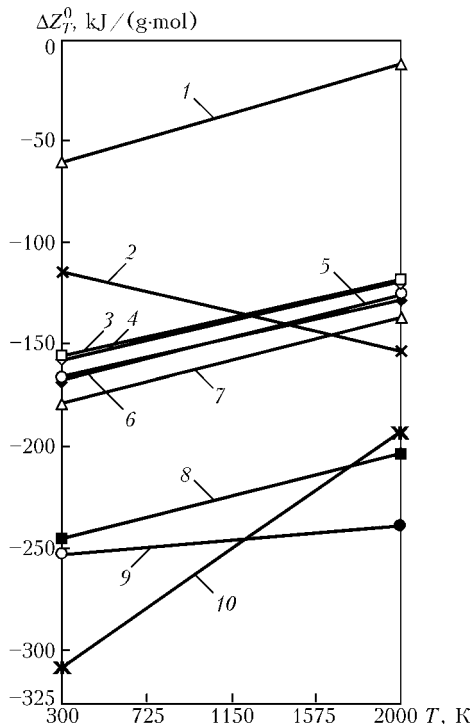


**Figure 1.** Isobaric potentials of reactions of formation of phosphides of alloying elements: 1 — SiP; 2 — NiP; 3 — Fe<sub>3</sub>P; 4 — AlP; 5 — Co<sub>2</sub>P; 6 — WP; 7 — MnP; 8 — Cr<sub>3</sub>P; 9 — Mo<sub>2</sub>P; 10 — V<sub>2</sub>P

metal is less probable in terms of thermodynamics, although, like iron, they may be contained in phosphides, the formation of which is thermodynamically more probable.

Experimental flux-cored wires 2 mm in diameter were (Table 2) made for evaluation of the effect of the strongest phosphide-forming elements on the morphology of the phosphide phase in the deposited metal. The wires were alloyed only with phosphorus, with vanadium and phosphorus, molybdenum and phosphorus, and titanium and phosphorus. Although we did not find in literature any comprehensive data on thermodynamic characteristics of titanium, we chose it for the investigations as an element that forms the most refractory phosphides [6]. Such phosphides should be the first to precipitate in solidification of the weld pool. And although titanium is rarely used for alloying the deposited metal in compositions close in type to tool steels, it is by all means added to the charge of self-shielding flux-cored wires to deoxidise this type of metal.

The calculated content of phosphorus in the experimental wires was 1 and 2 wt.%. According to the data of [5], solubility of phosphorus in pure iron is 1 %, and no network of grain-boundary phosphide eutectics should be formed at this content of phosphorus.

**Table 2.** Chemical composition (wt.%) of metal deposited with experimental flux-cored wires

Wire grade	C	Mn	Si	P	Ti	Mo	V
PP-Np-GSP	0.11	0.81	0.92	0.89	--	--	--
PP-Np-P2GS	0.13	0.67	0.83	1.86	--	--	--
PP-Np-M6GSP	0.14	0.79	0.86	0.97	--	5.63	--
PP-Np-M12P2GS	0.11	0.71	0.96	1.77	--	11.26	--
PP-Np-T3GSP	0.12	0.90	1.01	0.82	2.56	--	--
PP-Np-T6P2GS	0.15	0.87	0.89	1.73	4.81	--	--
PP-Np-F4GSP	0.13	0.91	0.94	0.96	--	--	3.70
PP-Np-F8P2GS	0.12	0.83	0.90	1.82	--	--	6.35

Based on the stoichiometric ratio of elements in phosphides  $V_2P$  (about 3.3:1),  $Mo_2P$  (about 6:1) and  $Ti_2P$  (about (3:1)), the calculated content of corresponding alloying elements was selected so that theoretically all phosphorus is fixed to form the above phosphides.

Five-layer submerged-arc deposition of beads on plates of steel St3 was performed by using flux AN-26 under the following conditions: deposition current 220–250 A, arc voltage 22–24 V, and deposition speed 30 m/h. As shown by visual examinations, all the beads, except that deposited with wire PP-Np-P2GS, were crack-free. Specimens were cut out from upper layers of the deposited beads to examine their microstructure\*.

Unalloyed deposited metal 20GSP and 20P2GS, containing only phosphorus, had ferritic structure (Figure 2, a, b). Microhardness of ferrite was  $HV0.05$  244–303. At a phosphorus content of about 1 wt.%, isolated inclusions of the phosphide eutectic appeared in structure of the deposited metal (Figure 2, a). With the phosphorus content increased to 1.89 wt.%, the eutectic formed a continuous network along the grain boundaries (Figure 2, b). Microhardness of the phosphide eutectic was  $HV0.05$  321–412.

The addition of molybdenum did not change the matrix structure of deposited metals 20M6GSP and 20M12P2GS, i.e. it remained ferritic (Figure 2, c, d). Its microhardness did not practically change either ( $HV0.05$  221–303). At a molybdenum content of about 6 wt.% and phosphorus content of about 1 wt.%, deposited metal 20M6GSP contained no inclusions of the phosphide eutectics (Figure 2, c). With the phosphorus content increased to 2 wt.%, isolated inclusions of the phosphide eutectic appeared in deposited metal 20M12P2GS. However, they did not form a continuous grain-boundary network (Figure 2, d). Microhardness of the phosphide eutectic was  $HV0.05$  412. Alloying the deposited metal with molybdenum promoted globulisation of phosphides with a much high microhardness ( $HV0.05$  606–824).

Ferritic-pearlitic structure with a negligible amount of very fine inclusions was formed in deposited

metal 20F4GSP (Figure 2, e). Microhardness of the matrix was  $HV0.05$  232–250. Increase in the content of vanadium and phosphorus led to a dramatic change in structure of deposited metal 20F8P2GS, and to decrease in volume content of the pearlitic component (Figure 2, f). Microhardness of the matrix increased to  $HV0.05$  303–321. A large amount of very fine phosphide inclusions formed in the bulk of grains. Because of their small size, it was impossible to measure microhardness of both types of the deposited metal.

Deposited metal 20T3GSP had a ferritic-pearlitic structure with phosphide and phosphide eutectic inclusions (Figure 2, g). Microhardness of ferrite was  $HV0.05$  286–303, and that of the pearlitic component was  $HV0.05$  271–286. The eutectic and compact phosphide inclusions were located inside the pearlitic colonies. Microhardness of phosphides amounted to  $HV0.05$  644. And microstructure of deposited metal 20T6P2GS was mostly ferritic, the grain size ranging from 6 to 9 (Figure 2, h). Microhardness of the matrix was a bit higher than that of deposited metal 20T3GSP ( $HV0.05$  391–412). Many fine inclusions with microhardness of  $HV0.05$  554 were found in the bulk of grains.

Therefore, examinations of microstructure of different types of the deposited metal showed that all the three alloying elements (molybdenum, vanadium and titanium) formed compact phosphide inclusions with a shape close to spherical. Such inclusions should promote improvement of crack resistance of the deposited metal, which makes it possible to use phosphorus in surfacing consumables alloyed with these elements.

The effect of phosphorus on crack resistance of the high-alloy deposited metal was evaluated by using three experimental flux-cored wires (PP-Np-35V9Kh3GSF, PP-AN132 and PP-AN147) developed by the E.O. Paton Electric Welding Institute for surfacing of tools operating under conditions of hot deformation of metal. These wires provide the deposited metal of the type of tool steels with the Fe–Si–Mn–W–Cr–V, Fe–Si–Mn–Cr–Mo–V–Ni and Fe–Si–Mn–

\* Examinations of microstructure of the deposited metal were completed by Dr. D.P. Novikova and Eng. I.L. Bogachuk.

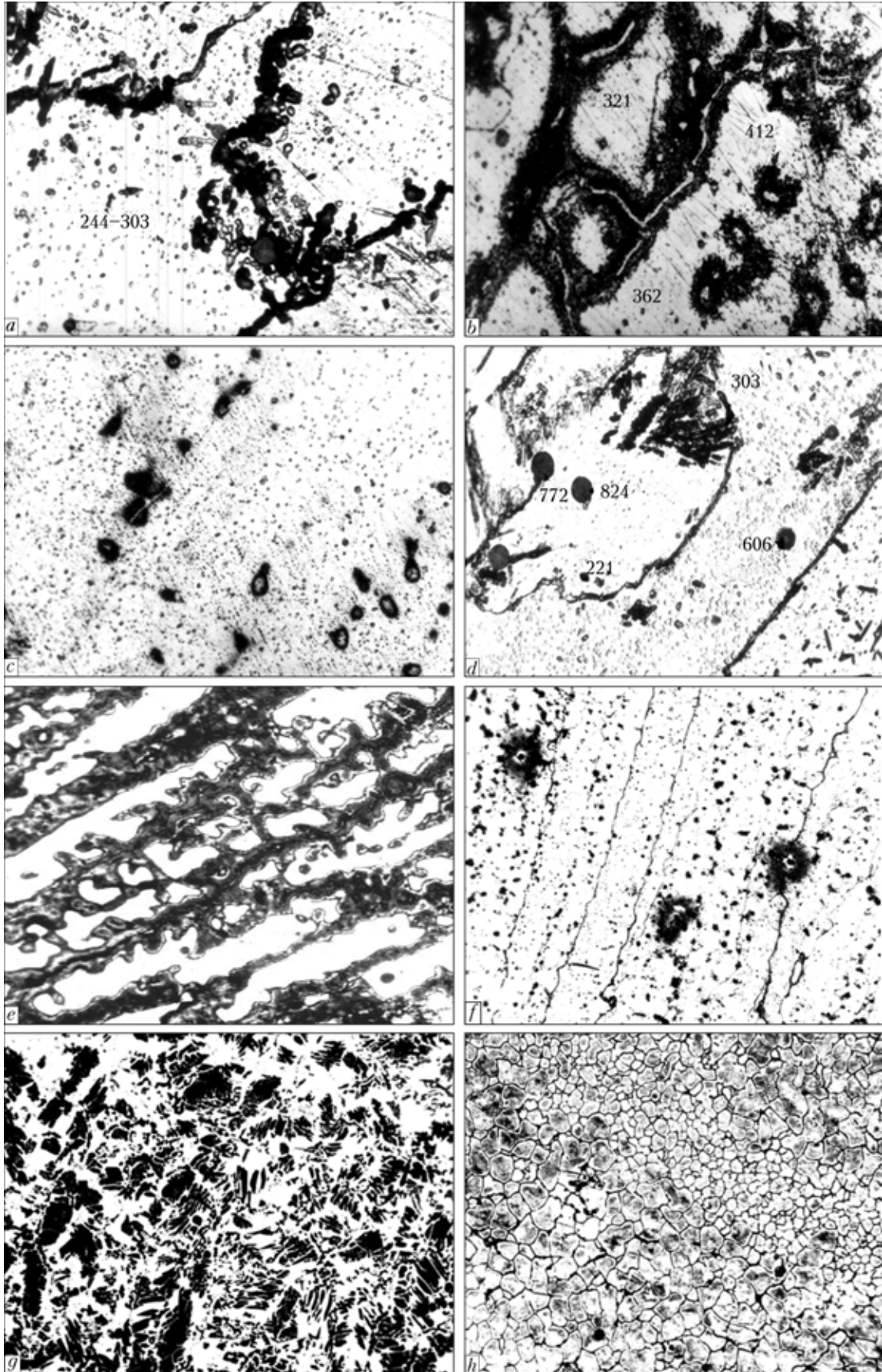


**Figure 2.** Microstructure of deposited metal of the type of 20GSP (a), 20P2GS (b), 20M6GSP (c), 20M12P2GS (d), 20F4GSP (e), 20F8P2GS (f), 20T3GSP (g) and 20T6P2GS (h) ( $\times 500$ )



Cr–Mo–V–W alloying systems. 1.5 wt % P was additionally introduced into the charge of each flux-cored wire, which provided high wear resistance of the deposited metal [3].

Four-layer isolated beads of the type of the restraint test specimens in the form of a cylindrical sample of steel 30Kh, 220 mm in diameter, were deposited by the submerged-arc surfacing method using three experimental flux-cored wires and flux AN-26 (Figure 3). Surfacing was performed without preheating under the following conditions: arc voltage 30–32 V, surfacing current 280–320 A, and surfacing speed 25 m/h. After surfacing, the sample was subjected to slow cooling under the flux layer. As shown by visual examinations, the deposited beads after cooling exhibited a good formation, and deposited metals of the above three types were crack-free.

## CONCLUSIONS

1. The probability of formation of phosphides in simultaneous alloying the deposited metal with several alloying elements (V, Mo, Cr, Mn, Co, W, Al, Fe, Ni, Si) was determined by means of thermodynamic calculations of isobaric potentials of the reactions of formation of phosphides.

2. Results of examinations of microstructure of metal deposited with the experimental flux-cored wires containing only phosphorus, vanadium and phosphorus, molybdenum and phosphorus, and titanium and phosphorus, showed that all the three alloying elements promote formation of phosphide inclusions of a spherical shape, the presence of which does not decrease crack resistance of the deposited metal.

1. Kuskov, Yu.M., Ryabtsev, I.I., Doroshenko, L.K. et al. (2002) Peculiarities of melting and solidification of 20KhGS type deposited metal alloyed with phosphorus. *The Paton Welding J.*, **8**, 21–24.
2. Ryabtsev, I.I., Kuskov, Yu.M. (2003) Prospects for applying phosphorus in iron-base surfacing consumables (Review). *Ibid.*, **1**, 12–16.
3. Ryabtsev, I.I., Kuskov, Yu.M., Grabin, V.F. et al. (2003) Tribological properties of the Fe–Cr–Si–Mn–P system deposited metal. *Ibid.*, **6**, 16–20.
4. Ryabtsev, I.I., Kuskov, Yu.M., Novikova, D.P. (2006) Effect of phosphorus on crack resistance of low-carbon depos-

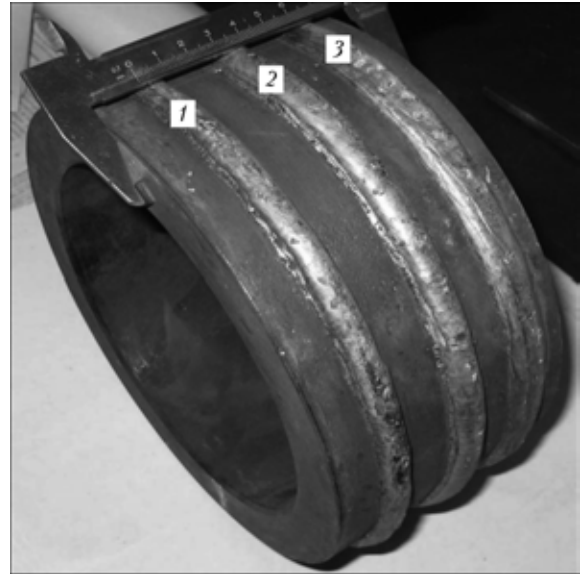


**Figure 3.** Appearance of cylindrical sample of steel 30Kh surfaced with experimental flux-cored wires: 1 — PP-Np-35V9Kh3SF; 2 — PP-AN132; 3 — PP-AN147

- ited metal of Fe–Mn–Si–Cr alloying system. *Ibid.*, **5**, 12–15.
5. Lunev, V.V., Averin, V.V. (1988) *Sulphur and phosphorus in steel*. Moscow: Metallurgiya.
6. Gordienko, S.P. (1987) *Thermodynamic characteristics of hard binary phosphides*: Preprint 15 of Institute of Problems of Materials Science. Kiev.
7. Vladimirov, L.P. (1970) *Thermodynamic calculations of equilibrium of metallurgical reactions*. Moscow: Metallurgiya.
8. Frumin, I.I. (1961) *Automatic electric arc surfacing*. Kharkov: Metallurgizdat.
9. [www.qivx.com/ispt/elements/ptw-022.php](http://www.qivx.com/ispt/elements/ptw-022.php), [ptw-040.php](http://www.qivx.com/ispt/elements/ptw-040.php), [ptw-023.php](http://www.qivx.com/ispt/elements/ptw-023.php), [ptw-041.php](http://www.qivx.com/ispt/elements/ptw-041.php), [ptw-042.php](http://www.qivx.com/ispt/elements/ptw-042.php), [ptw-074.php](http://www.qivx.com/ispt/elements/ptw-074.php), [ptw-024.php](http://www.qivx.com/ispt/elements/ptw-024.php), [ptw-025.php](http://www.qivx.com/ispt/elements/ptw-025.php), [ptw-026.php](http://www.qivx.com/ispt/elements/ptw-026.php), [ptw-029.php](http://www.qivx.com/ispt/elements/ptw-029.php), [ptw-027.php](http://www.qivx.com/ispt/elements/ptw-027.php), [ptw-028.php](http://www.qivx.com/ispt/elements/ptw-028.php), [ptw-013.php](http://www.qivx.com/ispt/elements/ptw-013.php), [ptw-014.php](http://www.qivx.com/ispt/elements/ptw-014.php), [ptw-015.php](http://www.qivx.com/ispt/elements/ptw-015.php), [ptw-016.php](http://www.qivx.com/ispt/elements/ptw-016.php)
10. Muchnik, S.V. (1982) *Study of interaction of transition metals with phosphorus under burning conditions*: Syn. of Thesis for Cand. of Chem. Sci. Degree. Kiev.
11. Mayers, C.E., Conti, T.J. (1985) Vaporization behavior, phase equilibria and thermodynamic stabilities of nickel phosphides. *J. Electrochem. Soc.*, **132**(2), 454–457.
12. Schlesinger, M. (2002) The thermodynamic properties of phosphorus and solid binary phosphides. *Chemical Rev.*, **102**(11), 4267–4302.
13. Niessen, A.K., de Boer, F.R. (1981) The enthalpy of formation of solid borides, carbides, nitrides, silicides and phosphides of transition and noble metals. *J. Less-Common Metals*, **82**(1), 75–80.



# PECULIARITIES OF PLASTIC DEFORMATION OF NEAR-WELD ZONE METAL IN EXPLOSION WELDING ACCORDING TO SCHEME OF DOUBLE-SIDED SYMMETRICAL CLADDING

S.V. KUZMIN, V.A. CHUVICHILOV and V.I. LYSAK  
Volgograd State Technical University, Volgograd, Russia

Results of analysis of strain-time conditions in formation of joints and plastic deformation of the near-contact metal layers in explosion welding of metal according to different collision schemes are presented.

**Keywords:** explosion welding, plane-parallel and battery schemes of welding, welded joints, boundary-adjacent volumes of metal, plastic deformation of metal

One of the factors, determining formation of a joint in explosion welding, is intensive common plastic deformation of the metal of colliding plates. Investigations of authors of [1–8] allowed detecting and generalizing main regularities of the metal plastic deformation in a near-weld zone (NWZ) in welding of similar and dissimilar materials, whereby majority of the experimental data were obtained when using asymmetrical plane-parallel scheme of collision (Figure 1, a).

At the same time, taking into account recently obtained experimental results that prove increase of the volume of the involved into plastic deformation metal in welding according to the scheme of double-sided symmetrical cladding (hereinafter the battery scheme) due to increase of the deforming pressure pulse in the collision zone [8, 9], of a significant scientific and practical interest is investigation of peculiarities of the NWZ metal plastic flow in such scheme of welding.

The goal of this work was investigation of regularities and peculiarities of plastic deformation of the

boundary-adjacent volumes of metal under conditions of explosion welding according to the battery scheme.

For achievement of the set goal, a series of comparative experiments in explosion welding of two- and three-layer aluminium specimens according respectively to traditional plane-parallel and battery schemes were carried out (Figure 1) with construction according to results of each experiment of the diagrams of the residual shear plastic deformations  $g_{\max}$ , registered in the target plates. For this purpose special windows-wells were milled in the latter, into which a lamellar model insert was placed (see Figure 1), made from a preliminarily breathed rolled aluminium foil of 0.025–0.030 mm thickness.

Two series of the experiments were carried out --- for plane-parallel (thickness of layers was 4 + (2 + 16) mm) and battery (4 + (2 + 16) + 4 mm) schemes of welding. Speed of the contact  $v_c$  for two series corresponded to 2400 m/s; speed of collision  $v_{\text{col}}$  for first series was 220, for second series --- 370 m/s. After explosion welding of experimental specimens microsections of the joint zone were made that included the lamellar insert. Digital photography of polished and etched surfaces of the microsections was made on the Carl Zeiss Axiovert 40 ( $\times 200$ ) microscope. For construction of diagrams of maximal shear strains a special EWD 1.0 program was used [2] that allowed automating process of construction of the dependences  $g_{\max} = f(y)$ .

Parameters of the welding were selected in such way that residual pressure of the detonation products  $p_{d,p}$  of the explosive was certainly higher than dynamic yield strength  $\sigma_y^d$  of the metal both at the instant of collision of the plates and in a certain time, which ensured in welding of two-layer specimens arrival into the joint zone of the stress relief wave, first of all on the side of the target plate. This condition was fulfilled at small values of the relative welding gap  $h/H$  of about 0.05–0.07.

Analysis of the NWZ configuration of welded specimens, produced according to both schemes of cladding in two series of the experiments, showed that within the whole range of the target plate thicknesses

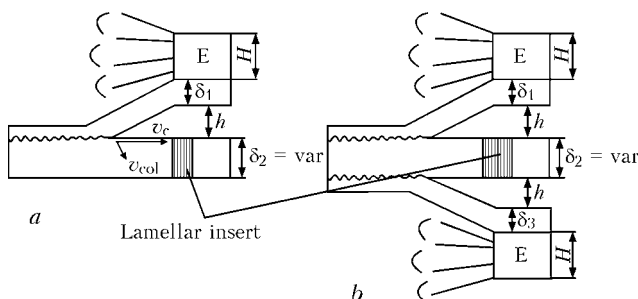


**Figure 1.** Scheme of collision of layers in two- and three-layered packages with application of lamellar model inserts in explosion welding according to plane-parallel (a) and battery (b) schemes: E --- explosive; H --- height of explosive charge;  $\delta_1$ ,  $\delta_3$ ,  $\delta_2$  --- thicknesses of respectively flyer ( $\delta_1 = \delta_3$ ) and target plates;  $h$  --- welding gap at package boundary;  $v_c$ ,  $v_{\text{col}}$  --- respectively speeds of contact and collision



the joint line had a wavy profile, whereby as it was shown, for example in [9], in case of the target plate thicknesses  $\delta_2$  increase in welding according to plane-parallel and battery schemes, character of change of the wave parameters in the joint was different (Figures 2 and 3). In welding of two-layer specimens sizes of the waves (length  $\lambda$  and amplitude  $2a$ ) first intensively grow, achieve at a certain value  $\delta_2$  maximal value and practically do not change with further increase of the target plate thickness. In battery scheme the opposite picture is observed — reduction of  $\lambda$  and  $2a$  by means of  $\delta_2$  increase [9].

It follows from analysis of Figure 2 that for selected conditions of welding according to the battery scheme of a three-layer package the limit thickness of the target plate  $\delta_2^1$ , beginning from which parameters of the waves do not change and are equal to sizes of the waves in the two-layer joint, produced according to the plane-parallel scheme, constitutes respectively for first and second series 8 and 10 mm. In both cases at  $\delta \geq \delta_2^1$  shear plastic deformation proceeds in a narrow NWZ of not more than 0.15–0.30 mm thickness. Values of maximal shifts  $g_{max}$  in immediate proximity from the joint line constitute 100–120 and 130–150 %

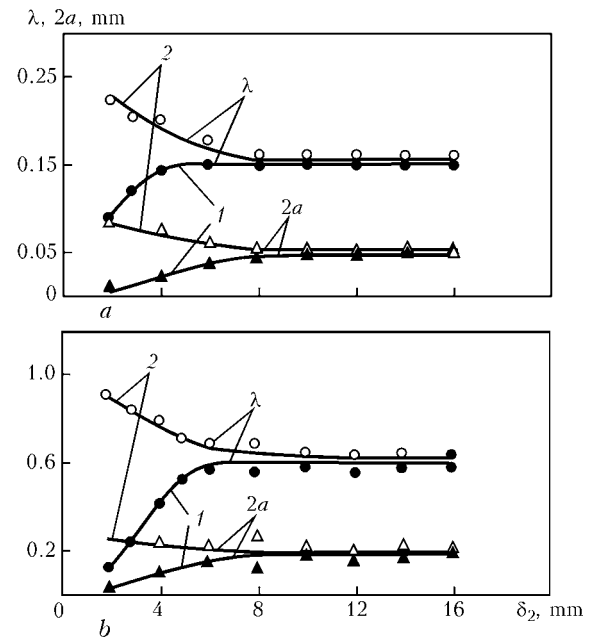


Figure 2. Dependence of length  $\lambda$  and amplitude  $2a$  of waves at boundary of two- and three-layer joints of aluminium plates upon middle plate thickness  $\delta_2$ : a —  $v_{col} = 220$ ; b —  $370$  m/s; 1 — plane-parallel; 2 — battery scheme

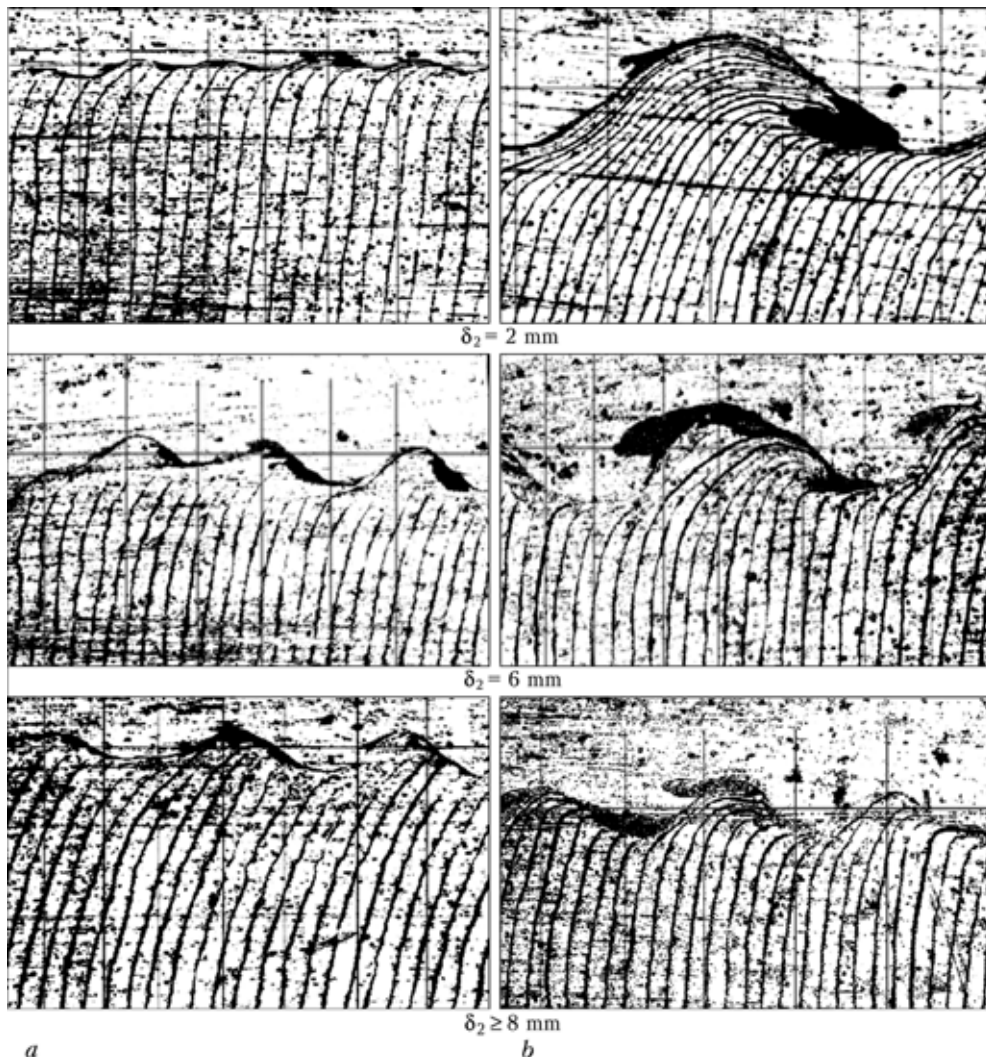
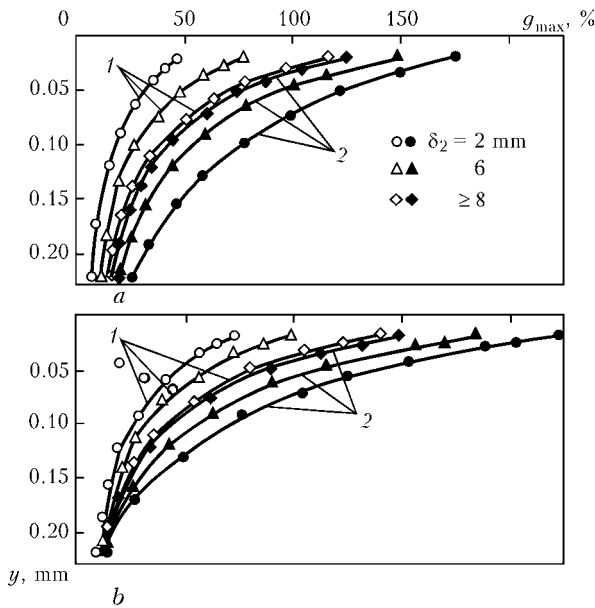


Figure 3. Macrostructures of model specimens from aluminium produced in explosion welding according to plane-parallel (a) and battery (b) schemes at  $v_{col} = 220$  m/s ( $\times 200$ )



**Figure 4.** Diagrams of shear plastic deformations obtained on specimens welded according to plane-parallel (1) and battery (2) schemes of welding ( $v_c = 2400$  m/s): a —  $v_{col} = 220$ ; b —  $370$  m/s

respectively for first and second series of the experiments.

In case of reduction of the target plate thickness ( $\delta_2 < \delta_2^1$ ), quality and quantitative differences start to be manifested in plastic deformation of the NWZ material in the considered schemes of welding (Figure 4).

So, in case of reduction of the thickness  $\delta_2$  from 8 to 2 mm in the two-layer specimens, produced according to the plane-parallel scheme, value  $g_{max}$  measured in immediate proximity to the joint line reduces approximately two-fold and constitutes approximately 50 and 75 % at  $v_{col}$  220 and 370 m/s respectively (Figures 4 and 5). In case of the battery scheme  $g_{max}$  of the contact-adjacent layers, on the opposite increases, achieving approximately 180 and 250 % respectively for first and second series of the experiments (see Figures 4 and 5). One may explain change of the level of maximal shear strains in the contact-adjacent layers of two- and three-layer specimens, welded ac-

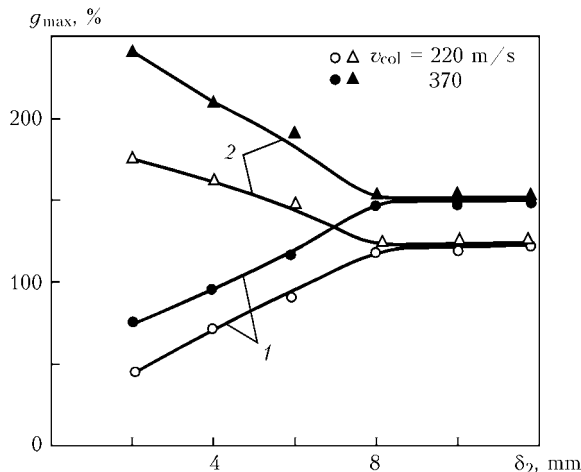


**Figure 5.** Dependence of shear plastic deformation of metal  $g_{max}$  in contact-adjacent layers of two- (1) and three-layer (2) explosion welded specimens upon thickness of target plate  $\delta_2$

ording to the plane-parallel and battery schemes respectively, detected at change of the target plate thickness, from position of the deforming pressure pulse  $I_d$  as an integral parameter that takes into account pressure in the collision zone and time of its action [9, 10].

Let us first consider the situation that occurs in case of the target plate thickness change in welding of a two-layer composition. As it was shown above, by means of increase of the target plate thickness  $\delta_2$  shear plastic deformation of contact-adjacent layers of the metal (similar to change of the wave parameters in a two-layer joint) first increases up to the maximum and then, beginning from a certain  $\delta_2$  value, remains constant at unlimited increase of the target plate thickness (Figure 5, curves 1). Value of the deforming pressure pulse  $I_d$  may be according to [9, 10] assessed by the formulas depending upon ratio of the time of the stress relief wave arrival from a free surface of the target plate  $\tau_{s,r}$  and time of the NWZ metal deformation behind the contact point  $\tau_c$  (Figure 6):

at  $\tau_{s,r} < \tau_c$

$$I_d = \int_{\tau_0}^{\tau_{s,r}} p_{max} e^{-\tau/\theta} d\tau = p_{max} \theta(1 - e^{-\tau_{s,r}/\theta}); \quad (1)$$

at  $\tau_{s,r} > \tau_c$

$$I_d = \int_{\tau_0}^{\tau_c} p_{max} e^{-\tau/\theta} d\tau = p_{max} \theta(1 - e^{-\tau_c/\theta}), \quad (2)$$

where  $p_{max}$  is the maximal (peak) pressure in the pulse, determined by the collision speed;  $\theta$  is the time constant that depends upon properties of the materials being welded.

At small thicknesses of the target plate ( $\delta_{21}$  in Figure 6) time of the stress relief wave arrival on the side of free surface of the lower plate  $\tau_{s,r1} = 2\delta_{21}/c_0$  ( $c_0$  is the speed of sound in the metal), pressure in the joint zone within this time will change from  $p_{max}$  to  $p_1$ , and value of pulse  $I_{d1}$ , calculated according to formula (1), corresponds in this case to the area, limited by the figure 0 —  $p_{max}$  —  $p_1$  —  $\tau_{s,r1}$  (Figure 6). Arrival of the stress-relief wave does not let deformation processes to develop to full degree in the contact-adjacent volumes of the metal behind the contact point (in the joint zone a «frozen» picture of the metal plastic flow with a respective level of shear deformations is observed).

Increase of  $\delta_{21}$  to the  $\delta_{22}$  value (Figure 6) or, which is the same,  $\tau_{s,r1}$  to  $\tau_{s,r2}$  causes respective increase of  $I_d$  with involvement into plastic deformation of big volumes of the metal and occurrence of significant shear deformations of the contact-adjacent volumes of the metal. In case of  $p$  reduction to the value of dynamic yield strength of the metal  $\sigma_y^d$ , which corresponds to time  $\tau_c$  in Figure 6, deformation processes in NWZ proceed in full volume (under these conditions of collision), and degree of plastic deformation  $g_{max}$

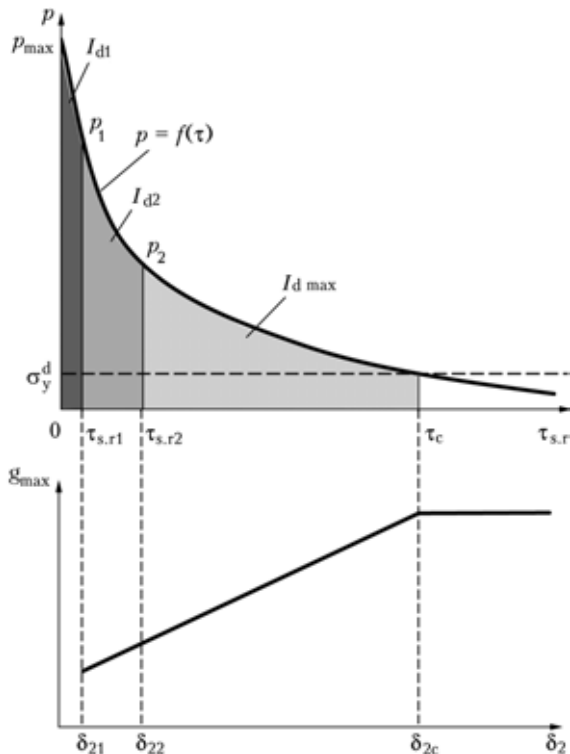


**Figure 6.** Increase of shear plastic deformation level in joint zone  $g_{max}$  in case of change of deformation pulse  $I_d$  due to time of pressure action  $\tau$

achieves its maximal possible value, which does not change at unlimited increase of  $\delta_2$ .

Quite different strain-time conditions occur in the joint zone in welding according to the battery scheme. Here at small thicknesses of the target plate  $\delta_2$  after passage of time  $\delta_1 = \delta_{21} / c_0$  a pressure pulse, occurring at collision on opposite boundary of the package being welded, starts to exert additional force action on the contact-adjacent layers of the metal that are plastically deformed by the pressure pulse which occurred at the considered boundary (Figure 7), whereby total deforming pulse, corresponding to the area limited by geometric figure  $0 - p_{max} - p_1 - p'_1 - p_{col} - \tau_c$  (Figure 7), turns out to be significantly greater than the deforming pulse, acting on the contact-adjacent layers of the metal in welding of a two-layer composite according to the plane-parallel scheme (see Figure 6). This causes, in its turn, significant increase of the level of plastic shear deformations of the NWZ metal.

Time of the pressure pulse arrival from the opposite boundary (in case of welding according to the battery scheme) also increases in case of  $\delta_2$  increase, while total pressure pulse reduces. In the limit case, when  $\delta_2 \geq \delta_2^1$ , pressure pulse arrives from the opposite boundary after termination of the deformation processes at the considered boundary of the composite ( $\tau > \tau_c$ ) and is not able to additionally deform stress-relieved NWZ metal.

So, it was experimentally shown that in explosion welding according to the battery and plane-parallel schemes strain-time conditions of a joint formation

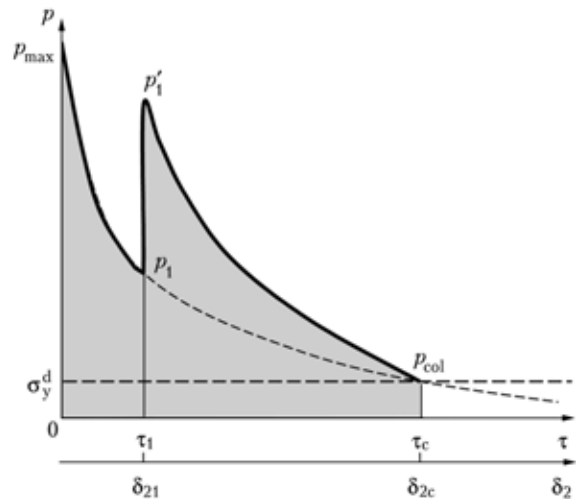


**Figure 7.** Change of pressure in joint zone in explosion welding according to battery scheme (target plate thickness  $\delta_{21}$ )

and plastic deformation of the contact-adjacent metal layers significantly differ: in welding according to the battery scheme values of maximal shear deformations  $g_{max}$  occurring near the joint line at  $\delta_2 < \delta_2^1$ , exceed several times respective values, characteristic of plane-parallel scheme, which is connected with additional force action of the pressure pulse, occurring in collision at opposite boundary of the joint.

The results obtained have to be taken into account when designing technological processes of explosion welding with application of the scheme of a two-sided symmetrical cladding, because at excessive shear deformations in the NWZ metal (at small target plate thicknesses  $\delta_2$ ) in the joint zone, areas of flashed metal and other defects will form that negatively affect quality of the produced composite material.

1. Sedykh, V.S., Sonnov, A.P., Shmorgun, V.G. (1988) Study of flow metal nature in high-velocity explosion cladding on lamellar models. In: *Interinst. Transact. on Explosion Welding and Properties of Welded Joints*. Volgograd: VolgPI.
2. Kuzmin, S.V., Lysak, V.I., Chugunov, E.A. et al. (2000) New procedure for investigation of plastic deformation of metal in near-weld zone of explosion welded joints. *Fizika i Khimiya Obrab. Materialov*, **2**, 54–60.
3. Chugunov, E.A., Kuzmin, S.V., Lysak, V.I. et al. (2001) Main principles of deformation of near-weld metal zone in explosion welding of aluminium. *Ibid.*, **3**, 39–44.
4. Kuzmin, S.V., Lysak, V.I., Chugunov, E.A. et al. (2000) Welded joint formation in explosion welding of metals. *The Paton Welding J.*, **11**, 26–30.
5. Peev, A.P., Kuzmin, S.V., Lysak, V.I. et al. (2003) Peculiarities of plastic deformation of near-weld metal zone in explosion welding of copper with aluminium. *Fizika i Khimiya Obrab. Materialov*, **1**, 71–76.
6. Gulbin, V.N., Kobelev, A.G. (1998) Plastic deformation of metals in explosion welding. *Svarochn. Proizvodstvo*, **10**, 9–12, 55–56.
7. Kriventsov, A.N., Sedykh, V.S. (1969) About role of plastic deformation of metal in explosion welded joint zone. *Fizika i Khimiya Obrab. Materialov*, **1**, 132–141.
8. Bondar, M.P., Ogolikhin, V.M. (1985) About plastic deformation in explosion clad joint zone. *Fizika Goreniya i Vzryva*, **21**(2), 147–157.
9. Kuzmin, S.V., Chuvichilov, V.A., Lysak, V.I. (2005) Time conditions of joint formation in explosion welding. *Perspekt. Materialy*, **1**, 85–91.
10. Lysak, V.I., Kuzmin, S.V. (2005) *Explosion welding*. Moscow: Mashinostroenie.



# CORRECTION OF A MANIPULATION ROBOT MOTION PATH TAKING INTO ACCOUNT ADDITIONAL MEASUREMENTS

G.A. TSYBULKIN

E.O. Paton Electric Welding Institute, NASU, Kiev, Ukraine

The paper deals with issues associated with ensuring the required accuracy of robot motion along paths, the spatial position of which is not known exactly beforehand. The law of corrective control has been formulated, which is based on utilization of additional measurements during the motion, and which guarantees the preset movement accuracy. Modeling of the dynamics of a system realizing this law has been performed.

*Keywords:* robotic arc welding, welded joints, corrective control, manipulation robot, motion path

One of the complicated problems arising at control of the motion of manipulation systems along preset paths is ensuring the required motion accuracy. This problem is traditionally addressed using methods [1–4], aimed at reduction of dynamic errors of local systems (LS), included into the composition of a multichannel manipulation control system. Also known are non-traditional approaches, which were suggested at some time by M.B. Ignatiev [5], and became further developed in studies [6–9]. Unlike [1–4], these methods envisage introduction of additional feedbacks into the multichannel system, which provide minimization of the path error by correction of relationships between dynamic errors along individual coordinates [7–9], or corrective control of the tempo of system motion in the function of LS dynamic errors [5, 8, 9].

However, increase of motion accuracy with the above methods can be guaranteed only provided the programmed paths are always adequate to the required (desired) paths. In practice it is quite often the case, when the desired paths do not coincide with programmed paths for this or that reason. Such situations are found, in particular, in robotic arc welding of large-sized items, when because of the large dimensions and weight of the parts being welded, they cannot always be placed exactly into the position specified for welding, or they have too large dimensional allowances. It is clear that in this case the spatial position of the actual joint lines of the parts being welded can differ essentially from the position of the programmed lines.

The program of robot motion can be corrected, if data about the deviation of the actual lines (desired paths) from the preset ones are available. For this purpose, the robot is usually fitted with a special device, which during motion at each moment of time  $t$  measures, for instance, the distance from the electrode tip to the desired path, and correction of the programmed path is performed based on  $\rho(t)$  signal characterizing this distance. In those cases, when the paths are rectilinear and are located along one of the

coordinates of the robot envelope, their correction is performed in a comparatively simple manner [10–12]. However, when the paths are curvilinear, it is still unclear, how the  $\rho(t)$  signal should be «split» into components by coordinates, so as to implement corrective control. Dynamic properties of such systems are not known, either.

In this paper the law of corrective control is plotted, which ensures robot motion along a desirable path irrespective of its shape or location in the robot envelope, and modeling of system dynamics implementing this correlation law is performed.

**Synthesis of corrective control law.** Let the specified path of motion of the robot actuator be given by the following equations

$$F(x_1, x_2) = 0, \quad (1)$$

implicitly establishing quite definite relationships between the set motions

$$x_1^0(t) = X_1(s(t)), \quad x_2^0(t) = X_2(s(t))$$

in the Cartesian system of coordinates  $Ox_1x_2$ . Here,  $X_1(s)$ ,  $X_2(s)$  are the known continuous and differentiable functions of parameter  $s$ , which is the length of the arc of the path, which connects the image point of assigning  $P_0$  with initial point  $P_{in}$  (Figure 1). It is assumed that in this case condition  $F(x_1^0(t), x_2^0(t)) = 0$  is certainly fulfilled, and the connection between the input actions of the manipulation robot  $\mathbf{q}^0 = \{q_j^0(t)\}$ ,  $j = 1, 2, \dots, n$  and coordinates  $\mathbf{x}_0 = \{x_i^0(t)\}$ ,  $i = 1, 2$  is described by dependence  $\mathbf{x}_0 = \mathbf{A}(\mathbf{q}^0)$ , in which  $\mathbf{A}(\cdot)$  is the vector-function generated by the kinematics of a specific manipulation robot.

Let us assume that desired path  $G(x_1, x_2) = 0$  does not coincide with path  $F(x_1, x_2) = 0$ , as shown in Figure 1. Let us denote the distance from point  $P_0$  to point  $N$  located on the intersection of path  $G(x_1, x_2) = 0$  with the normal to path  $F(x_1, x_2) = 0$  in point  $P_0$ , as  $\rho$ . The purpose of corrective control consists in ensuring fulfillment of requirement  $|\rho(t)| \leq \rho_0$ , where  $\rho_0$  is a positive number characterizing the assigned accuracy of robot motion.



From Figure 1 it is seen that in order to reduce  $\rho$ , it is rational, simultaneously with motion of the point along path  $F(x_1, x_2) = 0$  to additionally move it along coordinate  $x_1$  for distance  $\xi_1 = \rho \sin \alpha$ , and along coordinate  $x_2$  --- for  $\xi_2 = \rho \cos \alpha$ , where  $\alpha$  is the angle between the tangent in point  $P_0$  and axis  $x_1$ . Such a displacement is possible, if signals proportional to current values of  $\xi_1(t)$  and  $\xi_2(t)$ , respectively, are continuously added to input signals  $x_1^0(t)$  and  $x_2^0(t)$ . Such reasoning leads to an idea that the law of corrective control should be plotted in the integral form:

$$\begin{aligned} \xi_1(t) &= K \sin \alpha(t) \int_0^t \rho(t) dt, \\ \xi_2(t) &= -K \cos \alpha(t) \int_0^t \rho(t) dt, \end{aligned} \quad (2)$$

where  $K$  is the coefficient of proportionality selected from the condition of system stability.

It is easy to see that the current values of  $\sin \alpha(t)$  and  $\cos \alpha(t)$  can be obtained directly during system motion along assigned path  $F(x_1, x_2) = 0$ . Indeed, angular coefficient of the tangent in point  $P_0$  is defined as  $\text{tg } \alpha(t) = \frac{dx_2^0}{dt} / \frac{dx_1^0}{dt}$ .

Hence,

$$\sin \alpha(t) = \frac{1}{v} \frac{dx_2^0}{dt}, \quad \cos \alpha(t) = \frac{1}{v} \frac{dx_1^0}{dt}, \quad (3)$$

where  $v = \sqrt{\left(\frac{dx_1^0}{dt}\right)^2 + \left(\frac{dx_2^0}{dt}\right)^2}$  is the velocity of motion of point  $P_0$  along path  $F(x_1, x_2) = 0$ .

Thus, the law of corrective control (2), allowing for (3), takes the following final form:

$$\xi_1(t) = \frac{K}{v} \frac{dx_2^0}{dt} \int_0^t \rho(t) dt, \quad \xi_2(t) = \frac{K}{v} \frac{dx_1^0}{dt} \int_0^t \rho(t) dt. \quad (4)$$

**Modeling the control system.** Computer simulation of the dynamics of a two-channel control system for the case, when  $q_1^0(t) = x_1^0(t)$ ,  $q_2^0(t) = x_2^0(t)$ , was conducted for experimental verification of the effectiveness of synthesized law (4) of corrective control of the manipulation robot motion. As is seen from Figure 2, correction device (CD) is added to this system. In blocks  $B_1$  and  $B_2$  corrective signals are formed by (4) on the basis of the data on deviation  $\rho(t)$  and on derivatives of input signals  $x_1^0(t)$  and  $x_2^0(t)$ . Signals  $x_1^k(t) = x_1^0(t) + \xi_1(t)$  and  $x_2^k(t) = x_2^0(t) + \xi_2(t)$ , which, essentially, are a corrected program of robot motion, come to the inputs of local systems  $LS_1$  and  $LS_2$ , included into the two-channel system.

For modeling convenience it is assumed that  $LS_1$  and  $LS_2$  are identical, are characterized by astaticism of the first order, and in the open-loop state they are described by transfer function

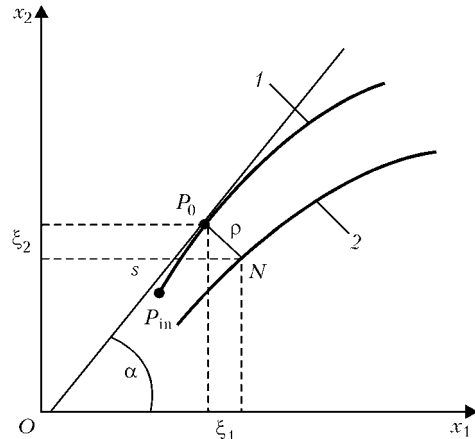


Figure 1. For calculation of corrective signals  $\xi_1(t)$  and  $\xi_2(t)$ : 1 —  $F(x_1, x_2) = 0$ ; 2 —  $G(x_1, x_2) = 0$ ; for other designations see the text

$$W(p) = \frac{K_0}{p(Tp + 1)}, \quad (5)$$

where  $K_0$  is the transfer coefficient;  $T$  is the time constant;  $p$  is Laplace operator.

The following values of transfer function parameters were taken (5):  $K_0 = 75 \text{ s}^{-1}$ ,  $T = 0.11 \text{ s}$ . Circular arcs described by the following equations were considered as the programmed and desired paths:

$$x_1^0(t) = R(1 - \cos \omega t), \quad x_2^0(t) = R \sin \omega t, \quad (6)$$

$$x_1^0(t) = R + a - R \cos \omega t, \quad x_2^0(t) = b + R \sin \omega t, \quad (7)$$

where  $R$  is the arc radius;  $\omega = v/R$  is the parameter selected from the condition of provision of the required speed  $v$  of robot motion;  $a, b$  are the initial deviations of the desired path (7) from the programmed one (6) by coordinates  $x_1$  and  $x_2$ , respectively.

Paths (6) and (7) were selected so that distance  $\rho(t)$  at any moment of time  $t$  could be easily calculated under the conditions of the model experiment. It is obvious that  $\rho(t)$  can be found from the following formula:

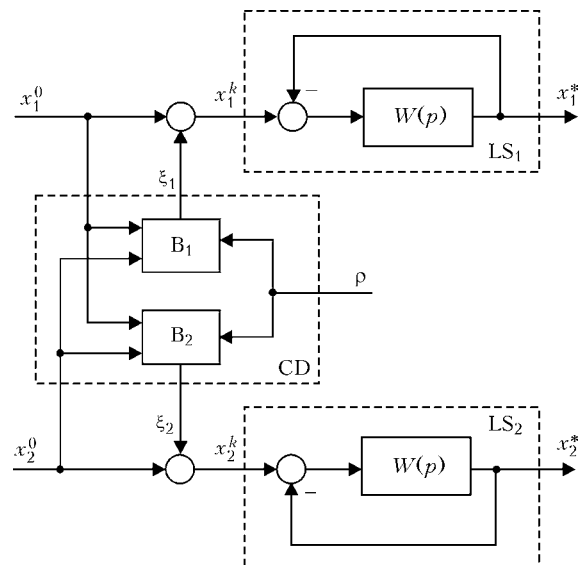


Figure 2. Block-diagram of the corrective device control system

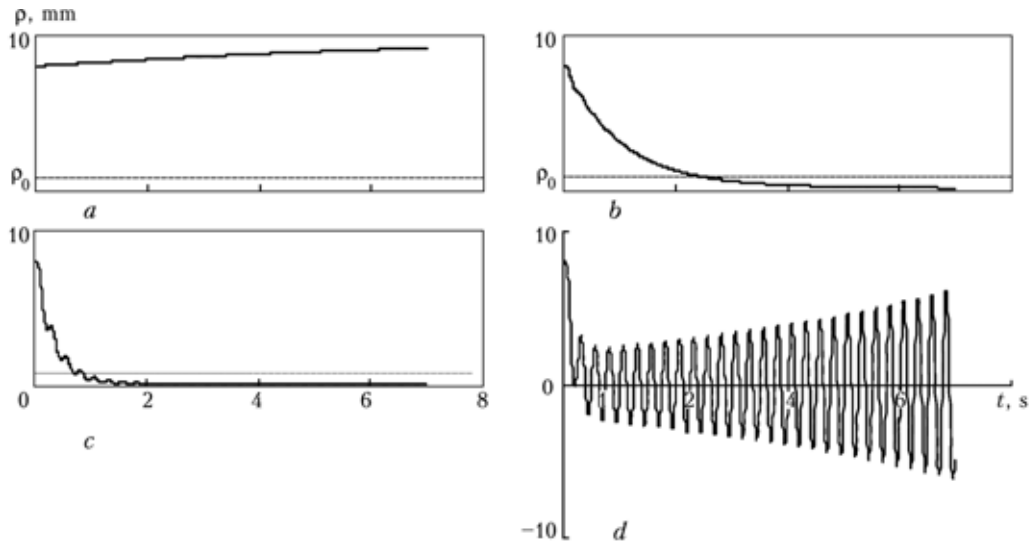


Figure 3. Graphs of function  $\rho(t)$  plotted by simulation results: a —  $K = 0$ ; b — 1; c — 3; d —  $6.6 \text{ s}^{-1}$

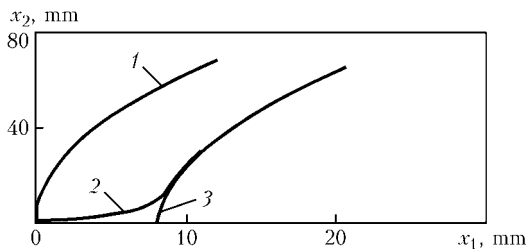


Figure 4. Motion paths: 1 —  $F(x_1, x_2) = 0$ ; 2 —  $\Phi(x_1^*, x_2^*) = 0$ ; 3 —  $G(x_1, x_2) = 0$ , for other designations see the text

$$\rho(t) = \sqrt{(x_1^*(t) - R - a)^2 + (x_2^*(t) - b)^2} - R,$$

where  $x_1^*(t)$  and  $x_2^*(t)$  are the coordinates of the actual position of the robot actuator.

Figures 3 and 4 present the results of simulation of a two-channel control system at the following parameter values:  $s = 70 \text{ mm}$ ;  $R = 200 \text{ mm}$ ;  $\omega = 0.05 \text{ s}^{-1}$ ;  $a = 8 \text{ mm}$ ;  $b = -5 \text{ mm}$ ;  $\rho_0 = 1 \text{ mm}$ . Figure 3 shows the processes of the change of  $\rho(t)$ , depending on the value of coefficient  $K$  in the corrective control law (4). Analysis of these curves showed that in the absence of correction ( $K = 0$ ) distance  $\rho(t)$  is large enough compared to  $\rho_0$  (Figure 3, a), but it decreases abruptly (Figure 3, b, c), if corrective control is applied ( $K > 0$ ).

Comparison of curves in Figure 3, b and c shows that the time of correction, i.e. time interval, during which distance  $\rho(t)$  becomes smaller than  $\rho_0$ , depends essentially on the value of coefficient  $K$  (with its increase the correction time becomes smaller). It should be noted, however, that at  $K$  increase  $\rho(t)$  variations develop, and at  $K \geq K_{ad}$  the automatic correction process becomes unstable (Figure 3, d) (in our experiment the admissible value  $K_{ad} = 6.3 \text{ s}^{-1}$ ). It is clear from here that the value of coefficient  $K$  should be selected in each individual case, proceeding from compromise considerations.

Figure 4 shows  $\Phi(x_1^*, x_2^*) = 0$  path, along which the robot motion is performed as a result of correction of the programmed path  $F(x_1, x_2) = 0$  at  $K = 3 \text{ s}^{-1}$ . It is seen from the Figure that  $\Phi(x_1^*, x_2^*) = 0$  path starts in  $F(x_1, x_2) = 0$  path and after some time the correction

practically coincides with desired path  $G(x_1, x_2) = 0$ , located at a rather large distance from  $F(x_1, x_2) = 0$ , which is indicative of high accuracy of corrective control synthesized by (4).

On the other hand, it should be noted that at robot motion along curvilinear paths a path error  $\varepsilon(t)$  develops, even in such a favourable case, when the programmed and desired paths coincide. As is known [9], error  $\varepsilon(t)$  increases with increase of velocity  $v$  of motion along the path and its curvature. As  $\varepsilon(t)$  is just a part of the overall deviation from the path determined by distance  $\rho(t)$ , the synthesized law of automatic correction (4) ensures the requires accuracy of motion along the path, irrespective of the cause for this deviation.

Thus, computer simulation demonstrated a sufficiently high effectiveness of the proposed law of correction of the programmed motion path at its random orientation in the robot envelope.

1. Timofeev, A.V. (1980) *Design of adaptive control systems of program motion*. Leningrad: Energiya.
2. Vukobratovich, M., Stokich, D., Kirchansky, N. (1989) *Nonadaptive and adaptive control of robotic manipulators*. Moscow: Mir.
3. Bobtsov, A.A. (2003) Algorithm of robust control in the problem of calibration signal tracking. *Avtomatika i Telemekhanika*, **6**, 104–113.
4. Krutko, P.D., Golovanov, M.A. (2005) Trajectory control of automatic manipulator movement in performance of technological operations. *Problemy Mashinostroeniya i Nadyozhnost Mashin*, **3**, 88–95.
5. Ignatiev, M.B. (1963) *Holonomic automatic systems*. Leningrad: AN SSSR.
6. Tsybulkin, G.A. (1988) Coordinative control of movement by two-dimensional variety with cross coupling between the reproducing systems. *Avtomatika*, **2**, 83–86.
7. Miroshnik, I.V. (1990) *Coordinated control of multichannel systems*. Moscow: Energoatomizdat.
8. Tsybulkin, G.A. (2002) About one non-traditional approach to the problem of improvement of the accuracy of movement in selected trajectories. *Upravl. Systemy i Mashiny*, **2**, 20–25.
9. Tsybulkin, G.A. (2003) Stabilization of lateral deviation of a program-controlled object in movement along the trajectories of variable curvature. *Ibid.*, **3**, 12–17.
10. Gao, X., Huang, S., Yu, Y. (1999) An artificial neural network for detecting weld position in arc welding process. *China Welding*, **8**(1), 74–80.
11. Sugitani, Y. (2000) Making best use of the arc sensor. *J. JWS*, **69**(2), 46–50.
12. Tsybulkin, G.A. (2000) Situation algorithms of automatic correction of the robot motion path in arc welding. *The Paton Welding J.*, **11**, 11–14.

# DEVELOPMENT AND APPLICATION OF TUBULAR WELDED STRUCTURES

E.F. GARF<sup>1</sup> and V.V. SNISARENKO<sup>2</sup>

<sup>1</sup>E.O. Paton Electric Welding Institute, NASU, Kiev, Ukraine

<sup>2</sup>OJSC «Ukrstalkonstruksiya», Kiev, Ukraine

Development and application of welded structures made from tubes is inseparably linked to improvement of welding as technological process for material joining, and involves fulfillment of requirements for assurance of quality and strength of the welded joints. It is shown that Ukraine has many-year traditions in the field of fabrication of tubular structures, and that it has preserved its scientific and industrial potential for further development of this field.

*Keywords:* welding, welded joints, welded structures, tubular structures, nodal connections, strength, stability, economic indices

Welding as a technological process of producing permanent joints created prerequisites for effective application of tubes in structures for the most diverse purposes. While the traditional sections of elements (angles, channel bars, etc.), widely used in welded structures, were taken from riveted structures, tubes are a type of sections, the application of which became possible and justified only due to welding. At present it is difficult to imagine a tubular structure (pipeline, tower or truss) made using riveted or bolted joints.

On the other hand, tubular welded structures make certain requirements of the welding technology. So, it is difficult to develop efficient structures without the possibility of producing butt joints of tubes, equivalent to the base metal. This requires welding consumables, providing such properties of welded joints which are not inferior to those of the base metal in a wide range of steel classes, and joining technologies capable of ensuring high quality of the joints not only at two-sided, but also at one-sided welding. Owing to modern achievements in welding production, these problems are successfully solved for different steel classes and tube diameters.

Expansion of the areas of tube application in welded structures offers a number of advantages, characteristic for this type of the section:

- high and uniform in all the directions values of geometrical characteristics of sections, such as radius of inertia and moment of inertia, which allows effective use of tubes in rods loaded by axial and eccentric compression, as well as torsion. This opens up the possibilities for more effective utilization of steels of higher and high strength in frame structures;

- increased local stability of tube walls, allowing use of thin-walled sections. Increase of the ratio of tube diameter to its wall thickness  $D/t$  leads to more efficient utilization of tubes in compressed elements from the viewpoint of longitudinal bending, but a moment may come, when local stability will determine their load-carrying capacity. For tubular elements

with  $D/t < 100$  ratio under the condition of a uniform distribution of stresses across the section, there is no risk of local stability loss. However, at non-uniform distribution of stresses across the section, as is the case in tubular nodal connections without gussets, loss of local stability can occur at  $100 > D/t > 50$ . Figure 1 shows the effectiveness of tubular sections, depending on their wall thickness [1]. As is seen from the Figure, in latticed structures, where a certain non-uniformity of stress distribution across the tube section is always found in the nodal connections,  $50 \geq D/t \geq 40$  ratio can be regarded as optimum. As the tubes feature the best fairness of the section of those applied in structures, such a relationship ensures a lowering of the wind and wave load on the construction, and, therefore, allows additional reduction of the structure weight. This is exactly the reason why the mast and tower structures are mostly made of tubes, and in such constructions as oil and gas off-shore platforms other profiles are practically not used for the columnar supports;

- increased corrosion resistance, which is due to a relatively smaller area of the corroding surface, surface accessibility for cleaning and painting, absence of

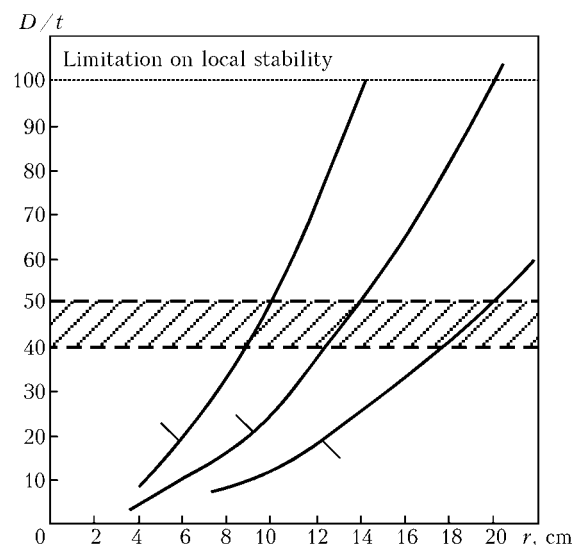


**Figure 1.** Dependence of radius  $r$  of inertia on  $D/t$  ratio at tube cross-sectional area of 50 (1), 100 (2) and 200 (3)  $\text{cm}^2$ ; area of optimum  $D/t$  ratio for tubular components is hatched

## Data on TV towers

City	Tower height, m	Development organization	Type of sections used	Material consumption		
				Rolled stock for tower, t	R-bars for foundation, t	Concrete for foundation, m <sup>3</sup>
Kiev	380 (385 m with flagpole)	USPK	Tubes	2737.7	23	1066
Tashkent	375	TsNIIPSK	Rolled shapes; tubes	5800	N/D	N/D
Riga	368	GSPI of USSR Communications Ministry	Sheet structural stock	4500	Same	Same
Almaaty	360	TsNIIPSK	Welded I-beams; rolled shapes	4760	»	»
St.-Petersburg	316	USPK	Tubes	1300	21.8	1664
Erevan	311.7	Same	Same	1757.8	18.6	1269
Tbilisi	274.4	»	Tubes, ropes	1242.5	31.5	1331
Vitebsk	243.9	»	Same	628	32.6	260
Kharkov	240.7	»	Tubes, rolled sheets	1233	45.3	1080

*Note.* USPK — Ukrainian Design Institute of Steel Structures, Kiev; TsNIIPSK — N.P. Melnikov Central R&D Institute of Steel Structures, Moscow; GSPI — State USSR Design Institute of the USSR Communications Ministry, Moscow.



**Figure 2.** TV tower in St.-Petersburg

slots, voids and pockets. However, in this case, it is necessary to take measures for ensuring the sealing of the inner, unpainted tube surfaces. Increased corrosion resistance allows lowering the operational costs and extending the operating life of tubular welded structures;

- esthetic and architectural perfection of tubular structures, as well as a broad range of the grades of commercially produced tubes, promote their application both in small architectural forms and in unique constructions.

Tower structures can serve as a confirmation of the rationality of tubular section application. Their operation is characterized by wind loads, which significantly exceed the loads from the weight of the structure proper and process equipment, a large proportion of the dynamic component in the total value of displacements and forces, as well as a strong dependence of the construction reaction to the main actions on the structural shape and shape of its elements [2].

The Table gives the data on TV towers built in ex-USSR in the second half of the previous century. We are limiting discussion on purpose to constructions built in ex-USSR, as they were designed using a common standard base. Without analyzing the features of designs and loads, the table data can lead to the conclusion of the advantages of tubular section application in terms of metal consumption. Let us briefly dwell on the most characteristic tubular constructions.

The TV tower in St.-Petersburg was built in 1962 (Figure 2). This tower was made all-welded of tubular elements for the first time in the construction practices. The load-carrying tower of a hexagonal section was made latticed with pre-tensioned tubular braces. It supported the frame of a technical building, above which was a stack of three prismatic sections of a

square cross-section. The tubes for the tower are made of low-alloyed steel of 15KhSND grade. The nodal connections of lattice element attachment to the girths were made using end plates --- lattice tube plugs to which gusset plates were welded. In site the lattice elements were joined to the girths by fillet welds. With such a technological solution, despite reinforcement of the end plate by additional stiffeners, a high stress concentration is found in the sections of gusset plate intersection with the brace tube. In order to reduce it, the thickness of the plug end plate was taken to be not less than  $1/6$  of the tube diameter.

It should be noted that at the moment of the tower design, investigations on selection of the optimum design solutions of the tubular nodal connections, providing a minimum concentration of stresses and maximum strength at static and cyclic loading, were not conducted on a sufficiently broad scale. The data deficit was partially compensated by the results of investigations performed at the E.O. Paton Electric Welding Institute [3, 4]. Nonetheless, after 40 years of operation the most heavy-duty components of the tower started developing fatigue cracks, which required thorough monitoring of the technical condition of the construction and timely repair of the detected damage.

In 1973 the towers of TV centers in Kiev and Tbilisi were constructed. By this time investigations in the field of tubular structures were developed further [5--7, etc.]. Their results confirmed the advantages of designing nodal connections based on direct (without gussets) abutment of the tubular elements.

The tower of the TV center in Tbilisi differs by that it has a non-symmetrical schematic and implements the idea of combining the load-carrying and enclosing functions in one of its girths (Figure 3). The vertical girth of the tower, extending into the antenna, at the same time is the lift shaft, and is supported by inclined tubular girths, connected to it by a system of braces from tubes and braces from high-strength ropes. Engineering buildings are located above the 71 m mark and below the 163.8 m mark. The angle between the tower side faces is equal to  $60^\circ$  in any horizontal section. The principles of direct abutment of tubes are used in most of the tower components, this ensuring a lowering of the level of stress concentration compared to the tube joining through the end plate and gusset.

In terms of design, the TV tower in Kiev (Figure 4) can be conditionally divided into three parts: base, latticed prismatic trunk and lift shaft with the antenna part. The tower base is a latticed octahedral mandrel to which spatial tetrahedral «legs» are attached. The latticed prismatic trunk of an octahedral section is restrained in the upper part of the base mandrel.

The upper part of the prismatic section of this tower supports the frame of an engineering building. The lift shaft is resting on a basement at the tower base and runs inside the latticed prismatic trunk, and above the trunk it extends into the antenna part. The



Figure 3. TV tower in Tbilisi

lift shaft and the antenna part are welded of cylindrical steel shells. The lift shaft is attached to the trunk by «ray» diaphragms.

A number of advanced and still novel solutions are used in the tower. In particular, high-strength steel of IZ 138 grade is used, nodal connections are mainly made without gussets, and an incremental mounting technique is implemented, thus providing guarantee



Figure 4. TV center tower in Kiev



Figure 5. Mounting the stadium roofing in Dnepropetrovsk

of sound performance of assembly-welding operations in site and shortening the construction time.

The last quarter of the previous century is characterized by increased interest to tube application in welded structures. It gradually becomes clear that optimum weight characteristics can be achieved by optimization of the sections of individual structure elements and ensuring the strength of nodal connections [8]. A number of works [9–12] prove the advantages of designing the nodal connections based on direct abutment of pipes, and large-scale investigations are conducted on development of the calculation procedures for nodal connections under static and periodical loading.

Scientific conferences on tubular welded structures are regularly conducted within the IIW framework. Such an increased interest to the problems of tubular welded structures is attributable primarily to intensive mastering of the world continental shelf and the need for a large-scale construction of off-shore platforms for oil and gas production.

Mastering the sea depth greater than 100 m, and, in particular, the North Sea shelf with its severe climatic conditions, necessitates evaluation of the strength of off-shore platforms at cyclic loads applied to the structure. It becomes clear that the strength of tubular structures at variable loads is always determined by fatigue resistance of nodal connections.

Features of the stress-strain state in the zone of tubular nodal connections eliminate the possibility of application of the results of fatigue testing of flat element welded joints in evaluation of their fatigue life. Evaluation of fatigue resistance of tubular connections requires development of special procedures of fatigue analysis. This research eventually led to development of the respective procedures for evaluation of the strength of connections at static and periodical loading and their inclusion into the codes on design of off-shore constructions of a number of developed countries [13–15]. Investigations in the above directions were intensively conducted also in ex-USSR [16, 17, etc.], as this was the period of active mastering of the southern sea shelves (Caspian, Azov and Black Seas), construction of the first platforms on the shelf

of Sakhalin island, and of preparation for mastering the shelf of the northern seas. A number of codes were developed, which specified design of off-shore structures [18–20].

In connection with disintegration of the USSR and the subsequent economic crisis, which also spread to Ukraine, construction of large facilities was practically stopped.

With the start of economic growth in Ukraine, re-birth of the building industry began and the interest to welded tubular structures became greater. The fact that the leading institutes in the field of metal structure design, namely OJSC «V.N. Shimanovskiy UkrNI-Proektstalkonstruksiya» (Kiev), «Institute «Shelf», Ltd. (Simferopol) and others managed to successfully overcome the crisis, had an important role here.

The almost completed construction of a roof over the stands of the stadium in Dnepropetrovsk should be regarded as one of the unique constructions built in the recent years using cylindrical pipes. The project was developed by the Department of New Types of Structures of «V.N. Shimanovskiy UkrNI-Proektstalkonstruksiya» (Project Engineer is I.N. Lebedich, Cand. of Sci. (Eng.) [21], and structure fabrication and mounting are performed by «Ukrstalkonstruksiya» (Kiev). The total weight of the roof metal structures is 1290 t.

The roofing over the stands is designed in the form of a system of flat cantilever truss structures of a variable height (Figure 5). For trusses above the stands the cantilever span from the support is equal to 27 m, and that of the tail part is 17.15 m. For the trusses over the VIP building the cantilever span is equal to 32.8 m, and that of the tail part is 14 m. The range of the seamless all-drawn pipes used in the roof design, includes sections from  $80 \times 5$  to  $426 \times 16$  mm. Tubes of  $299 \times 14$  mm section were used for truss girths. All the tubes are made of steel 20 in Nizhnedneprovsk pipe-rolling mill.

Predominantly nodular connections of tubular elements without gussets were specified. Plant butt joints are welded on a backing ring. In site, in order to reduce the volume of welding operations, the butts of compressed elements were made, as a rule, as flange joints using high-strength bolts, and for elements under tension kingpin joints with coupling bushings of 124, 164 and 194 mm diameter were used.

Another example of a successful use of tubes can be the covering of the International Exhibition Center in Kiev built in 2002. The metal structures of the Exhibition Center were designed by «V.N. Shimanovskiy UkrNI-Proektstalkonstruksiya» (Project Engineer is M.N. Palchik). The latticed covering in the form of trusses and secondary trusses and systems of ties fulfills not only the engineering, but also architectural functions. The trusses with the span of 24, 6, 30 and 48 m, have curvilinear lower and upper girths, secondary trusses with 60 m span have parallel girths (Figure 6). Thick-walled weldless tubes of  $377 \times 40$  mm section of steel 20 were used for the girths

and bearing braces of trusses with 60 m span, and tubes of  $152 \times 6$  up to  $325 \times 18$  mm section of the same steel were used for other truss elements. Initial tubular billets have the length of 12 m. All the factory-made butt joints were welded on backing rings, field joints of the upper compressed girth were also made on backing rings, and those of the lower girth under tension --- on half-couplings. Nodal tubular connections have no gussets with direct abutting of the lattice elements to the girths.

A feature of the truss design is fabrication of the girth elements with lattice element nipples in the connections. At mounting each of the lattice elements is connected to the respective nipples of the upper and lower girth connections by two butt joints which are made using two shaped half-couplings. This essentially simplifies the structure assembly in site, lowers the requirements to the blank fabrication accuracy, but, on the other hand, leads to increased consumption of the metal and welding consumables. With the modern development of welding technologies and materials such joints are made by welding from one side with ensuring the back bead formation. The latter is achieved, for instance, by using local electrodes of ANO-TM grade or LB-524 electrodes, manufactured in Japan.

The structures of the International Exhibition Center were made at the Dnepropetrovsk I.V. Babushkin Metal Structure Plant, mounting was performed by specialists of «Ukrstalkonstruksiya» and «Tsentrostalkonstruksiya» (Kiev).

A shop of OJSC «Vetropak Gostomel Steklozavod» built in 2004–2007 in the Kiev region can be an example of an effective use of tubes in industrial building coverings (Figure 7). The shop was designed by the same authors' team of «V.N. Shimanovsky UkrNIIproektstalkonstruksiya». Tubular constructions of the shop were made at the Chernigov Plant of Metal Structures and Metal Fixtures. Structure mounting was performed by «Ukrstalkonstruksiya» and «V.N. Shimanovsky UkrNIIproektstalkonstruksiya». For trusses of 42 m span seamless cylindrical tubes of steel 20 were used. Section of the truss girths is  $219 \times 8$  mm, that of the lattice is  $152 \times 6$  mm. Nodal connections are made by direct abutting of the lattice elements to the girth. Butt joints of tubes in the upper compressed girth were welded by circumferential welds on backing rings, those of the lower girth in tension were made using shaped put-on half-couplings. Such a technical solution, even though it is not optimum in terms of metal consumption, allows simplifying the structure assembly both in the shop and in site.

The list of tubular structures designed and built during the last decade, would not be complete without mentioning the continental shelf constructions.

A significant number of constructions in the continental shelf of Ukraine were designed by the «Institute «Shelf» Ltd. These mainly are off-shore platforms, designed for drilling and industrial production of oil and gas from the water areas of the Azov and



Figure 6. Tubular trusses of covering of the International Exhibition Center in Kiev

Black Seas. Over the last years more than a dozen major projects were developed, most of which were implemented. Platform design is usually selected allowing for the natural and climatic conditions of the construction area, availability of technical means for mounting and fastening of the structures, capabilities of enterprises making the structures, method of structure transportation to their mounting site.

It should be noted that in Ukraine there is no high-capacity specialized enterprise on fabrication of off-shore structures. For this reason, the structures are made in ship-building plants or special mounting sites located on the shore near the mastered site. In addition, tubes of the gas pipeline range have to be used for structural elements, having a relatively small wall thickness and ratio of their diameters to wall thickness  $D/t > 50$ . In this connection, at structure design special attention should be given to the issues of strength of the tubular nodal connections. Considering the shallow depths of the Azov Sea and currently mastered fields in the Black Sea, it is possible to do without the special tubes designed for off-shore platforms with the wall thickness of 30–40 mm. Mastering the fields at sea depth of more than 100 m will require manufacturing special tubes or buying them abroad.

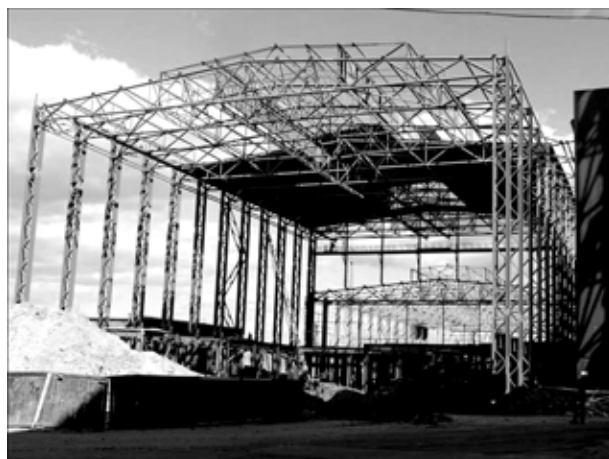


Figure 7. Tubular trusses of covering of a shop of OJSC «Vetropak Gostomel Steklozavod»



Effectiveness of tube application in welded structures greatly depends on their manufacturing technology. One of the labour-consuming processes of manufacturing tubular structures is cutting the element end to size and their subsequent assembly in the connections. These technological operations are greatly simplified when modern machines for gas-oxygen cutting are used.

In Ukraine only two organizations (OJSCs «Ukrstalkonstruktziya» and «V.N. Shimanovsky «UkrNIIproektstalkonstruktziya») have machines for pipe cutting with a six-coordinate numerical control system --- Tubosec «C» of RM 631-1500-5T grade (manufactured by Messer Griesheim, Germany). These machines perform cutting of pipe ends by the preset program, depending on the ratio of diameters of the abutted and main pipes, angle of inclination and wall thickness of the adjacent pipe. Severing of pipe edges for subsequent welding is performed simultaneously. Pipe diameter, which can be cut by this equipment, is equal to 80 to 1500 mm, their length is 700 to 10000 mm, maximum weight of the processed pipe is up to 5000 kg. Such pipe parameters allow using them in a wide range of welded structure types --- from lightweight trusses up to off-shore stationary platforms.

Owing to a high accuracy of the cut edges, machine cutting allows a cost saving during subsequent welding within 10--20 %. Cost advantages of its application in fabrication of tubular welded structures are so significant, that capital depreciation is ensured at one-shift operation and 60 % work load of the machine.

The given review does not completely cover the entire spectrum of tubular welded structures made in Ukraine or with participation of Ukrainian organizations, in the last years. Such structures also include pedestrian overpasses over highways and other design solutions developed recently.

On the other hand, the above data, in our opinion, are indicative of technical capabilities of Ukraine both in terms of design and manufacturing of critical structures using cylindrical tubes. This becomes extremely important in view of the forthcoming implementation of the project of a new safe confinement for the Chernobyl NPP which is a three-dimensional system, the main load-carrying elements of which are arches with 150 m span, consisting of tubular elements. The design and research institutes of Ukraine are quite capable of developing a reliable design of the sarcophagus, and industrial enterprises and organization are quite capable of manufacturing tubes of the required typesizes, fabricating the structures and mounting them.

## CONCLUSIONS

1. Owing to the available scientific potential, considerable experience of the leading project institutes and production facilities, fitted with sufficiently modern

equipment and technologies, in Ukraine all the conditions are in place for a wide use of cylindrical tubes in welded truss structures for different applications.

2. In design and fabrication of welded structures for civil and industrial applications, the optimum tube ratios and butt joint geometries are by far not always used, which is due to the desire to simplify their manufacturing, leading, however, to overconsumption of steel and welding consumables. Application of pipes of a higher and high strength in the tubular structures is not given sufficient attention.

3. A certain factor restraining tube utilization in the structures is absence of national general building standards, reflecting the features of tubular structure design, and in design of off-shore structures, there is a lack of standards specifying their fatigue analysis.

1. Garf, E.F. (2003) Design peculiarities of tubular welded structures. *Tekhn. Diagnostika i Nerazrush. Kontrol*, **4**, 11--17.
2. Shimanovsky, V.N., Garf, E.F., Permyakov, V.A. et al. (1997) *Welded building structures*. Vol. 2: Types of structures. Ed. by L.M. Lobanov. Kiev: PWI.
3. Novikov, V.I., Kovtunenکو, V.A. (1959) Attachment of tubular lattice elements to node gussets. *Avtomatich. Svarka*, **4**, 3--13.
4. Novikov, V.I., Kovtunenکو, V.A., Shumitsky, O.I. (1963) Some problems of design and construction of all-welded tower. *Ibid.*, **5**, 69--74.
5. Novikov, V.I., Kovtunenکو, V.A. (1969) Strength and calculation of welded connections without gussets. *Ibid.*, **9**, 70--71.
6. Hlavacek, V. (1970) Strength of welded tubular joints in lattice girders. *Costruzioni Metalliche*, **6**, 521--529.
7. Nakajima, T., Ishimazu, K., Shimizu, M. et al. (1971) Experimental study on the strength of thin wall welded tubular joints. *IIW Doc. XV-312-71*.
8. Marshall, P.W. (1984) Connections for welded tubular structures. In: *Welding of tubular structures*. Oxford: Pergamon Press, 1--57.
9. Marshall, P.W., Toprac, A.A. (1974) Basis for tubular joint design. *Welding Res. Supplement*, May, 1923--2013.
10. Pan, R.B., Plummer, F.B., Kuang, J.G. (1977) Ultimate strength of tubular joints. *J. Petrol. Technol.*, **29**(April), 449--460.
11. Kurobane, Y., Makino, Y., Mitsui, Y. (1976) Ultimate strength formulae for simple tubular joints. *IIW Doc. XV-385-76*.
12. Garf, E.F., Novikov, V.I., Litvinenko, A.E. et al. (1984) Study of strength and design of cylindrical tubular welded connections at static loading. In: *Welding of tubular structures*. Oxford: Pergamon Press, 359--372.
13. *BS 6235*: Code of practice for fixed offshore structures. Filed 28.09.84.
14. *API RP 2A*: Recommended practice for planning, designing and constructing fixed offshore platform. Filed Jan. 1983.
15. *Rules for the design construction and inspection of offshore structures*. Filed 1985.
16. Reshetnikov, B.N., Rivkin, A.M. (1971) Results of tests of truss frame models of high-strength pipes. *Prom. Stroitelstvo*, **1**, 31--35.
17. Garf, E.F., Tairli, Z.M. (1988) Static strength of welded tubular connections under complex loading. *Azerb. Neft. Khozaystvo*, **10**, 48--53.
18. *VSN 51.3-85*: Design of offshore stationary platforms. Filed 01.01.85.
19. *VSN 51.4-85*: Nodes without gussets in tubular structures of offshore oil-and-gas field constructions. Procedure of strength analysis. Filed 03.06.85.
20. *VSN 41.88*: Design of ice-resistant stationary platforms. Filed 03.01.89.
21. Lebedich, I., Kozyavkin, I. (2007) Construction of «Metalurg» stadium in Dnepropetrovsk. *A + C*, **1**, 160--164.

# ELECTROSLAG SURFACING OF ROTATING KILN GEAR SHAFT TEETH\*

S.M. KOZULIN<sup>1</sup>, I.I. LYCHKO<sup>1</sup> and G.S. PODYMA<sup>2</sup>

<sup>1</sup>E.O. Paton Electric Welding Institute, NASU, Kiev, Ukraine

<sup>2</sup>NTUU «Kiev Polytechnic Institute», Kiev, Ukraine

Described is the experience of application of electroslag surfacing for repair of manufacturing defects in teeth of sub-rim gear shaft of a rotating kiln.

*Keywords:* electroslag surfacing, gear shaft, teeth defects, recovery, involute profile, consumable nozzle, heating temperature, thermal cycle, residual stresses and deformations

Reconditioning of large-sized expensive machine components with application of electroslag welding and surfacing allows a considerable extension of their operating life, as well as decreasing the load on foundry and press shops by reducing the quantity of manufactured spare parts [1]. Repair of defects of parts and units developing during their manufacturing, is the less studied category of repair varieties known in practice.

Defects that were not repairable in accordance with the technology of such items manufacturing existing at the enterprise (Figure 1) were found in two teeth at the final stage of manufacturing the sub-rim gear shaft of a rotating kiln of  $3.6 \times 110$  m at PA «Volgotsemash». Gear shaft (tooth module  $m = 40$ , number of teeth  $z = 21$ , teeth length --- 700 mm, diameter of protrusions --- 920 mm, gear shaft mass --- 4150 kg) was manufactured from a solid forged piece of 34KhN1MA [2] steel and designed for delivery to Nikolaev Industrial Complex of Building Products for mounting into kiln unit.

After teeth cutting an inadmissible lowering of the slot and involute profile was found along the entire tooth length on one of the teeth, on the other tooth a part of the profile was cut away. As a result, the expensive part that passed practically all the stages of machining was found to be a definite reject by the plant Department of Quality Control.

However, the specialists of PWI of the NAS of Ukraine and the Department of the Chief Welder of «Volgotsemash» decided to recondition the rejected gear shaft by applying electroslag surfacing (ESS). ESS technology and special technological fixtures were developed for this purpose. It was necessary not only to ensure the quality of teeth reconditioning, but to also to preserve the geometrical dimensions of the gear shaft. The main objective was to avoid formation of longitudinal residual stresses in

the gear shaft body in the process of ESS that exceed the area of elastic deformations for the given structural material.

Considering that the gear shaft was manufactured from structural alloyed steel with a high content of carbon (0.3–0.4 %) [3], preheating and post-weld treatment is required at teeth reconditioning. Preheating temperatures were determined by well-known procedure described in study [4]. Calculation showed that the metal section of the gear shaft should be heated up to the temperature of 320 °C in surfacing zone. As it is impossible to apply general normalization of the item after surfacing in this case, it was decided to carry out only high tempering as an experiment.

Defective gear shaft was mounted on reusable bases in a strictly vertical position in one of the electroslag welding sections at PA «Volgotsemash». A special device was manufactured for monitoring the shaft bending deformation, where two pointer indicators

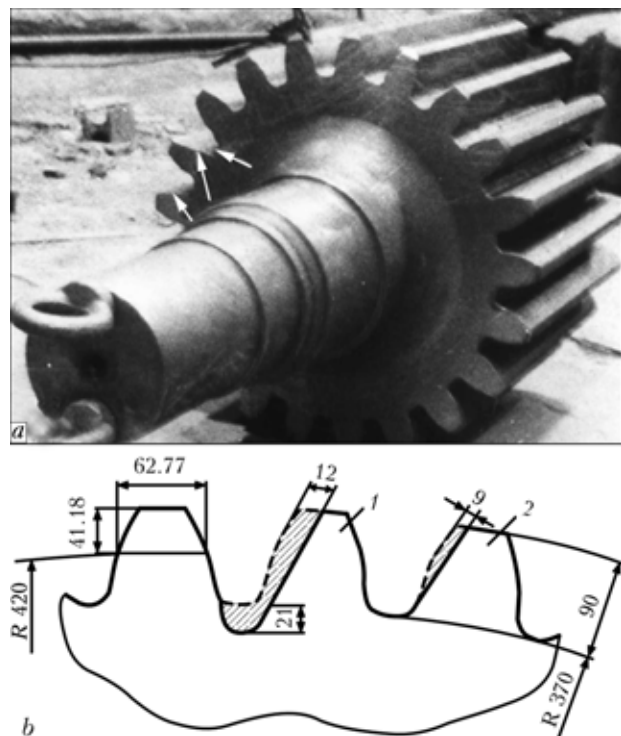


**Figure 1.** Gear shaft of kiln rotating drive with teeth defects formed in their manufacturing (a) and scheme of defects in the teeth (b): 1 --- tooth with lowered slot and cut away part of involute profile; 2 --- tooth with cut away part of involute profile

\* Employees of PA «Volgotsemash» A.P. Syatishev, engineer, D.I. Filchenkov and L.F. Bashev, Cands. of Sci. (Eng.), participated in gear shaft reconditioning.

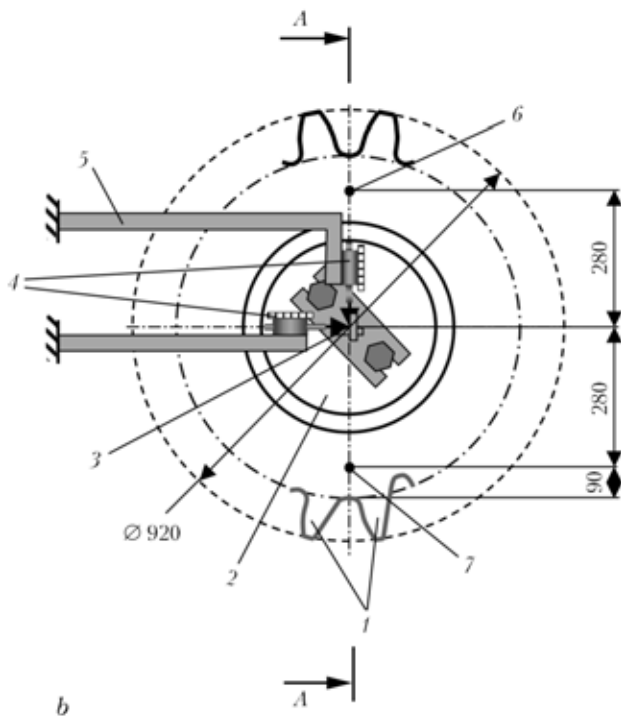
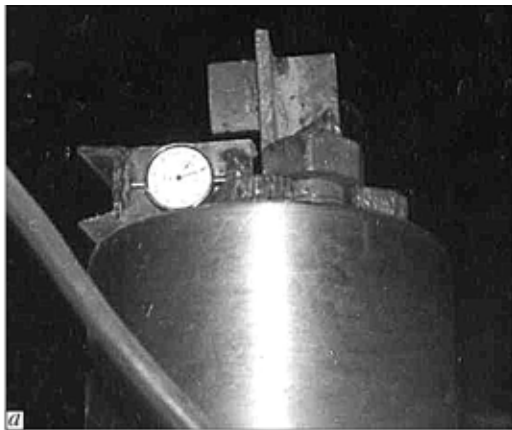


**Figure 2.** Device (a) and scheme for measurement of shaft end face deviation from the vertical axis during teeth surfacing and points of thermocouple mounting (b): 1 — defective teeth; 2 — shaft end surface; 3 — supporting straps; 4 — clock-type indicators; 5 — indicators fastening arm; 6, 7 — spot of placing thermocouples # 2 and 1, respectively

with measuring sensibility 0.01 mm were mounted. It was intended to measure the shaft axis deviations in horizontal plane on the level of the upper shaft end (Figure 2). One indicator fixed deviations in the plane passing in the middle of the slot located between the defective teeth, the second — the deviations in the perpendicular plane. Chromel-alumel thermocouples (Figure 2) were calked in the diametrically located sections on the end surface in the area of slot diameter to control the degree of gear body overall heating, as well as for temperature differences supervision. Automatic KSP-4 recorder performed temperature recording.

Considering that the tooth defects were located only on one side of the involute profile, it was decided not to remove the defective tooth body as it was usually done [1], but to perform one-sided surfacing of



**Figure 3.** Fragment of sub-rim gear shaft teeth recovery ( $m = 40$ ,  $z = 21$ ) with ESS application

each tooth with subsequent reconditioning of the working profiles using a modular milling cutter in a gear milling machine. Special technological fixture was manufactured for conducting the reconditioning work: a post with an outer support for holding the clock-type point indicators, plate with supporting straps, copper water-cooled coverplates of a special configuration, graphite crucible, graphite electrode with an electric holder, bottom trough and other.

In order to form the cavities for surfacing, water-cooled coverplates were mounted in parallel to the planes of the cut-off teeth profiles and changeable water-cooled coverplates were mounted at definite angle to them from the side of the tooth tops. The forming fixture was attached to the inlet and outlet pockets located on the tooth end parts to preserve the working surfaces of the teeth located next to the defective teeth. The beginning of electroslag process was performed by the «liquid» start technique for providing a guaranteed fusion in the lower (end) sections of the teeth, as well as required depth of the slag pool. For this purpose a bottom trough was mounted in the inlet pockets, through which strictly dosed portions of the liquid flux were poured in. The flux was melted in a graphite crucible using a graphite electrode. Surfacing was performed by a consumable nozzle using A-645 machine and TShS-3000-3 transformer (Figure 3). Consumable nozzle plates were manufactured of 34KhN1MA steel, using Sv-10G2 welding wire and AN8M flux. ESS conditions were calculated taking into account the recommendations given in study [1]. Preheating of the gear shaft was performed by a powerful flame torch of plant design using natural gas. Shaft neck surfaces accommodating the bearings were covered by asbestos cloth for preserving them from damage during tooth reconditioning. Experimental data of residual deformation measuring obtained at ESS of medium-carbon steels [5] were used, in view of the absence of a practical calculation method of anticipated deformations of items as a result of trans-

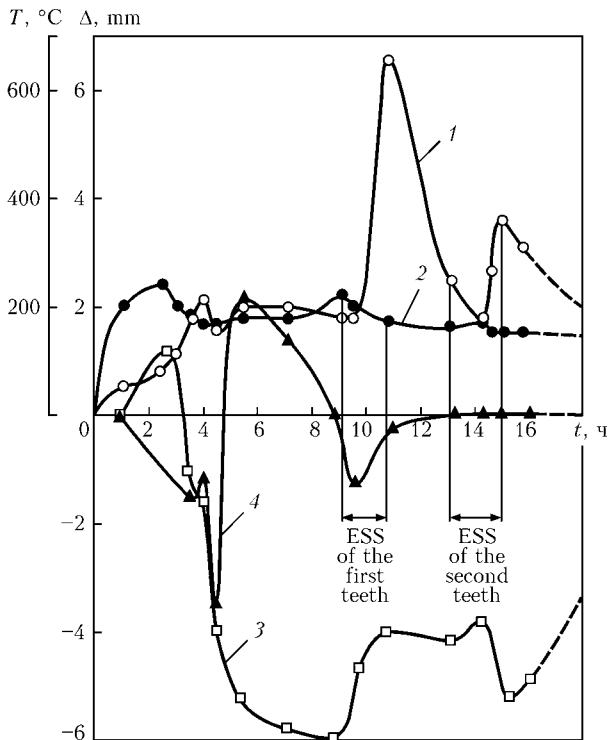


**Figure 4.** Thermal cycles of gear shaft heating in the spots of thermocouple placing and deviation of the shaft cantilever part from the vertical axis during preheating of gear shaft and repair of defects in teeth (see Figure 2): 1, 2 — metal heating in the spot of placing thermocouple # 1 and 2, accordingly; 3 — deviation in plane A-A passing between the repaired teeth; 4 — deviations in perpendicular plane A-A

verse and longitudinal shrinkage of the deposited metal.

Overall preheating of the gear shaft was done before tooth surfacing. Heating temperature and deformations values were controlled by thermocouples and clock-type indicators (see Figure 2). Flame torch was placed from the side of the defective teeth before surfacing for compensation of longitudinal shrinkage influence on geometrical sizes of the item, and local heating of treated surfaces up to the specified temperature was performed, the upper shaft end surface deviating to the side opposite to surfacing zone by 6 mm. The nature of thermal cycles of metal heating in the spots of thermocouples placing in combination with gear shaft vertical axis deformations caused by preheating and directly by ESS is given in Figure 4.

To eliminate the possibility of partial quenching of the end surfaces of the surfaced teeth, cutting off of the top sections by oxy-gas cutting was performed immediately after ESS. Top sections were cut off not completely, leaving the protruding sections of 15–20 mm high for their further machining. Then, the gear shaft was placed for not more than 30 min into the electric furnace heated up to 350 °C with drawout bottom for conducting high-temperature tempering. In the furnace, the gear shaft was placed on steel bases in the vertical position. Tempering was carried out in the following mode: heating up to 650 °C with the speed not higher than 50 °C/h, soaking during 8 h, cooling with the kiln up to the temperature of 80 °C.

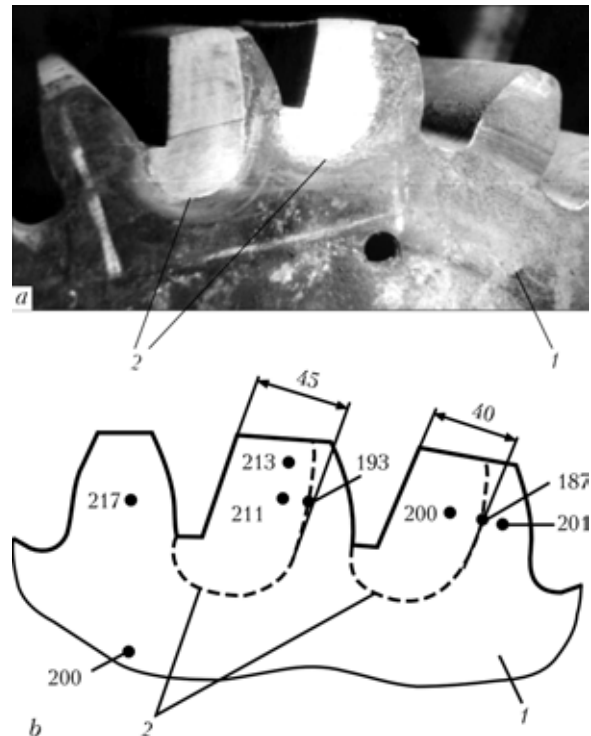


**Figure 5.** Appearance of end parts of the teeth after ESS and machining of top sections (a) and scheme of the shape and depth of teeth penetration (b): 1 — gear shaft end; 2 — penetration shape; spots and values of HB hardness are shown by dots

After complete cooling of the gear shaft, machining of deposited end faces of the teeth was carried out in lathe DIP-500 to the sizes shown in the drawing. Appearance of end faces of the surfaced teeth, penetration shape and results of hardness measurement performed with Poldy device, are shown in Figure 5. The results of ultrasonic testing of the surfaced teeth showed absence of defects in the deposited metal of the teeth and in the HAZ metal of gear shaft. Deposited metal hardness differed from the hardness of soft sections by not more than 8 %, that confirmed the correct choice of welding consumables.

Reconditioning of involute teeth profiles was performed by the standard modular milling tool in the gear-milling machine. Then the gear shaft was placed into the lathe. Control measurements of flange diameters and shaft journals for bearings, as well as radial run-outs of shaft sections were done with the clock-

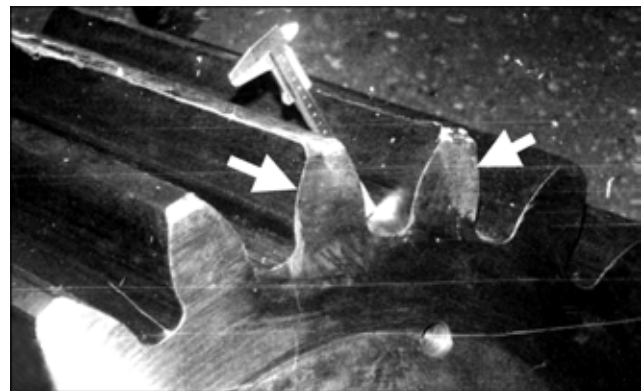


**Figure 6.** Appearance of teeth deposited by ESS after their machining in the gear-milling machine



type indicator and measuring clamps. Measurements showed that run-out of the teeth top surfaces (except for the recovered ones) do not exceed 0.1 mm along the entire length (admissible run-out is 0.15 mm), shaft journals run-out --- 0.05 mm (admissible value is 0.05 mm). Shaft diameters are also within the limits of admissible values [2]. Thus, shaft bending after ESS of two teeth turned to be minor. The height of the surfaced teeth and two adjacent ones decreased by 0.9–1.0 and 0.4–0.5 mm, respectively, compared with the drawing dimension. However, specialists from the Department of Quality Control of plant-manufacturer decided that such a minor decrease of teeth height will not impair their performance.

After hardening of the working surfaces, the gear shaft was recognized to be fit-for-service (Figure 6) and sent to Nikolaev Industrial Complex of Building Products, where it successfully operated for the specified service life.

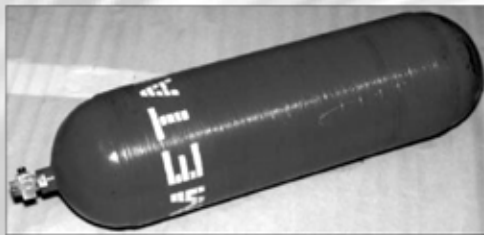
## CONCLUSIONS

1. Technology and technique were designed and successfully realized for repairing manufacturing defects of major module teeth ( $m = 40$ ,  $z = 21$ ) of sub-rim gear shaft by ESS method without subsequent high temperature treatment.

2. The results of performed work confirm that ESS is an effective method for repairing practically any defects formed in manufacturing or operation of major module gear shafts.

1. Sushchuk-Slyusarenko, I.I., Lychko, I.I., Kozulin, M.G. et al. (1989) *Electroslag welding and surfacing in repair work*. Kiev: Naukova Dumka.
2. OST 22-785-74: Girth gears and crowned gears of rotary kilns. Moscow: TsNIIEStroj mash.
3. (1989) *Reference book on steel and alloy grades*. Ed. by V.G. Sorokin. Moscow: Mashinostroenie.
4. Zemzin, V.N., Shron, R.Z. (1978) *Heat treatment and properties of welded joints*. Leningrad: Mashinostroenie.
5. (1980) *Electroslag welding and surfacing*. Ed. by B.E. Paton. Moscow: Mashinostroenie.

## AUTOMOBILE LIGHT-WEIGHT HIGH-PRESSURE CYLINDERS



At the E.O. Paton Electric Welding Institute a technology has been developed for manufacture of light-weight metal-plastic automobile welded cylinders, reinforced by a composite material.

They represent a combined structure, composed of a thin-walled welded sealed casing of a cylindrical shape with spherical bottoms, reinforced by a glass-reinforced plastics in a cylindrical part.

The reinforcement is realized by the method of a circular winding of a glassy roving, impregnated by a binder on the epoxy resin base.

The casing consists of a welded shell and stamped bottoms of alloyed high-strength steel.

- working pressure 20 MPa;
- strength safety factor  $> 2.6$ ;
- coefficient of mass perfection 0.6 kg/l;
- not less than 24,000 fillings at working pressure 20 MPa;
- splinter proof fracture at pressure of not less than 52 MPa;
- splinter proof fracture of filled cylinder in shooting with a 7.62 mm bullet;
- service life — 15 years;
- periodicity of inspection — 5 years.

**Purpose.** Cylinders are designed for storage and transporting of compressed natural gas and mounted in luggage compartments of motor cars and in special places of trucks and buses which use compressed natural gas (methane) as a motor fuel.

**Proposals for co-operation.** Development of designs of cylinders of required geometric sizes using Customer's material. Manufacture and testing the experimental samples. Implementation of technology of manufacture at the Customer's enterprise.

Contacts: Savitsky M.M.  
E-mail: savitsky@paton.kiev.ua

# PROCEDURE FOR REPAIR OF BLADES OF TITANIUM ALLOY VT3-1 BY ELECTRON BEAM WELDING

V.I. ZAGORNIKOV

E.O.Paton Electric Welding Institute, NASU, Kiev, Ukraine

Procedure for repair of complex-configuration titanium blades 1–2 mm thick in the welded joint location by using EBW is considered. The software program was developed for achieving the high-efficiency welding parameters (with speed of up to 50 mm/s) to provide quality weld metal. Refusal from heat treatment outside the welding vacuum chamber to provide the required quality of the titanium blades repaired by EBW is substantiated.

*Keywords: electron beam welding, titanium alloy, small thicknesses, repair method, high productivity, welding conditions, metallographic examinations*

Reported [1, 2] is the positive experience of using electron beam welding (EBW) for repair of steam turbine blades. The jet compressor blades made from heat-resistant titanium alloys require the high accuracy of fit-up of the parts to be butt welded and the minimal degree of buckling after welding. The EBW method meets all these requirements and is characterised by a number of technological peculiarities, which make it indispensable for manufacture of such parts [3–6]. Minimal heat inputs and distortions provide retention of the initial geometry of the repaired thin-wall blades and the satisfactory quality of the weld.

This article describes the procedure for repair of gas-compressor turbine blades made from titanium alloy VT3-1. The choice of the EBW method was based on the requirements for high efficiency and high operational reliability of such parts. The domestic experience of application of EBW for this type of parts having small thickness is very limited. Therefore, it was necessary to conduct a package of research to determine conditions providing the quality repair of complex-configuration blades of titanium alloys. It should be noted that available was the positive experience accumulated with application of EBW for thick-walled (up to 20 mm thick) forged billets of alloy VT3-1 [7]. Technological peculiarities of using EBW for joining thick-walled (100–160 mm) parts of titanium alloys, related to heterogeneity of the welds through thickness, are considered in study [8].

Our study relates to making sound EB welds on a thin-walled (1–2 mm) complex-configuration workpiece at a substantial ( $\geq 50$  mm/s) welding speed without heat treatment conducted outside the vacuum chamber and without the use of filler material. Moreover, it was necessary to make the welds of a small width, commensurable with thickness of a workpiece welded ( $\delta \leq 1$  mm). It was expected that there would be no inadmissible undercuts on the face and reverse side of the weld. To provide the full strength of the

workpiece (blade) through thickness, the shape of the weld walls in a cross section had to be close to parallel.

The repair consisted in cutting off of a defective part of the blades, and welding on of a new part of the airfoil of the same material as the blade material. The weld on the blade was located in the area of minimal vibration loads. Thickness of the blade can be restored by electron beam evaporation of metal of the same chemical composition as the blade material.

EBW was performed with a vertical beam in the flat position using small-size unit SV-112 with electron beam gun ELA 60/15. The work distance was 100 mm. The workpiece was secured in a special fixture for welding thin-walled curvilinear surfaces (blade elements) by maintaining minimal assembly gaps in a joint and in a location of tabs (Figure 1).

The experiments were first conducted at a welding speed of 15–25 mm/s. However, the substantial difference between the EBW speed and movement of the electron beam across the joint made it impossible to correctly guide the beam to the joint during welding. Later on we had to refuse from adjustment of the beam. So, EBW was carried out by the averaged position of the beam along the entire length of the joint, which was determined beforehand and fixed in the welding program. Removal of the above limitations on positioning allowed us to perform EBW at a speed of 50 mm/s, which was recommended for welding

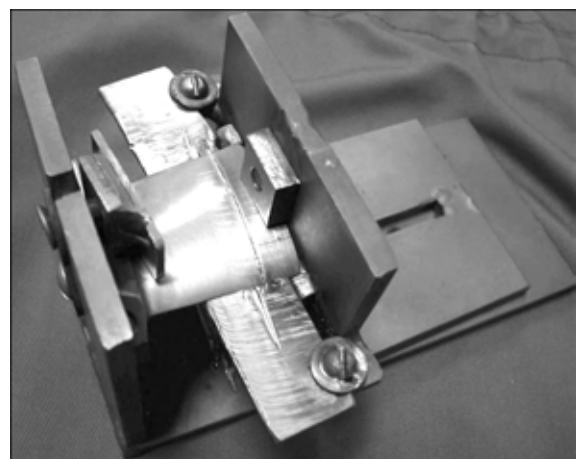
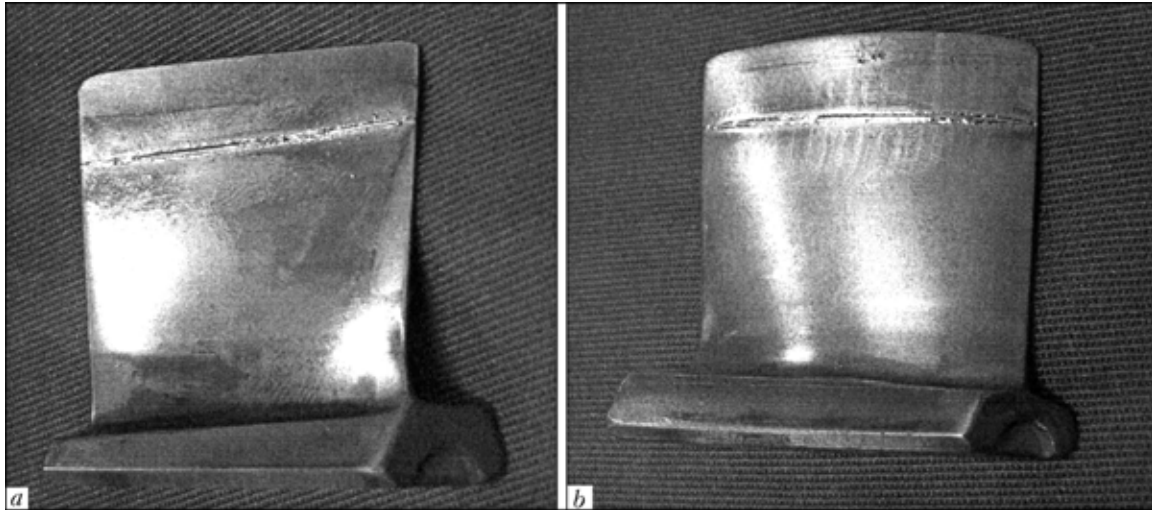


Figure 1. Assembly fixture for EBW of titanium alloys



**Figure 2.** Appearance of blade with repair weld: a — face side; b — reverse side

joints of a small thickness (0.8–1.6 mm), requiring minimal heat inputs [9].

Because the joint had a cross section varying through thickness, it was necessary to change the beam current at the blade input-output in the welding program. The focusing lens current was left unchanged. In EBW of experimental samples with normal focusing (by the minimal focal spot on the workpiece surface), we produced welds with the walls in a cross section close to wedge-shaped, which was intolerable in our conditions. It was decided to perform EBW with re-focusing of the beam, which provided the weld with almost parallel walls through the entire thickness of a workpiece, and with a relatively wide flush penetration and insignificant reinforcement. That levelled the risk of latent lacks of penetration related to inac-

curacies of fit-up or guiding of the beam to the joint. Decrease in the weld reinforcement at thin ends (0.5–0.6 mm) of the blades and insignificant undercuts formed on the face side of the penetration (Figure 2), caused by a high rate of the transient process of welding, were removed where necessary by making decorative local passes.

A more labour-intensive welding technique was used to produce welds of the required shape. To avoid probable undercuts and weld thinning in the transient mode of EBW, the input-output of the welding current at the blade ends was done at a minimal possible length of the weld, and the values of the current were selected on the basis of thickness of the joint region being welded. The rate of rise of the welding current and location of its input-output were determined ex-

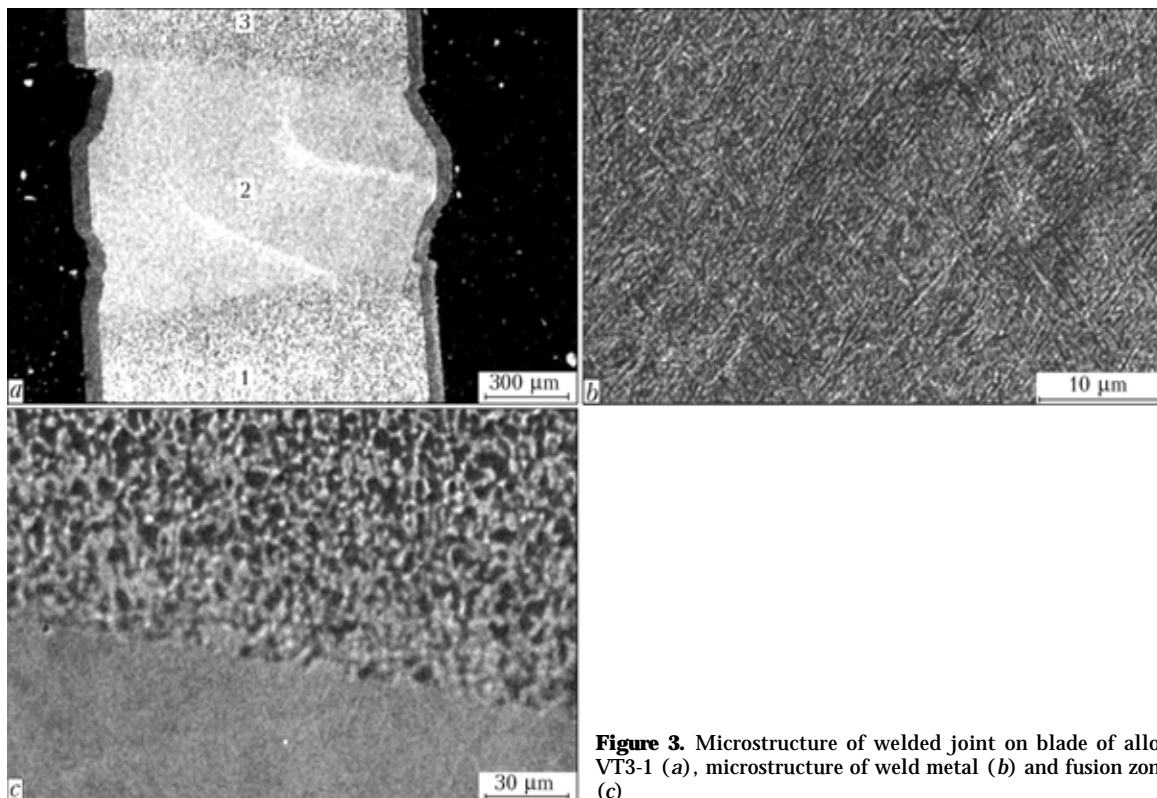


**Figure 3.** Microstructure of welded joint on blade of alloy VT3-1 (a), microstructure of weld metal (b) and fusion zone (c)

Content (wt.%) of main chemical components of the EB weld made on blade of alloy VT3-1

Weld region	Spectrum of analysis at points acc. to Figure 3, a	Al	Si	Ti	Cr	Fe	Mo
Base	1	6.48	0.62	89.18	0.16	0.14	3.42
Weld	2	6.44	0.43	89.46	–	0.13	3.53
Base	3	6.07	0.58	89.74	–	–	3.62

perimentally and fixed in the EBW program. The welding current in the main region of the weld was 30 mA.

Pulsed EBW with a frequency of 25–100 Hz and on-off time ratio of 1:4 was tried out as an alternative. With this welding method, the inconsistent formation of a wedge-shaped weld with incomplete filling of metal (voids in the weld root) occurred in some cases. It is likely that realisation of advantages of the pulsed welding mode at a high speed and through penetration is problematic.

Different methods were suggested in many studies [7, 9, 10] to improve performance of the welds on titanium alloys of the VT3-1 type (heat resistant  $\alpha + \beta$ -alloys), such as heat treatment, use of adapters of less strong and more ductile materials, or addition of alloying elements and modifiers to the weld metal. Because of high labour intensity of the above methods, they have almost no commercial application abroad. Only annealing is employed in a number of cases. The required mechanical properties of the welded joints and removal of structural heterogeneity are provided by optimising the thermal-deformation cycle of EBW.

Certain difficulties in providing the full-strength EB welds may arise because of their drastic cooling after the thermal welding cycle (with a substantially higher rates in the near-weld zone (HAZ), compared, for example, with argon-arc welding). At the same time, overheating of the weld and HAZ on titanium  $\alpha + \beta$ -alloys of the martensitic type may have a negative effect on the grain size of metal, state of grain boundaries and, therefore, impact toughness. That is why one should take care when using preweld and/or postweld heat treatment to provide high mechanical properties of the EB welded joints. Upon evaluating performance of the resulting welded joints under operating loading, it is possible to fully refuse from the heat treatment performed outside the welding vacuum chamber.

Owing to the optimised EBW procedure, in this study we produced the defect-free joints with an acceptable structure of the HAZ metal.

Microstructure of a cross section of the welded joint on a blade is shown in Figure 3, a. Width of the weld metal is no more than 1 mm. Structure of the weld metal is characterised by a grain size of 30–60  $\mu\text{m}$ . The weld metal has a martensitic structure (Figure 3, b) with microhardness  $HV$  4140 MPa. Microhardness of the HAZ region (Figure 3, c) is  $HV$  3090 MPa. The base metal has microhardness  $HV$  3090 MPa. Width of HAZ, where decomposition of the oversaturated solid solution took place due to the thermal effect, was 30–50  $\mu\text{m}$ .

Investigation of chemical composition of the EB weld showed that there was no chromium in the weld region (Table). Most probably, it sublimates from the melt during the welding process.

Investigations of mechanical properties of the resulting welded joints show that this procedure of repair EBW can be recommended for commercial application.

- Zhivaga, L.I., German, S.I., Levenberg, N.E. et al. (1981) Electron beam welding of steam turbine vanes. In: *Proc. of 7th All-Union Conf. on Electron Beam Welding* (Kiev, 8–11 Dec., 1980). Kiev: PWI, 37–40.
- German, S.I., Levenberg, N.E., Sitnitsky, A.A. et al. (1981) Application of electron beam welding for recovery of steam turbine blades. *Ibid.*, 40–41.
- Zhemanyuk, P., Petrik, I. (2001) Main tendencies in development of welding production at Open Joint Stock Company «Motorsich». Problems and prospects. *Dvigatel*, 3 (May–June), 30–32.
- Bykov, I., Kresanov, I. (2001) Advanced processes of metallurgical production as a basis of high quality product assurance. *Ibid.*, 28–29.
- Zhadkevich, M.L., Bondarev, A.A., Zelenin, V.I. et al. (2002) Technology of restoration of gas turbine blades. *The Paton Welding J.*, 2, 52–53.
- Gajkin, V. (2003) Perfection of engines is determined by perfection of technology. *Dvigatel*, 6, 11–16.
- Balabanov, V.A., Kovalev, V.V., Lupyri, V.F. et al. (1981) Comparative investigations of electron beam and arc welding of structures from forged billets of titanium alloy VT3-1. In: *Proc. of 7th All-Union Conf. on Electron Beam Welding* (Kiev, 8–11 Dec., 1980). Kiev: PWI, 55–58.
- Ardentov, V.V., Shestakov, A.I., Petrenko, V.R. et al. (1981) Technological peculiarities of producing quality electron beam welds on titanium alloy plates. *Ibid.*, 106–109.
- (1987) *Technology of electron beam welding*. Ed. by B.E. Paton. Kiev: Naukova Dumka.
- Kurochko, R.S., Ioda, A.V., Khorev, M.A. (1982) Heat treatment of welded joints made on alloy VT-23 by electron beam welding. *Aviats. Promyshlennost*, 5, 58–59.

# SAFE LEVEL OF ELECTROMAGNETIC FIELD INTENSITY IN RESISTANCE WELDING

O.G. LEVCHENKO and V.K. LEVCHUK

E.O. Paton Electric Welding Institute, NASU, Kiev, Ukraine

Sources and shapes of signals of the magnetic fields, generated by resistance welding equipment, have been analyzed to perform their reliable hygienic evaluation in line with new standards of Ukraine. Results of investigations of spectral composition and intensity of the magnetic fields, generated using different resistance welding methods, are presented. Recommendations for protection of welders against magnetic fields are suggested.

*Keywords:* resistance welding, electromagnetic radiation, magnetic fields, intensity, spectral composition, maximum-permissible levels, protection of welders

Wide application of resistance welding in automobile, aviation, electron and other branches of industry of Ukraine caused creation of a big stock of electric equipment and welding machines (mainly designed for alternating current of 50 Hz) of different types and designation, having power more than dozens and hundreds kilovolts per ampere. During operation of this equipment in working places of welders magnetic fields (MF) of significant intensity (up to 80 kA/m) are generated.

Lately special attention is paid to harmful action on organism of electromagnetic fields (EMF) [1–4]. One of the groups of workers, subjected to action of EMF of high intensity, are welders. It should be noted that in relation to a welding process only magnetic component of EMF is of sanitary-hygienic significance [5].

Sources of the radiation are a welding transformer that is not completely screened by housing of the machine and, as a rule, non-screened high-current elements of the welding circuit (arms, plugs, electrodes). Results of previously carried out investigations proved local formation of dissipation MP near resistance machines. Welding equipment may be located close to a welder, and welding cables may be in direct contact with his body (in case of welding using manual tools in the form of tongs, guns, etc.). Long action of mentioned factor negatively affects health of workers and causes certain functional changes in the organism. EMF may affect cardio-vascular system and cause pathological changes in nervous, endocrine and other systems. The data also exist that prove carcinogenic character of EMF action. In this connection since long exists acute need in constant check of electromagnetic situation at the working place of welders and ensuring of safe conditions of their work.

Recently in connection with introduction in Ukraine of new norms DSN 3.3.6.096–2002 [5] (which regulate conditions of safety in work with constant MF; constant MF, created by rectified three-phase current; alternative MF of 50 Hz frequency; EMF within the range 1 kHz–300 MHz and pulsing

EMF within spectral range of 0–1000 MHz frequencies) the need occurs to measure and evaluate MF signals taking into account their spectral composition.

The goal of this work is to make on basis of analysis of the shape and intensity of the MF signals adequate hygienic evaluation of electromagnetic safety when using main methods of resistance spot welding and determine required efficiency of protection against these fields.

**Character of MF in resistance welding.** One of the main factors of MF origination in resistance welding is the kind of the power source current (alternating or direct one), stored energy (capacitor, induction welding, etc.), and conditions of welding.

The greatest influence on selection of welding conditions exerts electric and heat conductivity of the metal being welded. Electric conductivity determines necessary for welding value of current, while heat conductivity — duration of heating and compression force.

Properties of a metal may significantly change in heating. Need in welding materials with different thermophysical properties stipulates following conditions of resistance welding: single pulse (welding pulse); two-pulse (first pulse is an additional preheating one) — «soft» conditions of welding (duration of welding is approximately 3.5 times longer); three-pulse (two additional pulses: preheating + annealing ones); conditions for thick sheets with free cooling; welding by modulated pulse of current.

Very thin components ( $\leq 0.25$  mm) are welded under especially rigid conditions with duration of welding less than 0.01 s. Rigid conditions are ensured on capacitor machines. Main and additional pulses of current have independent adjustment and they may be fed with a pause or without it. Main pulse has modulation of leading edge  $t_1 = 0.025$  s;  $t_w = 0.03$ – $0.07$  s.

Seam and relief welding are similar to the spot one and have the same modes. However, seam welding has in addition step and continuous modes when welding current may be fed by pulses with long pauses or without the latter.

The most widely used carbon or medium-alloy steels have relatively low electrical resistance. Such steels are welded at the long flow of current, value of which achieves 25 kA. In welding of non-ferrous

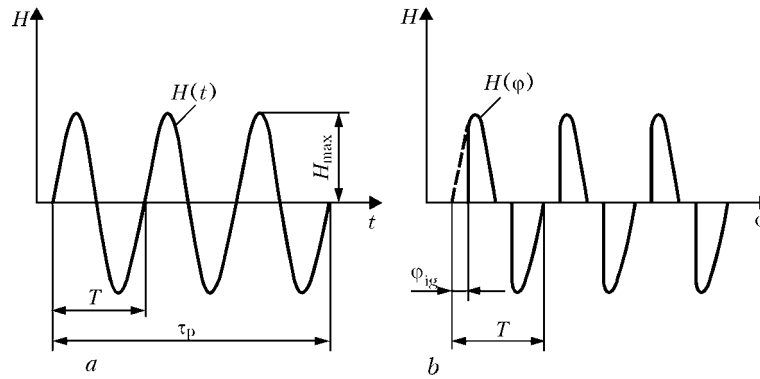


**Figure 1.** Shape and characteristics of radio pulse signals of single-pulse MF: *a* — regulation of pulse-welding current duration; *b* — phase regulation of current (designations see in the text)

metals and their alloys of the same thickness even higher values of current are needed.

Analysis of the welding circuit shape of the machines shows that it may be attributed to one of the classes of geometric figures. In particular, for considered resistance welding machines it represents a non-closed on one side rectangle, and cables of a suspended spot machine — two parallel lines. Main geometrical dimension of the radiation source configuration for the rectangle is half of the distance between the conductors. Working area of a welder (operator) is determined relative welding circuit of the machine by conditions of its work and technological process of processing of the items.

Presence in the welding current circuit of a variable parameter («welding spot» resistance) predetermines transformation (change) of the input signal (spectrum); shape of the MF signal is completely determined by shape of the welding current curve.

*Single-pulse spot and relief welding by alternating current of 50 Hz frequency.* In welding by alternating current of 50 Hz frequency MF are formed, which have shape of radio pulses (Figure 1). Radio pulse is a series of high-frequency oscillations, which may be represented as a result of 100 % amplitude modulation of high-frequency oscillations by a video pulse. Electric equipment of the welding mode control envisages in this case, as a rule, adjustment of the welding current pulse duration  $\tau_p$ , phase adjustment of current (Figure 1, *b*), and modulation of leading and falling edges of the pulses.

It should be noted that it was admitted in previous sanitary norms [6] that MF radio pulses that are created in resistance welding with application of alternating current of 50 Hz frequency have insignificant distortions due to transition processes in the welding machine and variable resistance in the molten metal. It was also assumed that comparatively long duration of these pulses ( $\tau_p > 0.02$  s) and insignificant changes of the sinusoid shape allow not taking into account composition of the spectrum, considering that main part of the field energy is concentrated in area of low (up to 50 Hz) frequencies (from zero to  $f = 1/\tau_p$ , 90 % of the whole signal energy is contained). Nowadays hardly these assumptions may be considered correct.

It is also known that the pulse spectrum in the shape of the sinusoid section, which consists of several periods  $n$ , is determined by the expression [7]

$$H_{xx} = \int_0^{nT/2} e^{-j\omega t} \sin \omega_0 t dt = 2S_{xx} \int_{-nT/2}^{nT/2} e^{-j\omega t} \sin \omega_0 t dt = \frac{4j\omega_0}{\omega_0^2 - \omega^2} (-1)^n \sin n\pi \frac{\omega}{\omega_0}, \quad (1)$$

where  $H_{xx}$ ,  $S_{xx}$  are respectively the single- and the two-side spectral density of the MF intensity amplitude;  $T$  is the period of oscillation;  $\omega$  is the circular frequency;  $n$  is the number of the sinusoid periods after switching on.

Actually this is a current single-side spectrum of the sinusoid (Figure 2). Spectral density of the amplitude at frequency  $\omega = \omega_0$  (50 Hz) increases in time linearly according to the expression

$$H_{xx_n} |_{\omega = \omega_0} = n \frac{T}{2}, \quad (2)$$

i.e. at beginning of the process the spectrum is homogeneous (contains big number of harmonics) and just gradually forms maximum at the frequency  $\omega = 0$ .

*Multipulse seam (two- and three-pulse spot and relief) welding using alternating current of 50 Hz frequency.* The MF pulses, formed in welding in this case, are repeated in a certain interval of time and form in seam welding repeating series, which are called pulse packets. Originated sequence of radio pulses (Figure 3, *b*) may be presented as result of change of the enveloping high-frequency oscillation according to the sequence of video pulses (Figure 3, *a*).

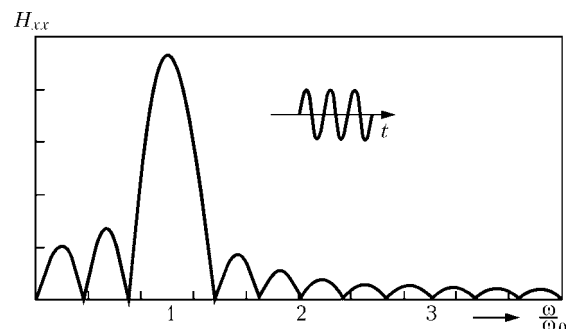


**Figure 2.** Spectrum of sinusoid section (phase distributions)

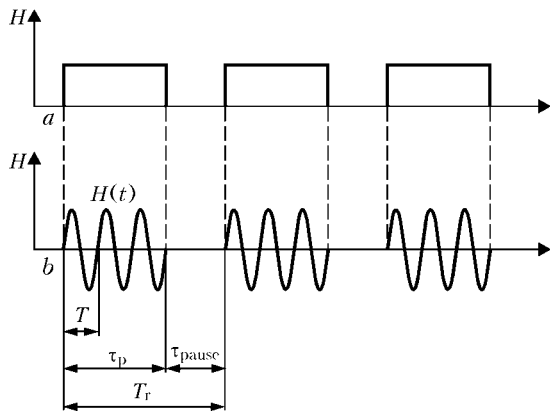


**Figure 3.** Shape and characteristics of radio pulse signals of multiple MF: a — character of change of envelope of radio pulses; b — packet of MF radio pulses in multipulse seam welding

Such modulation is frequently called the pulse one. However, in this case takes place not modulation, but switching on of the welding current source at the instants of origination of the pulses and its switching off at the instant of their cessation. The fact that at the beginning of each pulse oscillation is established anew exerts significant influence on spectrum of succession depending upon the period of repetition of the pulses  $T_r$  and  $Q$ -factor  $Q = \tau_{\text{pause}} / \tau_p$ , where  $\tau_{\text{pause}}$  is the pause time.

If occurring in the considered methods of welding and shown in Figure 3, a sequence of radio pulses is periodic and initial phases of high-frequency filling of the radio pulses (Figure 3, b) are the same («tied» to the front), then due to the modulation sequence of radio pulses is produced, which represents periodic function of time with a period, equal to the period of repetition  $T_r$  of the video pulses. Spectrum of such oscillation, containing frequencies multiple to frequency  $\omega$  of video pulses, is shown in Figure 4.

Like in considered above case of spot welding, electric equipment of the welding machine control ensures adjustment of the pulse duration  $\tau_p$ , phase regulation of current  $\tau_{\text{ig}}$  (see Figure 1, where  $\tau_{\text{ig}}$  is the angle of ignition of force thyristors), and modulation of leading and falling edges of the pulses.

**Capacitor-type welding.** In welding using direct current and stored energy the pulses of MF are created that have shape of video pulses. Video pulses are the increase of the amplitude of positive or negative polarity from zero to maximum and then its reduction to zero (Figure 5). Shape of a video pulse may be

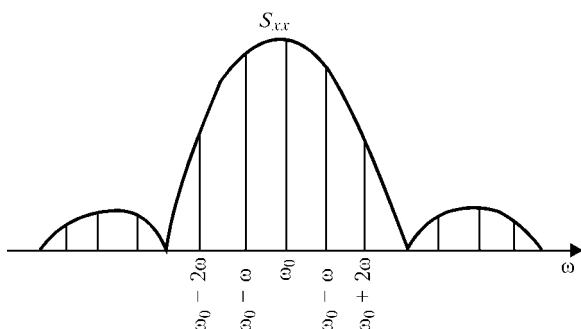


**Figure 4.** Spectrum of multipulse welding

different: triangular, step- and bell-like, whereby the pulses may be single (in spot welding) and may be repeated in a certain time interval (in seam welding).

Main time characteristics of a pulse MF is duration of a pulse  $\tau_p$ , duration of a pause  $\tau_{\text{pause}}$  and a period of repetition  $T_r$  ( $Q$ -factor  $Q = \tau_{\text{pause}} / \tau_p$ ). In addition, a pulse is characterized by duration of the leading edge  $t_l$  and of the fall  $t_f$  — time of increase and reduction of intensity within the range from  $0.1H_m$  to  $0.9H_m$ . Steepness of the edge characterizes speed of increase and reduction of the MF intensity respectively:  $S_l = H_m / t_l$ ,  $S_f = H_m / t_f$ .

MF, formed in welding using direct current and stored energy, are non-periodic and their form differs significantly from the harmonic one. Spectrum, formed by such signals, depends upon duration of the pulses and their edges, and is determined by the expression

$$S_{xx}(j, \omega) = \int_{-\infty}^{\infty} H(t) e^{-j\omega t} dt, \quad (3)$$

where  $S_{xx}(j, \omega)$  is the two-sided spectral density of the MF intensity;  $H(t)$  is the MF intensity.

Reduction of the pulse duration and increase of the edge steepness causes expansion of the spectrum in the area of high frequencies. In Figure 6, a theoretical spectrum of a single exponential pulse in capacitor welding is shown, in Figure 6, b — appearance of spectrum of the packet from three similar pulses at interval between the pulses  $T_r = 3\tau_p$ . Dash lines show spectral density of a single pulse. By means of increase of number of pulses  $n$  in the packet spectral density splits more and more and at  $n > \infty$  assumes linear structure of the spectrum of periodic function. This provision also relates to the multipulse welding.

So, presented analysis of the considered technologies and welding equipment shows that interrupted-pulsed MF are formed in welding in this case in the working zone, i.e. the fields, which within a certain period of time differ from zero value and stochastically repeat. Intensity of radiation of those working depends upon the type of used welding equipment (amplitude and duration of the welding current pulse, duration of a pause, number of cycles, duration of leading edges of the pulses, phase adjustment,  $\cos \varphi$ , etc.), geometric dimensions and configuration of the MF sources, and arrangement of working places relative these sources.

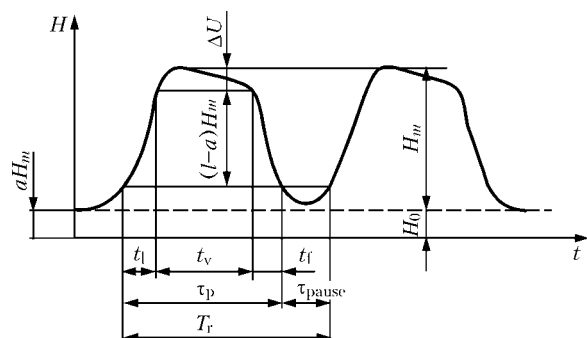


**Figure 5.** Shapes and parameters of MF video pulse signals



**Normalization of MF.** Maximum permissible levels (MPL) of intensity of pulsed fields within spectral range of frequencies from 0 Hz to 1000 MHz are determined at working places proceeding from permissible energy load and period of action by the formulas:

$$E_{MP} = \sqrt{EH_{E_{MP}}/T}, \quad (4)$$

$$H_{MP} = \sqrt{EH_{H_{MP}}/T}, \quad (5)$$

where  $E_{MP}$  and  $H_{MP}$  are the MPL of intensity of electrical (V/m) and magnetic (A/m) fields;  $T$  is the time of action, h;  $EH_{E_{MP}}$  and  $EH_{H_{MP}}$  are the maximal permissible values of energy load of respectively electrical  $((V/m)^2 \cdot h)$  and magnetic  $((A/m)^2 \cdot h)$  fields within a working day.

Maximum permissible amplitude values of MF intensity within spectral ranges of frequencies are determined by Table 1.

If within frequency range below 300 MHz operate sources, for which different MPL are established, it is necessary to observe following requirements:

$$\frac{E_1^2}{MPL_1^2} + \frac{E_2^2}{MPL_2^2} + \dots + \frac{E_k^2}{MPL_k^2} + \frac{H_1^2}{MPL_1^2} + \frac{H_2^2}{MPL_2^2} + \dots + \frac{H_k^2}{MPL_k^2} + \frac{W_1}{MPL_1} + \frac{W_2}{MPL_2} + \dots + \frac{W_k}{MPL_k} \leq 1. \quad (6)$$

For considered in this article cases expression (6) takes the form

$$\frac{H_1^2}{MPL_1^2} + \frac{H_2^2}{MPL_2^2} + \dots + \frac{H_k^2}{MPL_k^2} = \sum_n \frac{H_{mk}^2}{MPL_k^2} \leq 1. \quad (7)$$

Permissible duration of welding  $T_{w.p}$  is determined from formulas (5) and (7).

When performing experiments at this stage of the works the following prerequisites were taken into account. General character of MF propagation around a circuit with the configuration, shown in Figure 7, is known. In Figure 8 intensity of MF is presented in the form of lines of equal total intensity  $H_0 = H_{x,y,z} = \sqrt{H_x^2 + H_y^2 + H_z^2}$ . Real intensity  $H_{real}$  in

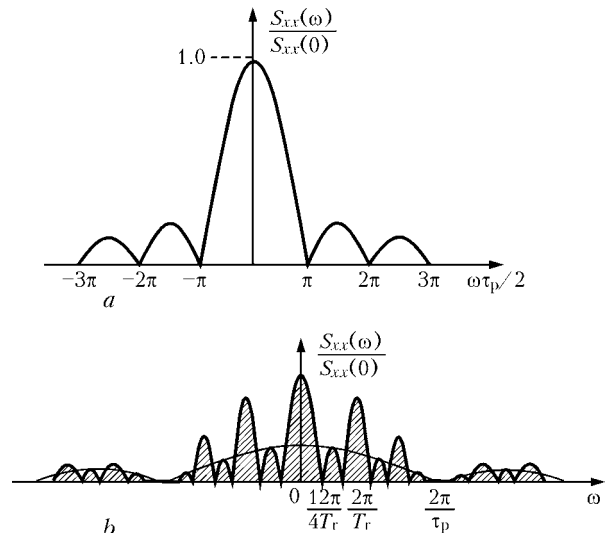


**Figure 6.** Examples of spectra of video pulses: a — theoretical spectrum of MF of single exponential pulse in capacitor-type welding; b — MF spectrum of packet from three equal pulses at interval between pulses  $T_r = 3\tau_p$

any point is calculated according to formula:  $H_{real} = H_0 I_w$ . Data from [8] were obtained at long engagement of welding current, duration of which was determined by time of «dampening» of the measuring millivoltmeter needle and time of recording the readings. In this work levels of MF were determined, which affect work of located in proximity electron-measuring and control equipment.

Analysis of presented data shows that zone of the lowest MF intensity is located in plane  $XOZ$  in front of the circuit (Figure 8, a). The experiments were carried out on the MT-1223 spot welding machine with rated long-term secondary current  $I_{2H} = I_w = 5600$  A. Under these conditions main parameters of MF ( $H_m$  and  $t$  — time of action), created by the resistance welding machines operating on alternating current of 50 Hz frequency, were regulated according to all sanitary norms [6] by the diagram, presented in Figure 9. So, at distance 0.4 m at the contact point level of the electrodes in plane  $XOZ$  (see Figure 8, a)  $H_m = 1.41 H_0 I_w = 3950$  A/m, whereby net time (total time of all welding current pulses within a

**Table 1.** Normative requirements to MF

Parameter	Maximum permissible amplitude values of magnetic field intensity within spectral ranges of frequencies*								
	0–5 Hz	5–50 Hz	0.05–1 kHz	1–10 kHz	10–60 kHz	0.06–3 MHz	3–30 MHz	30–300 MHz	0.3–1 GHz
$E_{MP}$ , V/m	60000	35000	3500	1000	300	200	150	100	80
$EH_{MP}$ , $(V/m)^2 \cdot h$	$3.2 \cdot 10^9$	$2.0 \cdot 10^8$	$1.6 \cdot 10^6$	120000	7200	3200	1800	800	500
$E_{MP}$ , V/m (8 h)	20000	5000	447	120	30	20	15	10	8
$T$ , h (at $E_{MP}$ )	0.89	0.16	0.13	0.12	0.08	0.08	0.08	0.08	0.08
$H_{MP}$ , A/m	30000	10000	850	100	85	70	--	--	--
$EH_{MP}$ , $(A/m)^2 \cdot h$	$1.4 \cdot 10^8$	$1.6 \cdot 10^7$	70000	1300	900	400	--	--	--
$H_{MP}$ , A/m (8 h)	4200	1400	94	13	11	7	--	--	--
$T$ , h (at $H_{MP}$ )	0.16	0.16	0.10	0.13	0.12	0.08	--	--	--

\* In all cases in determination of frequency ranges each range excludes lower and includes upper frequency limit.

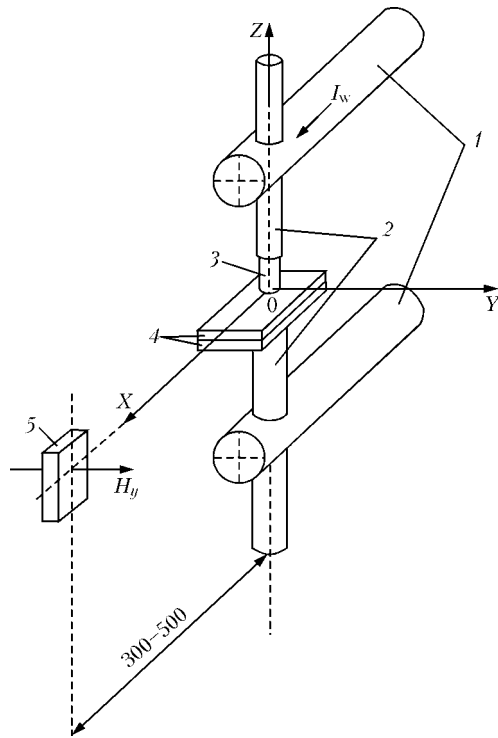


**Figure 7.** Schemes of MF intensity measurement: 1 — welding machine arms; 2 — water-cooled plugs; 3 — electrode; 4 — parts being welded; 5 — MF sensor

working shift), within which a welder is located in this zone should not exceed three hours.

**Methodology of MF intensity determination.**

Taking into account that within frequency range of radiations 50–1000 Hz sanitary norm is 15 times more stringent in comparison with the range 5–50 Hz, within which, as it was assumed earlier, these radiations exist, the need occurred in experimental determination of pulsed MF intensity spectra. For this purpose it was necessary first to develop methodology of measurements and choose the measuring equipment, determine MF spectra, analyze obtained data accord-

ing to the new sanitary norms [5], evaluate influence of regulation of main welding cycle parameters on MF spectra for the purpose of their optimization, etc. At this stage of work spectra in the MF minimal intensity zone were determined (Figure 7), which allowed preliminary interpolating obtained data over the whole space of the working zone (Figure 8).

Requirements of new sanitary norms to the level of pulsed electromagnetic radiations, taking into account their spectral composition, unambiguously indicated the need in using as a registration instrument a digital storage oscillograph combined with a personal computer with a respective software. As sensors the instruments, based on galvano-magnetic phenomena in semiconductors or induction coils, may be used.

For experimental check of mentioned above and measurement and analysis of investigated MF the following instruments were used: the DMP-1 induction sensor of magnetic field; the GFI-1 measurer of magnetic field induction (Hall sensor); the PCS-500 digital oscillograph with FFT (fast Fourier transform) function with PC «Ezbook-700»; the TDS-1002 digital storage oscillograph with FFT function.

Certified sensors and oscillographes ensured measurements of spectral intensity components of variable and pulse MF (see Table 1) from 10 to 160,000 A/m. Non-linearity of amplitude-frequency characteristic of the DMP-1 sensor within frequency range 40–500 Hz did not exceed ±10 %, and of Hall sensor within 0.2–2000 Hz range — ±5 %.

For the purpose of determining accuracy of measurements evaluation of error of the instruments at the most unfavorable combinations (method of determined evaluations) of partial errors was made, which constituted

$$\epsilon_{instr} \cong \epsilon_{sens} + \epsilon_{osc} \cong 9 \%, \quad (8)$$

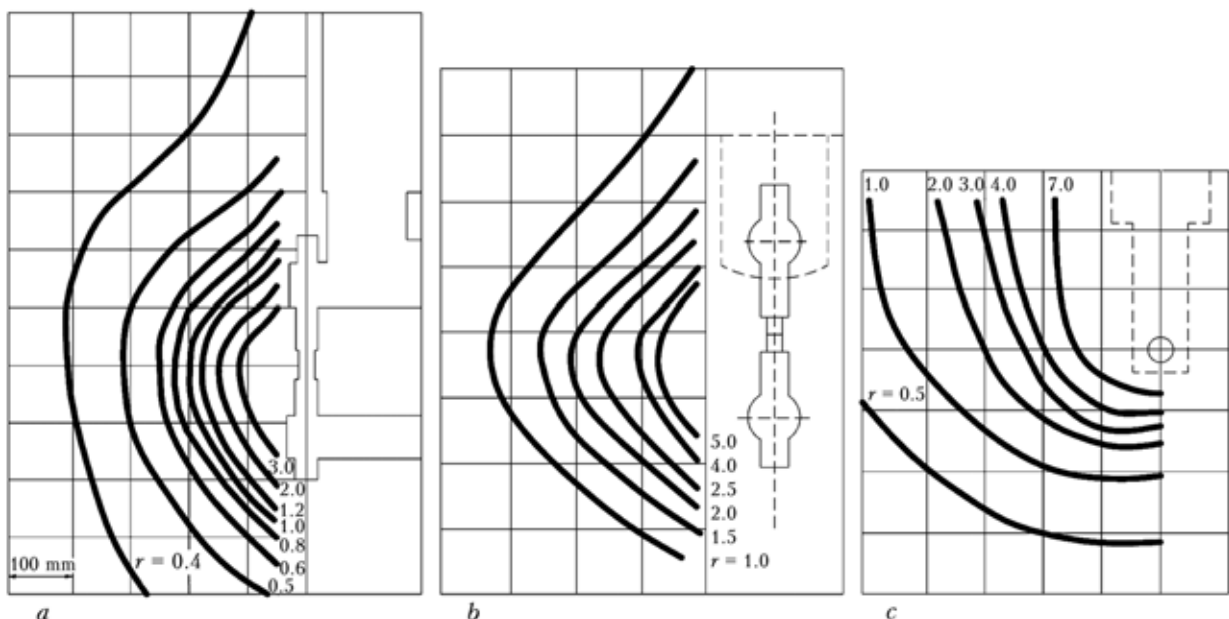


**Figure 8.** Distribution of MF intensity in planes XOZ (a), YOZ (b), XOY (c)



where  $\epsilon_{sens}$  is the main error of sensors  $\pm 5\%$ ;  $\epsilon_{osc}$  is the oscillograph error  $\pm 4\%$ .

Occasional «smoothed» error of spectral evaluation, averaged by  $n_d$  (non-superimposed, separate, equal sections of  $t_{obs}$  length [9]) constituted

$$\epsilon_r \left[ \left| \hat{H}_{xx}(f, t_{obs}) \right|^2 \right] \cong \frac{1}{\sqrt{n_d}} = 14\%$$

Resulting error of evaluation of spectra constituted  $\epsilon = \epsilon_{instr} + \epsilon_r = 23\%$ .

Results of the measurements and calculations of the MF parameters are obtained according to the requirements [5], i.e.  $\sum \frac{H_{mk}^2}{MPL_k^2} = \sum \frac{H_{xxk}^2}{MPL_k^2}$  for each

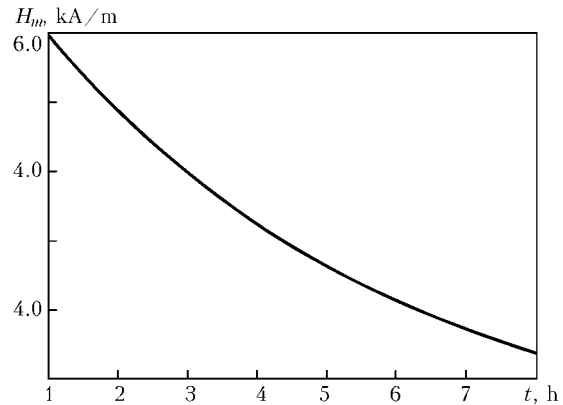
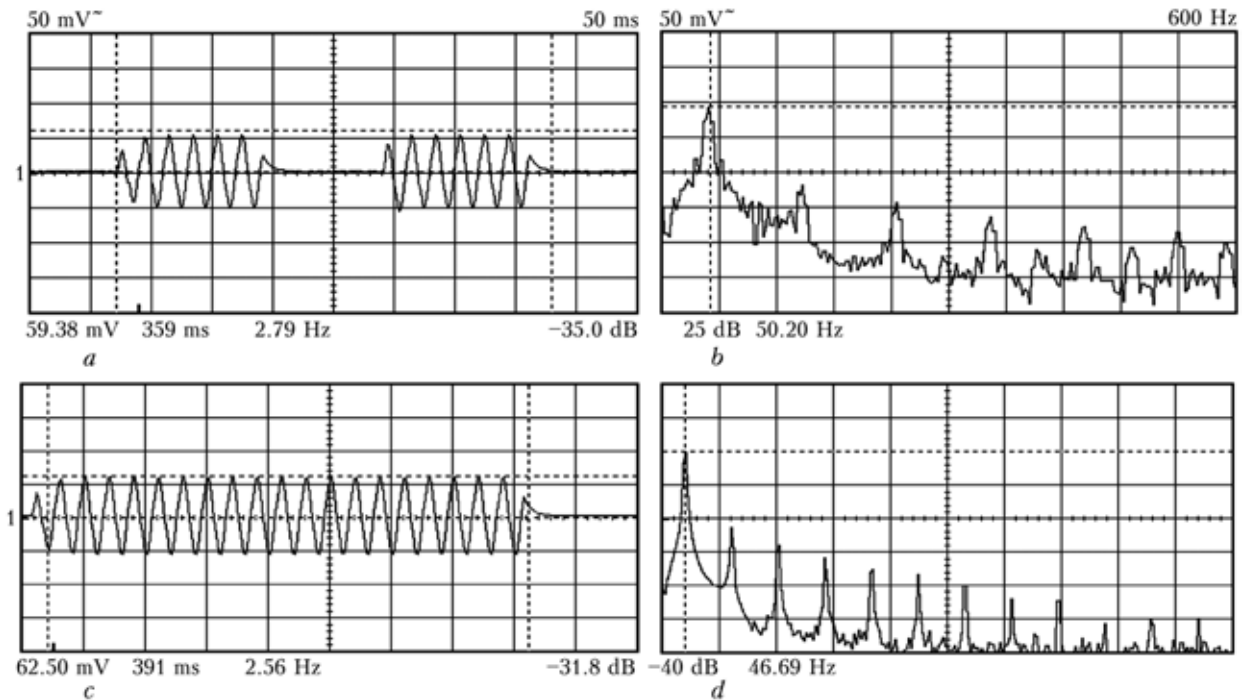


Figure 9. Dependence of maximal permissible values of intensity of continuous and discontinuous MF ( $\tau_p \geq 0.02$  s;  $\tau_{pause} \leq 2.0$  s) of 50 Hz frequency upon time of action

Table 2. Results of MF hygienic evaluation

Welding equipment, method of welding, kind of current	Welding conditions		Measurement zone	Frequency range, Hz	$\sum_k \frac{H_{mk}^2}{MPL_k^2}; T_{w.ad.}, h$
	Cycle duration; kind of pulse	Transformer stage			
Gun MTP-1110, resistance spot welding (manual), alternating current (welding of galvanized metal sheets on frame of minibus)	0.650 s; 2 pulses with modulation of leading and falling edges of pulses --- 1 period	1 (minimal)	Near mains cable	5-50 50-1000	<<1; -- 4.2; 1.9
	Same	Same	Arms (between handles of welding gun at distance 0.1 m from ferromagnetic parts)	5-50 50-1000	<<0.23; -- 25.8; 0.31
	»	4 (maximal)	Same	5-50 50-1000	6.8; 1.17 172; 0.047
Gun for stud welding ELOTOP-502 of Koester company, arc-butt type, direct pulse current (welding of studs of 3 mm diameter to steel sheets)	0.28 s; direct current pulse	Same	»	0-5 5-50 50-1000	<<1; -- <<1; -- 1.01; 8.0
Stationary machine MTK-2202 for spot welding of sheet metal, alternating current	0.360 s; 2 pulses with modulation of leading and falling edges of pulses --- 1 period	4 (maximal)	In plane of welding circuit of machine at distance 0.3 m from contact point of electrodes	5-50 50-1000	<1; -- 3.0; 2.7
	Same	Same	In plane of welding circuit of machine at distance 0.5 m from contact point of electrodes	5-50 50-1000	<<1; -- 1.45; 5.5
	0.420 s; 1 pulse with modulation of leading and falling edges of pulses --- 1 period	»	Same	5-50 50-1000	<<1; -- 1.6; 5.0
	0.416 s; 1 pulse with modulation of falling edge. Angle of adjustment of thyristors is about 40°	»	In plane of welding circuit of machine at distance 0.3 m from contact point of electrodes	5-50 50-1000	<<1; -- 23.7; 0.3
Stationary machine MTK-2201 for spot capacitor-type welding of 0.8 mm thin-sheet metal, direct current	10 ms; arc voltage is 700 V	»	Breast, arms (in plane of welding circuit at different distances from contact point of electrodes)	0-5 5-50 50-1000 0-5 5-50 50-1000	<<1; -- <<1; -- <<1; -- <<1; -- <<1; -- 14.14; 0.64



**Figure 10.** Oscillograms (a, c) and spectrograms (b, d) of resistance spot welding MF on MTK-2202 machine: a — 2 pulses; c — 1 pulse

method, conditions of the experiments, parameters of welding conditions and frequency range, whereby  $H_{mk} = \sqrt{2}H_{xx}(f, t_{obs}) = \sqrt{2}H_{xxk}$  is the amplitude value of  $k$ -th harmonic (see Tables 1 and 2), averaged by  $n_d = 50$  intervals (experiments). Resolution of spectrum by frequency  $\Delta f = 1/t_{obs}$ , where time of observation  $t_{obs} = H\Delta t$  ( $\Delta t$  is the signal quantization time, s;  $N$  is the number of observations for  $N$ -spot DFT (discrete Fourier transform) (resolution ADC).

**Results of investigations.** Measurements were carried out both in the PWI laboratories and under production conditions of enterprises where resistance welding is used. Organization of the working places (arrangement of the equipment, power and welding cables, etc.) may be considered typical (arbitrarily optimal) one. Conditions of carrying out measurements at the working places during performance of resistance welding, welding modes and results of measurement of the MP parameters are presented in Table 2. Conditions of the welding equipment operation during MF measurement may be characterized as rather medium in regard to the power, that's why in case of operation of this equipment at higher stages of regulation amplitude parameters of MF may significantly exceed values, presented in Table 2. Obtained oscillograms and spectrograms of the MF signals are presented in Figures 10–14.

Lets us consider the results obtained for each method of resistance welding.

**Resistance spot welding.** Results of the investigations showed that the following regularities are characteristic of all kinds of resistance spot welding. Shape of the welding current in the form of a short packet (packets) of sinusoidal pulses — sections of a sinusoid (Figure 10) determines MF spectrum, which has transitional character (intermediate between discrete and

continuous one). Spectrum components within frequency range 50–1000 Hz determine problems of magnetic safety of this method.

Modes in spot welding may be rather diverse from the viewpoint of the produced spectra of MF, which exert significant influence on its composition depending upon number of pulses in the packet and number of packets (up to three: preheating, welding, and annealing ones).

Even more significant factor, determining amplitude of the MF spectrum harmonics, is the welding current value, i.e. power parameters of the mode, determined by the «regulation stage» of the welding transformer (whereby investigation of  $\cos \varphi$  influence of welding machines on the welding current shape and spectra of MF signals at this stage of work was not carried out).

Phase regulation of the welding current thyristor contactors may exert significant influence on magnetic situation in the working zone and cause its drastic worsening. In this case MF spectrum shifts rightwards with main 100 Hz harmonic (see Table 2 and Figure 11), whereby  $T_{w.ad} \approx 0.3$  h. Modulation of leading and falling edges of pulses does not exert significant influence on MF spectra. These preliminary conclusions may be a priori transferred on methods of relief and seam welding.

One should also note unfavorable results, obtained in spot resistance welding by manual tools (tongs, guns, etc.). Oscillograms and spectrograms of this process are presented in Figure 12, conditions of carrying out the experiment — in Table 2. On pictures (Figure 15), illustrating conditions of work at Kiev automobile factory during manufacturing of minibus bodies, one may observe unfavorable spatial arrangement of working tools (the welding gun) relative body

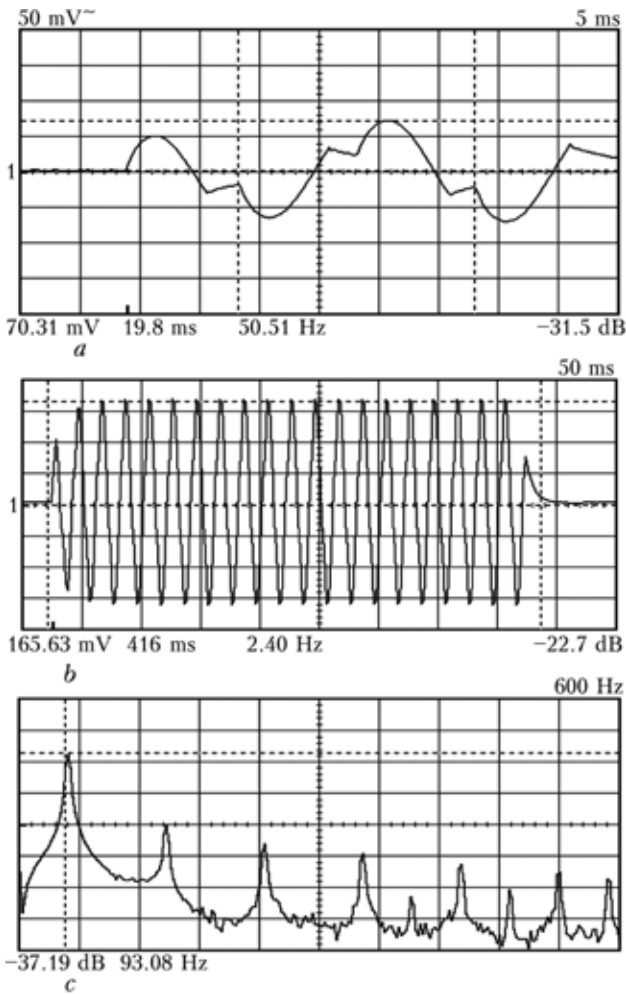


**Figure 11.** Oscillograms (a, b) and spectrograms (c) of MF of resistance spot welding by 1 pulse of welding current with phase regulation of thyristor contactor ( $\phi_{ig} \approx 40^\circ$ )

of a welder during performance of operations. Taking into account the fact that at this enterprise a 12-hour working day is established, duration of welding  $T_w$ ,

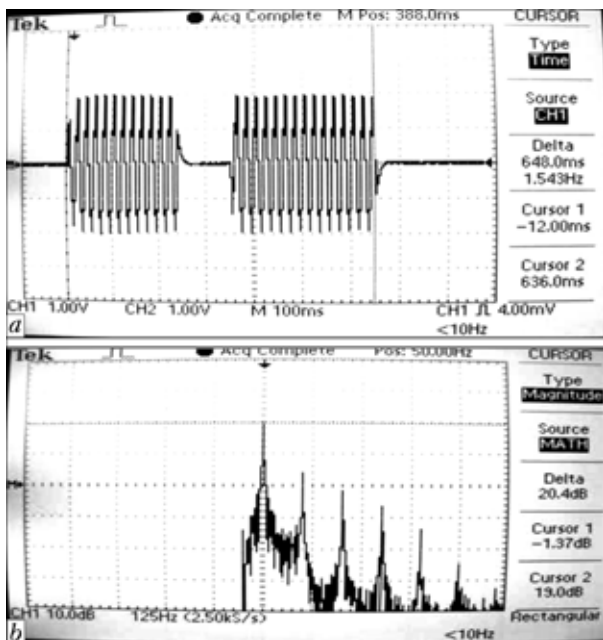


**Figure 12.** Oscillogram (a) and spectrogram (b) of MF between handles of MTP-1110 gun in manual spot resistance welding

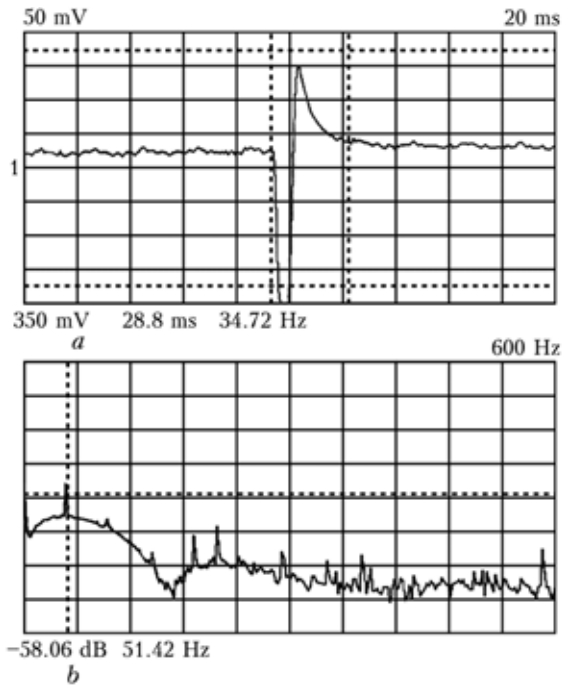


**Figure 13.** Oscillogram (a) and spectrogram (b) of MF of capacitor-type spot welding on MTK-2201 stationary machine

taking into account duration of engagement of the equipment, equals several hours. Analysis of obtained by us results of measurements of MF levels showed that  $T_{w.ad}$  for a welder on this technological operation may constitute just  $T_{w.ad} \approx 0.047$  h.

**Capacitor-type spot welding.** It is characteristic of all kinds of direct current capacitor spot welding that shape of the welding current in the form of a short-term exponential video pulse determines continuous spectrum of MF. Spectrum component within

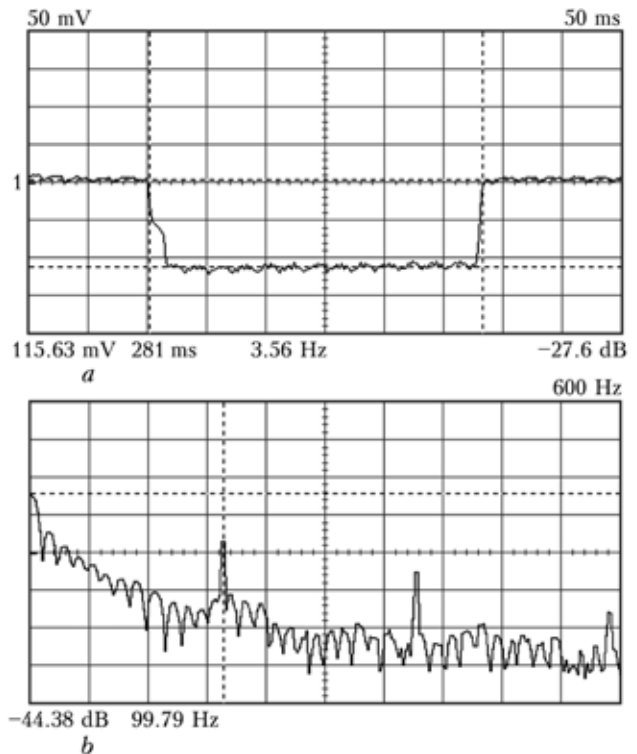


**Figure 14.** Oscillogram (a) and spectrogram (b) of MF of arc butt spot welding by ELOTOP gun (between gun handles)

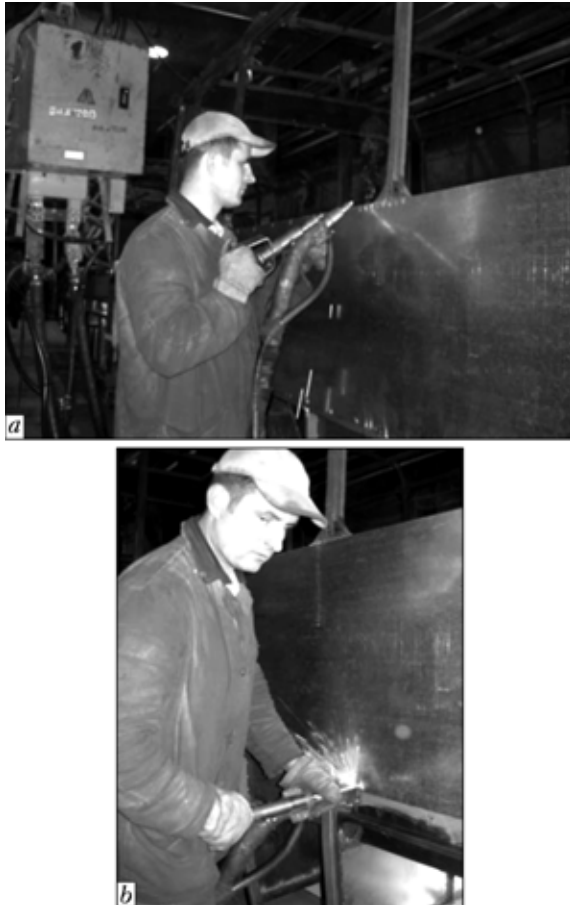


**Figure 15.** Manual resistance welding by MTP-1110 gun at level of shoulder (a) and waist (b)

frequency range 5–1000 Hz mainly determines sanitary problems of this method (see Table 2, Figure 13). In this case presented oscillogram proves disrepair of the MTK-2201 capacitor machine electrical circuit, in particular, pulse «overtravel» over zero during discharge of the capacitors, i.e. oscillation process during discharge should be excluded. So, the data obtained correspond to the real ones, but technical state of the welding machine does not meet technical requirements. In this case  $T_{w.ad} \approx 0.64$  h.

These conclusions may be also extrapolated on manual percussion capacitor welding (manual welding of studs of 2–12 mm diameter to sheets by a gun, the UDK-701 unit, developed by the E.O. Paton EWI) with a very probable assumption of higher magnetic radiation.

**Arc butt welding.** Investigation of MF, which occur in welding by the ELOTOP gun of the Koester company (Germany), designed for welding of studs of 3–6 mm diameter to sheets by a direct current pulse (the power source is characterized by absence of phase regulation of thyristors), showed that spectrum of the MF signal is of continuous character and shifted to frequency range 0–5 Hz (Figure 14), whereby  $T_{w.ad} \approx 8$  h, i.e. minimal influence of MF even on arms of a welder is ensured.

**Recommendations on protection of welders.** Obtained results of MF intensity measurements made it possible to determine necessary efficiency of protection in resistance electric welding (Table 3). Under

**Table 3.** Necessary efficiency of protection methods in resistance welding

Method of welding	Maximal MF intensity at working place within frequency range 50–1000 Hz, A/m	Necessary efficiency of protection, times
Spot (tongs)	580	6–8
Spot (stationary)	290	3–4
Spot (capacitor)	120	2
Arc butt (manual without phase regulation)	80	--
Seam	--	2–3
Relief	--	2

efficiency of protection devices the ratio of the MF intensity (maximal value) at the working place  $H_m$  to the maximal permissible one  $H_{MP}$ :  $E_{pr} = H_{mk} / H_{MP}$  is meant.

The most efficient solution of the electromagnetic safety problems in resistance welding may be technological methods, in particular: optimization of resistance spot, seam and relief welding conditions not just from technological but also electromagnetic safety viewpoint (duration, number and modulation of pulses, Q-factor, angle of phase regulation of thyristors, etc.); limitation of power of the resistance welding machines (especially table machines, spot tongs and guns).

Designers and manufacturers of new series equipment should take into account conditions of their application and valid sanitary norms, because application of this equipment in industry will be limited by the electromagnetic radiation levels in a working zone during tests at maximal power stage of the welding transformer with different combinations of the welding cycle regulator settings.

In case of exceeding of regulated by DSN 3.3.6.096–2002 electromagnetic radiation levels and insufficiency of technological measures, directed at their reduction, industrial workers must obligatory take such known additional measures of their protection as proper organization of a working place, which envisages protection by a distance, time of stay in a hazardous zone, and screening of the welding equipment.

1. Weman, K. (1994) Health hazards caused by electromagnetic fields during welding. *Svetsaren*, 48(1), 2.
2. Bourton, M. (1995) A review of arc welding and electromagnetic compatibility. *IIW Doc. VIII-G100–95*.
3. Epstein, R. (1995) Electromagnetic fields: how big a problem in Europe? *IIW Doc. VIII-C108–95*.
4. Couderc, M.P. (1999) Notes on magnetic fields in welding. *IIW Doc. VIII–99*.
5. *DSN 3.3.6.096–2002*: State sanitary codes and regulations in work with sources of electromagnetic fields. Kiev: Ministry of Health Protection.
6. *SN 3206–85*: Maximum permissible levels of magnetic fields of 50 Hz frequency. Moscow.
7. Kharkevich, A.A. (1962) Spectrums and analysis. Moscow: Fizmatgiz.
8. Chuloshnikov, L.P., Chalev, A.A., Orlov, B.D. et al. (1980) Study of electric field intensity in resistance welding. *Elektrotekh. Promyshlennost. Series Electric Welding*, Issue 3, 5–6.
9. Bendat, J., Pirsol, A. (1989) *Applied analysis of hash*. Moscow: Mir.



# APPLICATION OF EXPLOSION ENERGY FOR TREATMENT OF WELDED JOINTS ON DECOMPOSERS AND MIXERS AT THE NIKOLAEV ALUMINA PLANT

L.D. DOBRUSHIN, V.G. PETUSHKOV and A.G. BRYZGALIN  
E.O. Paton Electric Welding Institute, NASU, Kiev, Ukraine

Example is given of the efficient application of explosion energy for improving reliability of process equipment installed at the Nikolaev Alumina Plant by relieving residual welding stresses in welds on decomposers and mixers with a diameter of up to 14 m and height of up to 34 m.

*Keywords:* explosion treatment, welded decomposers, mixers, welds, residual stresses, extension of service life

Tensile stresses are the energy drivers of corrosion cracking of metals in alkalis [1–3]. Residual stresses present in welded structures cause cracking of the welds and lead to formation of leaks and a risk of major accidents [4]. Relieving residual stresses in large-size metal structures by heat treatment is a labour-consuming, expensive and inefficient operation [3, 4]. The E.O. Paton Electric Welding Institute developed the technology for relieving residual stresses by explosion treatment, which was applied to advantage in construction of new alumina plants and expansion of production of the existing ones in the territory of the former Soviet Union, in Ukraine and in Yugoslavia [2, 4, 5].

Substantial expansion of production capacities, which has been realised in the last years by the world-leading manufacturers of aluminium, resulted in revival of the insistent demand for commercial application of this technology. In 2007, the Joint Stock Company RUSAL completed construction of 15 decomposers and two mixers at the Nikolaev Alumina Plant by using the explosion treatment technology for relieving residual stresses in the welds. Diameter of the apparatuses was 12 and 14 m, and height was 15 to 34 m, thickness of the metal welded (steel St3sp (killed)) ranging from 8 to 40 mm. The work on ap-

plication of explosion treatment by the above technology was performed by specialists of the R&D Centre «Explosion Treatment of Materials» under the supervision of experts of the E.O. Paton Electric Welding Institute. Successful interaction with assembly organisations allowed the explosion treatment process to be logically integrated into the flow diagram of construction of tanks, which made it possible to perform explosion operations without any delay in assembly-welding operations.

Characteristically, explosion treatment was carried out by using the strictly portioned captive explosion charges located along the welds on the internal surface of a tank. The shape and linear weight of the explosion charges were set depending upon the thickness of the metal welded. The explosion charges were made beforehand, delivered to the welds to be treated, and fixed to the tank walls using adhesives (Figure 1). Explosion treatment, which is characterised by high reproducibility of results, is controlled by geometry of imprints of the explosive charges (Figure 2), which allows a substantial reduction of efforts associated with measurement of resulting residual stresses.

Another important moment is that in explosion treatment the tank itself plays the role of a sort of an explosion chamber and serves for protection of humans and nearby buildings from a harmful side effect of explosion. Maximal weight of the simultaneously mounted explosive charges is based, as a rule, on a condition of ensuring integrity of glasses [4]. From 20 to 180 running metres of the welds can be treated



Figure 1. Mounting of explosive charge

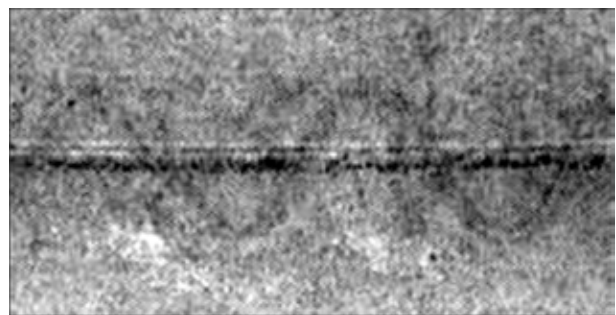


Figure 2. Trace of explosive charge after explosion treatment



per blasting, depending upon the conditions of performing the explosion operations and thickness of the metal treated. As proved by the many years' practical experience, explosion treatment is not hazardous for technological facilities having no glasses, for control equipment, as well as for service lines.

For example, at the Nikolaev Alumina Plant the nearby building (amenity building) was located at a distance of 40 m from the two mixers subjected to explosion treatment. The special pioneering protection device, which prevented destruction of glasses in the amenity building, including with the already existing cracks, was developed, manufactured and applied to provide the required productivity of the explosion operations.

The explosion treatment technology requires no special equipment or power supplies. It is sufficiently simple and can be implemented by workers of any specialised organisation under the supervision of the

technology developers. In addition to the welds on tank structures, the explosion treatment technology can also be used to relieve residual stresses in assembly butt joints on industrial pipelines, this, however, requiring special arrangements to be made to ensure safety of the explosion operations [5] because of the external location of explosive charges.

1. (1971) *Alkali brittleness and increase in resistance of alumina production equipment*. Ed. by V.I. Artemiev, O.I. Steklov. Moscow: TsNITEItsvetmet.
2. Artemiev, V.I., Pashchin, A.N., Petushkov, V.G. et al. (1978) Application of explosion energy for improving corrosion resistance of welded joints on decomposers. *Tsvet. Metallurgiya*, 5, 37-40.
3. Petushkov, V.G. (1994) Explosion treatment of welded joints. Ed. by B.E. Paton. In: *Welding and Surfacing Rev.* Harwood: A.P.
4. Petushkov, V.G. (2005) *Application of explosion in welding engineering*. Kiev: Naukova Dumka. 756 p.
5. Sushkov, A.I., Troitsky, I.A. (1965) *Metallurgy of aluminium*. Moscow: Metallurgiya.

## NEWS

### STEAM-PLASMA PROCESSING UNITS

Specialists of the E.O. Paton Electric Welding Institute of the NAS of Ukraine together with the Institute of Gas of the NAS of Ukraine, in collaboration with

gases emitted from the work chamber, independent cooling system, compressor station, gas analysis system, and other appropriate systems.



Experimental-industrial unit for steam-plasma processing of environmentally hazardous wastes

Research-Production Companies «Plazer» and «UkrSpetstekhnologii», based on in-house research, developed experimental equipment for processing and disposal of environmentally hazardous, including medical, wastes by the method of steam-plasma pyrolysis with synthesis-gas produced as a secondary product. The method can be used to process not only medical, but also other wastes, and first of all organic ones, e.g. wastes of plastics, etc. Based on the above equipment, the Institute of Gas arranged an integrated pilot section, which consists of two steam-plasma units equipped with the 180 kW plasmotrons with a design capacity of up to 100 kg/h (Figure), special system for gas cleaning with the equipment for chilling of

The section is equipped with the modern monitoring and control system. The steam-plasma pyrolysis technology provides practically complete processing of wastes with no emission to the atmosphere of such hazardous substances as dioxins, phenols, and different types of fumes. During processing, it is necessary to remove such dangerous elements as chlorine, fluorine, etc., which are parts of different plastic materials.

The units have no analogues in Ukraine. The world experience of application of traditional plasma methods for processing of hazardous wastes shows that plasma holds high promise for highly efficient, environmentally safe processing of different types of wastes.



## OUR CONGRATULATIONS

### To 80th anniversary of Prof. Boris A. Movchan



Known scientist in the field of materials science and electron beam technology, academician of Academy of Sciences of Ukraine Boris A. Movchan is 80 years of age.

Boris A. Movchan was born on 9th of January 1928 in village Makievka, Chernigov oblast. In 1944 he finished incomplete secondary school, in 1946 --- two years of Kiev Ship Building Technical School, and in 1951 --- physical faculty of the T.G. Shevchenko Kiev State University, where he specialized in «Physics of Metals».

Since 1951 till nowadays B.A. Movchan has been working in the E.O. Paton Electric Welding Institute of the National Academy of Sciences of Ukraine, first as a research assistant of the Institute, and from 1960 till 1994 as Head of the Department of Electron Beam Technologies; since 1994 he has been the founder and director of International Center for Electron Beam Technologies of the E.O. Paton EWI (IC EBT). Beginning from 2003 till nowadays B.A. Movchan has been occupying position of chief research assistant of the Department of Vapor-Phase Technologies of Non-Organic Materials of the E.O. Paton EWI and research assistant-consultant of IC EBT.

In 1954 B.A. Movchan defended thesis for scientific degree of candidate of engineering sciences, and in 1961 became doctor of engineering sciences. In June 1964 he was elected a corresponding member of Academy of Sciences of UkrSSR, and since March 1978 ---

academician of Academy of Sciences of UkrSSR in the field of «Materials Science and Strength of Materials».

Main direction of scientific activity of B.A. Movchan is structure and properties of non-organic materials, electron beam technologies, and new materials.

He may be rightfully called the founder of a new scientific school for producing new materials and multifunctional coatings by the method of electron beam technology of evaporation and condensation in vacuum. B.A. Movchan published more than 360 scientific works, 7 monographies and received more than 100 patents. He trained 56 candidates and 6 doctors of engineering sciences. He is member of the editorial boards of a number of scientific journals and scientific councils.

Scientific activity of B.A. Movchan is marked by a number of state awards. In 1974 he was awarded State prize of UkrSSR in the field of science and technology, in 1976 --- Order of the Red Banner of Labor, in 1981 --- second Order of the Red Banner of Labor, in 1984 --- Lenin prize for work in the field of electron beam technology, in 1988 --- order of Lenin, in 1989 --- Evgeny Paton prize of the NAS of Ukraine, in 1998 --- order «For Merits» of III degree. In 2004 Boris A. Movchan was awarded honorary title «Honoured Worker of Science and Technology of Ukraine». B.A. Movchan is marked by honorary diplomas of American Vacuum Society (1983, 1988) and Honorary diploma of Ministry of Aircraft Industry of China (1988).

Academician B.A. Movchan meets his 80th anniversary full of creative energy. We congratulate the hero of the anniversary, wish him good health, happiness, and further success for the welfare of our Ukraine.

*E.O. Paton Electric Welding Institute of NASU  
International Center  
for Electron Beam Technologies  
Editorial Board of «The Paton Welding Journal»*

# SUBSCRIPTION FOR «THE PATON WELDING JOURNAL»

If You are interested in making subscription directly via Editorial Board, fill, please, the coupon and send application by fax or e-mail.

The cost of annual subscription via Editorial Board is \$324.

Telephones and faxes of Editorial Board of «The Paton Welding Journal»:

Tel.: (38044) 287 6302, 271 2403, 529 2623

Fax: (38044) 528 3484, 528 0486, 529 2623.

«The Paton Welding Journal» can be also subscribed worldwide from catalogues of subscription agency EBSCO.

<b>SUBSCRIPTION COUPON</b>			
Address for journal delivery			
Term of subscription since	200	till	200
Name, initials	_____		
Affiliation	_____		
Position	_____		
Tel., Fax, E-mail	_____		



## ADVERTISEMENT IN «THE PATON WELDING JOURNAL» (DISTRIBUTED ALL OVER THE WORLD)

### «AVTOMATICHESKAYA SVARKA»

#### RUSSIAN VERSION OF «THE PATON WELDING JOURNAL» (DISTRIBUTED IN UKRAINE, RUSSIA AND OTHER CIS COUNTRIES)

**External cover, fully-colored:**

- First page of cover (190×190 mm) – \$570
- Second page of cover (200×290 mm) – \$400
- Third page of cover (200×290 mm) – \$400
- Fourth page of cover (200×290 mm) – \$400

**Internal cover, fully-colored:**

- First page of cover (200×290 mm) – \$400
- Second page of cover (200×290 mm) – \$400
- Third page of cover (200×290 mm) – \$400
- Fourth page of cover (200×290 mm) – \$400

**Internal insert:**

- Fully-colored (200×290 mm) – \$340
- Fully-colored (double page A3) (400×290 mm) – \$570
- Fully-colored (200×145 mm) – \$170

- Article in the form of advertising is 50 % of the cost of advertising area
- When the sum of advertising contracts exceeds \$1000, a flexible system of discounts is envisaged

**Technical requirement for the advertising materials:**

- Size of journal after cutting is 200×290 mm
- In advertising layouts, the texts, logotypes and other elements should be located 5 mm from the module edge to prevent the loss of a part of information

**All files in format IBM PC:**

- Corell Draw, version up to 10.0
- Adobe Photoshop, version up to 7.0
- Quark, version up to 5.0
- Representations in format TIFF, color model CMYK, resolution 300 dpi
- Files should be added with a printed copy (makeups in WORD for are not accepted)